

**INCORPORATING LINK CORRELATIONS IN
MODELS AND ALGORITHMS FOR
LOCALIZATION IN WIRELESS
SENSOR NETWORKS**

by

Piyush Agrawal

A dissertation submitted to the faculty of
The University of Utah
in partial fulfillment of the requirements for the degree of

Doctor of Philosophy

Department of Electrical and Computer Engineering

The University of Utah

May 2012

Copyright © Piyush Agrawal 2012

All Rights Reserved

The University of Utah Graduate School

STATEMENT OF DISSERTATION APPROVAL

The dissertation of Piyush Agrawal
has been approved by the following supervisory committee members:

<u>Neal K. Patwari</u>	, Chair	<u>01/06/2012</u> Date Approved
<u>Cynthia M. Furse</u>	, Member	<u>01/06/2012</u> Date Approved
<u>Rong-Rong Chen</u>	, Member	<u>01/06/2012</u> Date Approved
<u>Behrouz Farhang</u>	, Member	<u>01/06/2012</u> Date Approved
<u>Sneha K. Kasera</u>	, Member	<u>01/06/2012</u> Date Approved

and by Gianluca Lazzi, Chair of
the Department of Electrical and Computer Engineering

and by Charles A. Wight, Dean of The Graduate School.

ABSTRACT

In wireless sensor networks, knowing the location of the wireless sensors is critical in many remote sensing and location-based applications, from asset tracking, and structural monitoring to geographical routing. For a majority of these applications, received signal strength (RSS)-based localization algorithms are a cost effective and viable solution. However, RSS measurements vary unpredictably because of fading, the shadowing caused by presence of walls and obstacles in the path, and non-isotropic antenna gain patterns, which affect the performance of the RSS-based localization algorithms. This dissertation aims to provide efficient models for the measured RSS and use the lessons learned from these models to develop and evaluate efficient localization algorithms.

The first contribution of this dissertation is to model the correlation in shadowing across link pairs. We propose a non-site specific statistical joint path loss model between a set of static nodes. Radio links that are geographically proximate often experience similar environmental shadowing effects and thus have correlated shadowing. Using a large number of multi-hop network measurements in an ensemble of indoor and outdoor environments, we show statistically significant correlations among shadowing experienced on different links in the network. Finally, we analyze multi-hop paths in three and four node networks using both correlated and independent shadowing models and show that independent shadowing models can underestimate the probability of route failure by a factor of two or greater.

Second, we study a special class of algorithms, called kernel-based localization algorithms, that use kernel methods as a tool for learning correlation between the RSS measurements. Kernel methods simplify RSS-based localization algorithms by providing a means to learn the complicated relationship between RSS measurements and position. We present a common mathematical framework for kernel-based localization

algorithms to study and compare the performance of four different kernel-based localization algorithms from the literature. We show via simulations and an extensive measurement data set that kernel-based localization algorithms can perform better than model-based algorithms. Results show that kernel methods can achieve an RMSE up to 55% lower than a model-based algorithm.

Finally, we propose a novel distance estimator for estimating the distance between two nodes a and b using indirect link measurements, which are the measurements made between a and k , for $k \neq b$ and b and k , for $k \neq a$. Traditionally, distance estimators use only direct link measurement, which is the pairwise measurement between the nodes a and b . The results show that the estimator that uses indirect link measurements enables better distance estimation than the estimator that uses direct link measurements.

CONTENTS

ABSTRACT	iii
LIST OF FIGURES	ix
LIST OF TABLES	xii
ACKNOWLEDGEMENTS	xiii
CHAPTERS	
1. INTRODUCTION	1
1.1 Summary of Contributions	2
1.2 Models for the Received Signal Strength (RSS)	4
1.2.1 Single Link Channel Model	4
1.2.2 Extension to Multi-Hop Networks	5
1.3 Motivation for the Study of Kernel-based Localization Algorithms	7
1.4 Range Estimation in Wireless Sensor Networks	8
1.5 Outline	8
2. RELATED RESEARCH	10
2.1 Correlation in Shadowing	10
2.2 RSS-based Localization Algorithms	13
2.2.1 Model-based Algorithms	13
2.2.1.1 Range-based Algorithms	13
2.2.1.2 Range-ratio Algorithms	14
2.2.1.3 Range-free Algorithms	14
2.2.2 RSS Fingerprinting Algorithms	14
2.2.3 Discussion	15
2.3 Range Estimation in Wireless Sensor Networks	16
3. CORRELATED LINK SHADOW FADING IN MULTI-HOP WIRELESS NETWORKS	19
3.1 Abstract	19
3.2 Introduction	19
3.2.1 Single-Link Path Loss Model	21
3.2.2 Application in Multi-Hop Networking Research	22
3.2.3 Correlation Limits Link Diversity	24
3.3 Related Research	24

3.4	Motivation	26
3.4.1	Adaptation to Mobile-to-Mobile Link	27
3.4.2	Adaptation to Multiple Links	28
3.4.3	Summary	29
3.5	Joint Path Loss Model	29
3.5.1	Spatial Loss Field	30
3.5.1.1	Isotropy	31
3.5.1.2	Exponential Decaying Covariance	31
3.5.2	Shadowing Losses	32
3.5.2.1	Single-Link Properties	33
3.5.2.2	Joint Link Properties	34
3.5.3	Total Fading Model	34
3.5.4	Analysis Using Proposed Model	35
3.6	Experimental Validation	36
3.6.1	Measurement Campaign Overview	36
3.6.2	Controlled Measurement Campaign	37
3.6.3	Field Deployment Measurement Campaign	38
3.6.4	Statistical Analysis	41
3.6.4.1	Estimation of Large-Scale Path Loss Parameters	41
3.6.4.2	Estimation of Correlated Shadowing Parameters	42
3.6.4.3	Discussion	43
3.6.5	Verification	44
3.7	Application of Joint Model	46
3.7.1	A Three-Node Multi-Hop Path	48
3.7.1.1	Case of i.i.d. Shadowing	49
3.7.1.2	Case of Correlated Shadowing	49
3.7.2	A Four-Node Multi-Hop Network	50
3.7.3	Discussion	50
3.8	Conclusion	51
3.9	Acknowledgments	52
3.10	Appendix	52
4.	KERNEL METHODS FOR RSS BASED INDOOR LOCALIZATION	54
4.1	Abstract	54
4.2	Introduction	54
4.3	Kernel Methods	57
4.3.1	Problem Statement	58
4.3.2	General Mathematical Formulation	59
4.3.2.1	Determination of Kernel Parameters	60
4.3.2.2	Example Framework	61
4.3.3	LANDMARC Algorithm	63
4.3.4	Gaussian Kernel Localization Algorithm	65
4.3.5	Radial Basis Function Based Localization Algorithm	68

4.3.6	Linear Signal-Distance Map Localization Algorithm	71
4.3.7	Summary	74
4.4	Numerical Examples	74
4.4.1	Maximum Likelihood Coordinate Estimation	75
4.4.1.1	Estimating Coordinate from RSS	75
4.4.1.2	Implementation Details	76
4.4.2	Description of Comparison Example	76
4.5	Evaluation Using Measurement Data Set	84
4.5.1	Measurement Campaign Description	84
4.5.2	Evaluation Procedure	85
4.5.3	Results	86
4.5.3.1	Bias Results	86
4.5.3.2	RMSE Results	88
4.6	Discussion and Conclusion	88
5.	NETWORK DISTANCE: DISTANCE ESTIMATION	
	VIA MEASUREMENTS WITH NEIGHBORS	90
5.1	Abstract	90
5.2	Introduction	90
5.3	Related Work	92
5.4	Distance Estimation Model	93
5.4.1	Framework for Network Distance Estimation	94
5.4.2	Discussion	96
5.4.3	Transforming Dissimilarity to Geographical Distance	96
5.5	Expected Neighbors with Distance	97
5.6	Prior Range Estimation Algorithms	100
5.6.1	Direct Link Distance Estimation	101
5.6.1.1	Constant Per-Hop (CPH) Distance Estimator	101
5.6.1.2	RSS-based Distance Estimator	101
5.6.2	Neighbor Connectivity-based Distance Estimator	102
5.7	Experimental Setup	103
5.7.1	Measurement Campaign Description	103
5.7.2	Experimental Procedure	104
5.8	Results	108
5.8.1	Experimental Validation of Affine Approximation	108
5.8.2	Analysis of Network Distance	111
5.8.2.1	Analysis as a Function of τ	111
5.8.2.2	Analysis for Different Link Reliability	113
5.8.2.3	Discussion	115
5.8.3	Comparison of Network Distance with Other Distance Estimators	115
5.8.3.1	Comparison with Neighbor Connectivity (NC)-based Distance Estimator	115
5.8.3.2	Comparison with Constant Per-Hop (CPH) Distance Estimator	116

5.8.3.3	Comparison with RSS-based Distance Estimator	117
5.8.4	Distance Estimation Between Two-Hop Nodes	118
5.8.4.1	Validation of Affine Approximation for Two-Hop Links	118
5.8.4.2	Comparison with Other Distance Estimators	120
5.8.4.3	Comparison with Shortest-Path of One-Hop Network Distance	123
5.8.5	Distance Estimation for Non-Peer-to-Peer Systems	124
5.9	Localization Using Dissimilarities	126
5.9.1	Procedure	127
5.9.2	Preprocessing for Dissimilarity	127
5.9.3	Results	129
5.9.3.1	Using PRR on Direct Link	129
5.9.3.2	Using Neighbor Ratio	131
5.10	Conclusion	133
6.	CONCLUSION	135
6.1	Key Findings	135
6.2	Future Work	139
	REFERENCES	146

LIST OF FIGURES

1.1 Graphical depiction of different fading models.	6
1.2 A plot of the actual measured signal level, from [1] (used with permission from Sage publications).	6
1.3 Example of factor in shadowing loss correlation. Because link a and link b cross the same environment, their shadowing losses tend to be correlated.	7
3.1 Graphical depiction of (a) circular coverage model, and (c) coverage in the i.i.d. log-normal shadowing model, compared to the common depiction of (b) in which coverage area is a random shape. In (a) and (b), nodes are connected if and only if they are within the gray area, while in (c), nodes are connected with probability proportional to the shade (darker is more probable).	22
3.2 Example of factor in shadowing loss correlation. Because link a and link b cross the same environment, their shadowing losses tend to be correlated.	23
3.3 Example of the motion of mobile receiver and base station position in Gudmundson's model	27
3.4 A simple four-node ad hoc network its six pairwise links.	27
3.5 A link pair in an underlying spatial loss field $p(\mathbf{x})$	30
3.6 Figure (a) shows one realization of the network deployment at Albion Basin. The map constructed by such deployment of wireless sensors is shown in (b).	40
3.7 Example multi-hop networks of (a) three and (b) four nodes.	48
3.8 The percentage increase in P [link failure] for correlated, vs. i.i.d. shadowing, for three-node and four-node multi-hop network examples, as a function of $\bar{\beta}_{i,j}$	51
4.1 Flow chart showing the localization operation using kernel methods. . .	60
4.2 Position of APs and tags.	62
4.3 Position of APs and tags. There is a wall separating the network, represented by a black vertical line.	77
4.4 Plot showing the coordinate estimates for different localization algorithms along with the position of the tag. In (a) the tag is at the center of the network and in (b) the tag is at the edge of the network.	79

4.5	Bias plot showing the mean (\times) of tag location estimates over 500 trials for different localization algorithms. Actual tag location (\blacktriangle) is connected to the mean location estimate (---). Plot also shows $1\text{-}\sigma$ covariance ellipse (---) for the coordinate estimates. The APs (\bullet) are at the corners of the grid. The tag is located at the center of the network.	82
4.6	Bias plot showing the mean (\times) of tag location estimates over 500 trials for different localization algorithms. Actual tag location (\blacktriangle) is connected to the mean location estimate (---). Plot also shows $1\text{-}\sigma$ covariance ellipse (---) for the coordinate estimates. The APs (\bullet) are at the corners of the grid. The tag is located at the edge of the network.	83
4.7	Coordinates of APs in the measurement analysis. The APs represented by ($*$) are said to be in “sweet spot” of the deployment.	86
4.8	Bias plot showing the mean (\times) of location estimates of the APs when it is emulated as a tag. In all the plots, actual AP location (\bullet) is connected to the mean location estimate (---). The APs in “sweet spot” are marked with (\bullet) and are inside the box.	87
5.1	Two sensors (\bullet) and their coverage areas, including the area of coverage overlap.	98
5.2	The normalized areas of overlap and of non-overlap (one or the other but not both) of two circles of radius R , when their centers are separated by distance d . The plot also shows the first order approximation.	99
5.3	The normalized values of $E[\delta_{a,b}]/(\lambda\pi R^2)$ as a function of d/R . The plot also shows the first order approximation.	100
5.4	Block diagram showing the distance estimation in neighbor connectivity-based distance estimator.	103
5.5	Coordinates of the sensors (\bullet) in the measurement campaign.	104
5.6	Percentage of connected links that have $\text{PRR} > \gamma$ for different values of γ	105
5.7	Average number of (a) non-common and (b) common neighbors of the pairs of nodes, such that the link between the nodes have $\text{PRR} > \gamma$, for different values of γ and τ	106
5.8	Scatter plot of δ computed with (a) τ -connectivity and (b) τ -PRR vs. actual geographical distance d (\circ). Also shown is the least-squares linear regression line (a) $d = 0.48\delta + 10.05$ and (b) $d = 0.60\delta + 9.67$	109
5.9	MSE vs. model order.	110
5.10	MSE of network distance estimate vs. τ for different values of the PRR limit γ . In (a) τ -Connectivity weighing function is used while in (b) τ -PRR weighing function is used.	112

5.11	Normalized number of links in each PRR bin. The normalization is done such that the sum of the links in all the bins is one.	113
5.12	MSE vs. PRR limit γ	114
5.13	CDF plots of the squared errors for network distance estimators (τ -connectivity and τ -PRR), Neighbor connectivity (NC)-based distance estimator, constant per-hop (CPH) distance estimator and RSS-based distance estimator.	116
5.14	Scatter plot of δ computed with (a) τ -Connectivity and (b) τ -PRR vs. actual geographical distance d (\circ). Also shown is the least-squares linear regression line (a) $d = 0.72\delta + 14.90$ and (b) $d = 0.91\delta + 14.02$	119
5.15	MSE vs. model order for computing distance between nodes that are two hops away.	120
5.16	MSE of network distance estimates vs. τ for links that have PRR > 0.1	121
5.17	CDF plot of the squared errors for network distance estimators (τ -connectivity and τ -PRR) and direct-link measurement estimators (constant per-hop and RSS-based). The error is computed for distance estimation between nodes that are two hops separated.	122
5.18	MSE of the distance estimators for each ρ bin.	125
5.19	Figure showing the nodes in different clusters. Nodes in the same clusters are shown by the same marker type. Also shown are the reference nodes for each clusters, with black solid lines on the boundary of each marker type.	128
5.20	MSE of the location estimates using transformed dissimilarity as a function of τ . In (a), method a is used to determine the distance estimates $s_{a,b}$ in Isomap and in (b), method b is used to determine the distance estimates $s_{a,b}$ in Isomap	130
5.21	MSE of the location estimates using transformed dissimilarity with Method b on node pairs with neighbor ratio $\rho > 0.1$ as a function of τ	132

LIST OF TABLES

3.1 Summary of two measurement campaigns	43
3.2 Link geometry and correlation coefficients (observed, proposed model) .	45
4.1 Table showing an example RSS values (in dBm) measured by APs. . . .	62
4.2 Log-normal path-loss parameter description and values used in the running example framework.	62
4.3 Table summarizing the similarities and dissimilarities of LANDMARC (LM), Gaussian kernel (GK), radial basis function (RBF) and linear signal-distance map (SDM) localization algorithms.	75
4.4 Parameter description and values used in the simulation of network. The values are assumed to be <i>a priori</i> unknown to the localization algorithm.	78
4.5 Table showing the overall (O.A.) and sweet spot (S.S.) performance of different localization algorithms for the real-world measurement data. .	88
5.1 Table showing the MSE of the distance estimates between nodes that are one hop separated for different algorithms.	117
5.2 Table showing the MSE of the distance estimates between nodes that are two hops separated for different algorithms.	123
5.3 Table showing the MSE of the distance estimates between nodes that are separated by two hops for two possible network distance estimates.	123
5.4 Table showing the MSE of the different distance estimators for the links that have $\rho_{a,b} > 0.1$	126
5.5 Table showing the MSE of the location estimates for different distance estimators.	131
5.6 Table showing the MSE of the location estimates for different distance estimators using neighbor ratio as a parameter to determine the links. .	133

ACKNOWLEDGEMENTS

I would first like to acknowledge and thank my advisor and mentor Neal Patwari. Neal has been an absolutely great advisor and this dissertation would not have been possible without his constant guidance and motivation. He has been my role model and guide since the day I joined the SPAN lab. His support in performing measurements, his patience during delays for getting results, his humility in explaining difficult concepts are virtues that make him an excellent advisor, guide and role model. Working with him on this research has been a memorable experience for me, which I would cherish for the rest of my life. I feel extremely fortunate and blessed to have him as my advisor.

I am grateful to have found friends in my colleagues within SPAN lab: Jessica, Dustin, Yang, Joey and Merrick. Their unique skills and personalities have helped me during my research.

I want to express my love and regards to my family and friends. My parents, especially my mother, have been a tremendous support over time and gave me confidence that I can to accomplish my educational goal. I cannot thank you enough for your constant support and love during my studies.

CHAPTER 1

INTRODUCTION

Recent technological advances have enabled low-cost, inexpensive sensor devices to be deployed and interact with the physical environment, operating together in a wireless network. The advent of wireless sensor networks has enabled many location-based and remote sensing applications which include asset tracking [2, 3, 4, 5]; structural and seismic monitoring for timely response in the case of hazards [6, 7]; and security applications like radio tomographic imaging [8], among others.

In most wireless sensor networks applications, knowing the location of the sensor device is crucial. Without the knowledge of the location of a sensing device, the data sensed or measured by that device cannot be interpreted. When the sensor data are reported, it is essential to know where in space that data were measured to determine a meaningful information about the underlying physical world. In many scenarios, location information is itself the data that need to be “sensed.” For instance, in asset tracking and work flow applications, determining the location of devices is the main goal. In addition, sensor location information is the driving need for many geographical routing algorithms. The process of determining or estimating the location of a device, whose position is unknown *a priori*, is called *localization*. As such, a reliable and automatic localization scheme is a critical component of the wireless sensor networks [9, 6].

These applications can be made viable by deploying a vast number of sensors, for which the device cost has to be low, sensors would need to last for a long time without the need for constant replacement and the network should be configured automatically or with very less human moderation. Traditional localization techniques like GPS or radar are not suitable for these requirements. Including GPS on every device increases the overall system cost, and also the system energy requirements. In addition, GPS

is restricted to work in outdoor environments.

This dissertation, instead, considers the problem in which some small number of sensors, also called reference nodes, are deployed at known locations and the unknown location devices must determine their own location using pairwise measurements. In general, these measurements could be any physical reading that indicates distance or relative position, such as time-of-arrival (TOA), angle-of-arrival (AOA) and received signal strength (RSS). There has been considerable research in developing localization algorithms using different measurement types and the author refers to studies in [10, 11, 12, 6, 13] and the references within. Perhaps the most attractive candidate for localization is the RSS-based approach, which also forms the focus of this dissertation. RSS is the average power of the received RF signal over a signal packet and the RSS measurements are readily available in almost every wireless device, such as laptops and smart phones, without the need for additional hardware.

Even though the RSS-based localization approaches are cost effective and viable in indoor environment, the RSS measurements suffer from errors because of multipath fading, losses due to the presence of walls and obstacles in the path and non-isotropic antenna gain patterns. These errors cause unpredictability in the measured RSS, which affects the performance of the RSS-based localization algorithms. Efficient modeling and understanding of the statistics of these errors is of primary importance in any RSS-based localization algorithms.

This dissertation is an exploration of efficient models and algorithms to improve the performance of sensor localization. Motivated by the study of these models, we investigate and experimentally evaluate existing algorithms for wireless sensor network localization. In addition, we propose and develop a new algorithm for range estimation in wireless sensor network, which can improve localization performance.

1.1 Summary of Contributions

The research work presented in this dissertation have resulted in the following publications:

- Piyush Agrawal and Neal Patwari, “Kernel methods for RSS-based indoor

localization,” *Handbook of Position Location: Theory, Practice and Advances*, Eds. M. Buehrer and S. Zekavat, pp. 457 – 486, John Wiley and Sons, Inc., 2011.

- Piyush Agrawal and Neal Patwari, “Network distance: Distance estimation via measurements with neighbors,” *IEEE Transactions on Mobile Computing*, 2011 (to be submitted).
- Piyush Agrawal and Neal Patwari, “Correlated link shadow fading in multi-hop wireless networks,” *IEEE Transactions on Wireless Communications*, vol. 8, no. 8, 2009.
- Neal Patwari and Piyush Agrawal, “Effects of correlated shadowing: Connectivity, localization, and RF tomography,” In *Proceedings of the 7th International Conference on Information Processing in Sensor Networks (IPSN '08)*.
- Neal Patwari and Piyush Agrawal, “Nesh: A joint shadowing model for links in a multi-hop network,” In *IEEE International Conference on Acoustics, Speech and Signal Processing (ICASSP '08)*, 2008.
- Piyush Agrawal and Neal Patwari, “Correlated link shadow fading in multi-hop wireless networks,” Tech Report arXiv:0804.2708v2, 18 Apr 2008.
- Neal Patwari and Piyush Agrawal, “Calibration and measurement of signal strength for sensor localization,” *Localization Algorithms and Strategies for Wireless Sensor Networks*, Eds. Guoqiang Mao and Baris Fidan, IGI Global, Information Science Reference, page 122, May 2009.

In this dissertation I have made several contributions to channel modeling for multi-hop networks and RSS-based localization. Specifically, I have:

- Proposed, analyzed and validated a joint path loss model for multihop wireless networks, called network shadowing (NeSh) model [14]. This model provides an extension to existing channel models by modeling second-order statistics of the measured RSS on links.

- Motivated the importance of considering correlation in the shadowing loss between link pairs in applications such as localization and the design of reliable multi-hop networks. [14, 15].
- Investigated advantages of kernel methods in RSS-based localization [16]. Kernel methods are explicitly used to learn correlations in RSS measurements from training data.
- Proposed a novel algorithm for estimating distance between two radios using indirect link measurements and demonstrated using an extensive measurement campaign, that the estimator using indirect link measurements alone is better than estimator that uses direct link measurements alone.

In the rest of this introduction, I briefly motivate the need for better models for the RSS in multi-hop wireless networks. I, then, motivate the study of kernel methods in the RSS-based localization algorithms and provide an outline of the proposed range estimator. I end this introduction with the structure of the dissertation.

1.2 Models for the Received Signal Strength (RSS)

Typically, self-configuring wireless sensor networks are multi-hop networks wherein every sensor must not only capture and communicate its data, but also act as a relay for other sensors in the network. Current statistical channel models used for multi-hop networks consider RSS measurements on the links to be independent. This is a simplifying assumption, since shadow fading is determined by environmental obstructions, and geographically proximate links pass through similar obstructions. It can be hypothesized that links that pass through nearby parts of the environment will have correlation in their shadowing losses. In this section, we introduce current models for the measured RSS that are used in the current literature. We start with the introduction of the radio channel modeling for a single radio link.

1.2.1 Single Link Channel Model

Radio propagation measurement and modeling for a single radio link have been reported extensively over the past century [17, 18, 19, 20]. In general, when there

is no site-specific knowledge of the environment, the ensemble mean received power, $\bar{P}(d)$ (dBm), at a distance d from the transmitter, is [18, 19],

$$\bar{P}(d) = P_T - \Pi_0 - 10n_p \log_{10} \frac{d}{\Delta_0}, \quad (1.1)$$

where P_T is the transmitted power in dBm, n_p is the path-loss exponent, and Π_0 is the loss experienced at a short reference distance Δ_0 from the transmitter antenna. This model incorporates the free space path loss model when $n_p = 2$, and extends to practical (obstructed) multipath environments when $n_p > 2$.

On a particular link, received power will vary from the ensemble mean because of *fading*. The measured received power for the link between transmitter i and receiver j can be written as,

$$P_{i,j} = \bar{P}(d_{i,j}) - X_{i,j} - Y_{i,j}, \quad (1.2)$$

where, $d_{i,j}$ is the distance between nodes i and j , and $X_{i,j}$ is the dB shadowing loss and $Y_{i,j}$ is the dB non-shadowing loss and error. We refer to the total fading loss $Z_{i,j} = X_{i,j} + Y_{i,j}$. In general, shadow fading, narrowband or frequency-selective fading, and antenna and device losses all contribute to $Z_{i,j}$.

1.2.2 Extension to Multi-Hop Networks

Current channel models used for multi-hop wireless networks consider two types of fading models:

1. The circular coverage: $Z_{i,j} = 0$ for all the links and thus, the coverage is a perfect circle, as shown in Fig. 1.1(a).
2. The i.i.d. log-normal shadowing model: For all links the random variables $Z_{i,j}$ (in dB) are independently and identically distributed Gaussian distributed with zero mean and variance σ_z^2 . An example of the i.i.d coverage area is shown in Fig. 1.1(b).

We note that the two models are at opposite extremes, and both problematic. Note that “realistic coverage” is commonly depicted pictorially as a coverage area with random range as a function of angle [21, 22], as in Fig. 1.2, and neither fading model

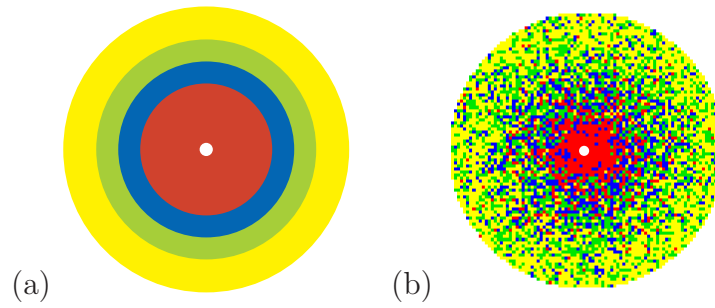
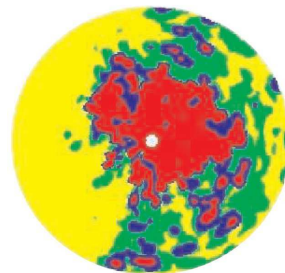


Figure 1.1. Graphical depiction of different fading models.

produces such a random shape. It is easy to recognize that the deterministic, circular coverage areas are unrealistic for wireless communications links. However, circular coverage has been a common assumption in ad hoc and sensor network research and has been used to generate foundational research results. It has been shown that the majority of papers which require radio propagation models in their simulation use the circular coverage model [23].

In comparison, the i.i.d shadowing model eliminates the concept of coverage area. Since the model has no spatial memory, even two nearly overlapping links would be represented as statistically independent. In reality, if an obstacle in one direction from a transmitter strongly attenuates its signal, any receiver behind the obstacle is likely to experience high fading loss. For example, if the environment in Fig. 1.3 causes severe shadowing, it is likely to cause additional path loss on both links a and b . In contrast, the i.i.d. log-normal shadowing model assumes that the shadowing across



Measured
Signal Level

Figure 1.2. A plot of the actual measured signal level, from [1] (used with permission from Sage publications).

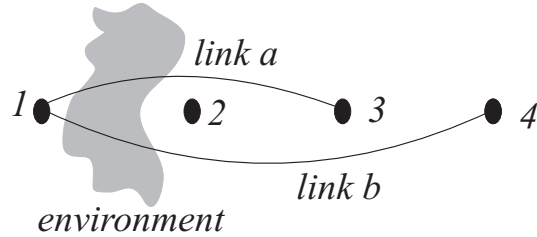


Figure 1.3. Example of factor in shadowing loss correlation. Because link a and link b cross the same environment, their shadowing losses tend to be correlated.

links a and b will be independent, which causes disconnect with the RSS measured in the real-world deployment.

1.3 Motivation for the Study of Kernel-based Localization Algorithms

Recent results in [15] have demonstrated that shadowing link correlation can be useful in improving the localization performance. In general, based on the results in [15], we argue that RSS-based localization algorithms should make use of the measurements made by the nodes with their in-range nodes in order to reduce the variance of the location estimation.

A large class of localization algorithms have applied statistical learning techniques to explicitly learn the correlation in the RSS measurements from training data, and then, use these correlations to classify or estimate the sensor’s location [24, 25, 26, 27]. Motivated by the results in [15] and the plethora of algorithms present in the localization literature, we study a special class of algorithms that uses *kernel methods* as a tool for learning correlation between the RSS measurements.

Kernel methods encapsulate the complicated relationship between the RSS and position, along with the correlation in the RSS measurements at proximate locations, in a kernel. The kernel can be assumed as a parametric “black box” that takes the measured RSS as inputs and gives a measure of position as output. Kernel methods are attractive because kernel models are typically linear with respect to the parameters, allowing good analytical properties, yet are nonlinear with respect to the RSS measurements. I provide an in-depth analysis of kernel methods in RSS-based

localization algorithms in [16].

1.4 Range Estimation in Wireless Sensor Networks

In addition to sensor localization, a large number of other applications of wireless sensor networks depend on the ability to estimate distance between pairs of radio devices. For instance, many communication and routing protocols use the knowledge of the distance to neighboring devices for routing of data packets [28, 29, 30]. In range-based localization, algorithms determine the location of the unknown location devices using the distance to a selected number anchor nodes [31, 32, 33].

When estimating the distance between two sensor nodes, a and b , most systems use a *direct link measurement* between a and b , for example, the received signal strength (RSS) between a and b [6, 34, 35, 36], or just whether a and b communicate [31, 33, 32, 37, 38]. Motivated by the fact that correlation in link RSS measurements can help in better localization performance, in this dissertation, we explore the capability to estimate range between two nodes a and b from indirect link measurements, that is, the measurement between a and k , for $k \neq a$ and b and k , for $k \neq b$.

The proposed range estimator is also motivated by the fact that two nodes that are near to each other will have similar connectivity measurements to other nodes in the network. These connectivity measurements with the other nodes in the network are embedded as a vector of high dimensional space. Such an embedding is commonly called *Lipschitz embedding* [39, 40, 41]. Using Lipschitz embedding, information about the relative distance of two nodes can be captured by the “dissimilarity” measure in the Lipschitz embedding space.

1.5 Outline

The structure of the dissertation is as follows. Chapter 2 presents an overview of the related work in wireless sensor localization. We briefly present some key research contributions in the field of sensor localization from various studies conducted in the literature.

In Chapter 3 we present a non-site specific statistical joint path loss model between a set of static nodes. Current statistical channel models used for multi-hop net-

works consider link path losses to be independent. This is a simplifying assumption, since shadow fading is determined by environmental obstructions, and geographically proximate links pass through similar obstructions. We hypothesize that links which pass through nearby parts of the environment have correlated shadowing losses. We conduct extensive measurements to verify this hypothesis and present a model which determines the second order statistics of the link path losses.

Chapter 4 is an exploration of kernel-based algorithms which attempt to determine the link correlation using a kernel. Kernel-based algorithms encapsulate the complicated relationship between RSS and position, along with correlation in the RSS at proximate locations, in a kernel, which can be assumed as a parametrized “black box” that takes the measured RSS as inputs and gives a measure of position as output. In this chapter, we describe four different kernel-based RSS localization algorithms using a common mathematical framework and compare and contrast their performance (to each other, and to a baseline model-based algorithm, the maximum likelihood estimator) using a simulation example and using an extensive experimental study. These algorithms include LANDMARC [42], Gaussian kernel localization [43], radial basis function localization [44], and linear signal-distance map localization [45].

Chapter 5 proposes a new algorithm to estimate the range between two radios using the indirect link measurements. When estimating the distance between two nodes a and b , current ranging algorithms use the direct link measurements between a and b . This chapter explores the capability to estimate the range between the two nodes a and b using only the indirect link measurements, that is, the connectivity measurements made with the in-range devices of a and the measurements with the corresponding in-range devices of b .

Chapter 6 forms the conclusion and presents avenues for future research.

CHAPTER 2

RELATED RESEARCH

Development of efficient RSS models and localization algorithms for wireless sensor networks is a broad and active area of research that spans the areas of signal processing, wireless channel modeling and algorithm design. In this chapter, we place our work in the context of the large body of literature, outlining key concepts and pointing out important previous studies. We first explore the work that has been done in modeling shadowing correlation.

2.1 Correlation in Shadowing

Shadow fading correlations have been measured and shown to be significant in other wireless networks. For example:

1. In digital broadcasting, links between multiple broadcast antennas to a single receiver have correlated shadowing which affects the coverage area and interference characteristics [46].
2. In indoor WLANs correlated shadowing is significant (with correlation coefficients as high as 0.95), and strongly impacts system performance [47].
3. In cellular radio, correlation on links between a mobile station (MS) and multiple base stations (BSs) significantly affects mobile hand-off probabilities and co-channel interference ratios [48, 49, 50].
4. In multi-antenna systems, fading on the link pairs between the antennas is found to be correlated and shown to limit diversity gain of the system [51, 52, 53].

5. In sensor networks, packet reception on different links is found to be correlated [54] which affects many data dissemination and opportunistic routing protocols [55].
6. In spectrum sensing, simulation results have shown that the performance of collaborative methods to “sense” the channel is significantly hampered by correlation in shadow fading [56, 57, 58, 59, 60].

An early study on the significance of spatial correlations between two links in a multi-hop network was done in [61]. In their work, RSS measurements in a single network of 44 sensors were used to quantify fading correlations between two links with a common node. Those results could not be complete because a single measured network does not provide information about an ensemble of network deployments. The study in this dissertation uses the data from two campaigns each consisting of multiple measured networks to examine many pairs of links with the identical geometry, both with and without a common node.

In cellular radio, the model of Gudmundson [62] is used to predict shadowing correlation for the link between a mobile station MS to a BS over time as the MS moves. However, this model cannot be directly applied to model the correlations among links in multi-hop networks. Wang, Tameh, and Nix [63] extended Gudmundson’s model to the case of simultaneous mobility of both ends of the link, for use in MANETs, and relate a sun-of-sinusoids method to generate realizations of the shadowing process in simulation. Both works use “correlated shadowing” to refer to the correlation of path loss in a *single link* over time, while the present work studies the correlation of *many disparate links* at a single time.

Since we presented the NeSh model in [14],[64], based on our model, a new ellipse overlap (EO) method is proposed in [65]. In the EO method, the shadowing region of a link is modeled as an ellipse. The correlation coefficient between two links is given by the intersection area of the ellipses around the links. The intersection space between the ellipses is divided into rectangles of a predetermined width. Then the area of intersection is approximately given by the sum of the area of these rectangles.

The authors of [65] claim that the computation cost of EO method is low compared to that of the NeSh model and the model agreement with the measurement, in general, improves. However, their model needs three parameters to be estimated, in contrast to two in the NeSh model.

Finally, we note that the performance of other RSS-based applications in wireless networks depend on the accurate modeling of shadowing correlation. Some of these applications are as follows:

- Collaborative spectrum sensing in cognitive radio networks using channel gain (CG) maps. Recent work by Kim *et al.* extends the NeSh model to model the temporal variations in the shadow fading [66, 67, 68].
- Evaluation of power control mechanisms in cognitive radio networks. The NeSh model is used for generating “realistic” spatial shadowing on links in various simulation-based studies of cognitive radio networks and also in the evaluation of different power control schemes in cognitive radio networks [69, 70].
- Cooperative localization in sensor and ad hoc networks uses signal strength to estimate node locations. The error performance of such estimators is dependent on the statistical model for path losses in the network. All previous analytical studies of location estimation bounds assume independence of links [71, 72, 73, 6, 74], but new work shows that bounds change when correlated shadowing is taken into account [15].
- Since multiple links will measure the shadowing caused by an attenuating object, the location of an attenuating object can be estimated. It was shown in [15] that tomographic imaging can be used to estimate and track the location of a moving RF attenuator such as a person. Accurate RF tomographic imaging requires a non-site-specific statistical model which relates the attenuation field to the shadowing losses measured on links.

2.2 RSS-based Localization Algorithms

Localization using RSS has been an active area of research for the past two decades. In this section, we provide a brief overview of some key research contributions to this area. Existing RSS-based localization approaches can be classified into two main categories:

1. RSS fingerprinting algorithms
2. Model-based algorithms

Kernel-based algorithms, which we investigate and experimentally evaluate in this dissertation, are the “middle ground” between model-based and RSS fingerprinting algorithms.

2.2.1 Model-based Algorithms

Model-based algorithms work by first estimating the relative distance between pairs of nodes and then estimating positions [75, 76, 77]. Model-based algorithms can be further classified into three categories: (a.) range-based algorithms, (b.) range-ratio algorithms, and (c.) range-free algorithms.

2.2.1.1 Range-based Algorithms

Range-based algorithms use standard statistical channel models to provide a functional relationship between distance and measured RSS (see an extended discussion about range estimation in Section 2.3). Using this functional relationship, the location of an unknown location node is estimated from the RSS measured by the in-range reference devices by first estimating the distance to the reference devices, and then using methods of lateration [76, 36, 77], multilateration [32, 78] or statistical inference [73] to determine the coordinates.

Some of the earliest range-based algorithms were proposed in [24, 79]. In these systems the relationship between measured RSS and distance is modeled by the log-distance path loss model [19, 80]. There are also approaches that fit into this category, which use sophisticated site specific ray-tracing models based on detailed floor maps [75].

2.2.1.2 Range-ratio Algorithms

In addition to the model parameters, measured RSS is a function of the transmit power of the device. Transmit power may vary from device to device because of manufacturing variations and may change as batteries on the sensor deplete. One could consider the transmit power of the device as an unknown parameter and can jointly estimate the transmit power, the model parameters and the position.

Alternatively, range-ratio algorithms can be used. Under this class of algorithms, instead of using the measured RSS, differences between the RSS measured at pairs of reference nodes for a single transmitting target (unknown location node) are considered [81, 82].

2.2.1.3 Range-free Algorithms

In contrast to range-based methods, range-free algorithms have also been proposed in the literature which use only the *connectivity* graph among the nodes to determine the location. By connectivity we mean a binary value indicating whether or not two devices can communicate. Some early work in this class of algorithms are DV-hop [31], N-hop multilateration by Savvides *et al.* [32], and MDS-MAP, also known as Isomap [38]. The principle of approaches in this class of algorithms is that the relative positions of the neighboring nodes in the network are found according to the proximity constraints. As a descriptive example, when two devices are not connected, their connectivity measurement can be seen to indicate to an algorithm to “push” each other to be outside the radio range. On the other hand, when the two devices are connected, their connectivity measurement can be seen to indicate to “pull” each other to be within the radio range, but this effort may be restricted by other devices in the network which do the same to them.

2.2.2 RSS Fingerprinting Algorithms

In contrast to the model-based approaches, RSS fingerprinting [24, 83] methods work in two phases - an offline training phase and an online estimation phase. In the offline training phase, RF signatures are collected at some known locations in the deployment region, which are then stored in a database. An RF signature is a

vector of RSS values measured by some predetermined known location devices. In the online estimation phase, an algorithm searches in the constructed database to find a location whose RF signature matches closely with the RF signature of the unknown location device.

Some research [35, 84, 85] also proposes using statistical models to create an entire radio map as a function of position, in which the location of the unknown location device is estimated directly from the RSS measured by the in-range reference devices. One key disadvantage of these methods is the large computation requirements in determining the estimates of the location. In addition, the model parameters need to be known *a priori*. Alternatively, the model parameters can be included as additional variables that are required to be estimated, in addition to the device’s location. This, however, increases the computational cost because in most cases a closed form solution is not available and one has to resort to numerical techniques. Recently, the EZ localization algorithm [86] was proposed which uses genetic search algorithm to reduce the “search space” for the solution.

The advantage of RSS fingerprinting is that the localization performance is, in general, better than the model-based algorithms. In fact, in a deployment area of 12600 m² with calibration data collected at every 3 m, the median error for a model-based algorithm is about 7 m, while that of RSS fingerprinting algorithm is 4 m, an improvement of 43% [86]. However, the downside is that intensive training and calibration are needed.

2.2.3 Discussion

Statistical channel models, in most cases, are unable to capture the complicated relationship between RSS and location in indoor environments. They also typically assume that shadow fading on links are mutually independent, even though environmental obstructions cause correlated shadowing as discussed in Section 2.1.

RSS fingerprinting methods, on the other hand, do not assume any prior relationship between RSS and position, but the training phase consumes a significant amount of time and effort [24, 44]. To some extent, the training effort can be reduced

via spatial smoothing [44, 87, 34], but this is possible only to distances at which the RSS is correlated. Some research has also suggested supplementing some of the measurements using predicted RSS using channel models [24]. Changes in the environment over time reduces the accuracy of the database, requiring recalibration.

In summary, model-based algorithms require the least training effort, but they rely heavily on the prior knowledge of the relationship between RSS and position. RSS fingerprinting algorithms, on the other hand, are not based on any prior knowledge of the relationship between RSS and position, but require considerable training effort and time.

In this dissertation we explore and experimentally evaluate kernel-based algorithms, which provide the ability to mix the features of both model-based and RSS fingerprinting algorithms. Kernel-based algorithms encapsulate the complicated relationship between RSS and position, along with correlation in the RSS at proximate locations, in a *kernel*, which can be assumed as a parametrized “black box” that takes the measured RSS as inputs and gives a *measure* of position as output. In this dissertation in Chapter 4, we study four different kernel-based RSS localization algorithms in a common mathematical framework and using extensive measurements compare and contrast their performance. These algorithms include LANDMARC [42], Gaussian kernel localization [43], radial basis function localization [44], and linear signal-distance map localization [45].

2.3 Range Estimation in Wireless Sensor Networks

A number of techniques for range estimation have been proposed in the literature. When determining the distance between two devices a and b , most range estimation algorithms use the direct link measurements between a and b , for example, the RSS between a and b [6, 34, 35, 36], or just whether a and b communicate [31, 33, 32, 37, 38].

Range estimation algorithms based on direct link RSS measurements use statistical channel models which relate measured RSS and distance. The most commonly used channel model is the log-distance path loss model, which expresses the ensemble mean of the RSS in dB as linear with the log of distance [19, 80, 14]. Suppose that

we want to estimate the distance between two devices a and b . Device a measures the RSS for the signal transmitted by b (similarly b measures the RSS for the signal transmitted by a), which we call the direct link RSS measurement. A standard estimator of distance is the maximum likelihood estimator (MLE) which determines what distance \hat{d}_{MLE} is “most likely” given the direct link RSS measurement between a and b and the log-distance path loss model [6, 88, 73].

In indoor or cluttered environment, however, RSS measurements deviate from the model because they suffer from multipath fading, shadowing, and non-isotropic antenna gain patterns, all of which cannot be known *a priori* [14, 15, 89]. Consequently, systems relying exclusively on the direct link RSS measurements for distance estimation remain inaccurate estimators.

In contrast, algorithms based on direct link connectivity measurements use the hop counts to determine the range between each pair of nodes [31, 90]. The hop counts are then converted into physical distances by multiplying the hop counts with the average distance per hop. In [31], the average distance per hop is computed by the anchors. Every anchor in the network obtains hop count information to all the other anchors in the network. The average distance per hop is then computed by every anchor as the ratio of the average distance to the other anchors in the network and average hop counts to them. The *Amorphous Positioning* algorithm, proposed in [90], employs the similar approach and determines the hop counts between two nodes. However, it uses a different, centralized approach to determine the average distance per hop. The Amorphous Positioning algorithm assumes that the density of the network is known *a priori* and uses the Kleinrock and Sliverster formula [91] to determine the average distance per hop.

A major advantage of using connectivity measurements for estimating the range is the inherent simplicity of the algorithm using them. On the other hand, the drawback is that algorithms using connectivity measurements only work for isotropic networks, *i.e.*, when the properties of the graph are the same in all directions, so that the average distance per hop can reasonably be used to estimate the distances between hops.

In this dissertation, we propose and evaluate a method to estimate range between two nodes a and b from measurements on *indirect links*, which are the measurements made by the nodes a and b with their neighbors, but not the direct link measurements between a and b . Specifically, indirect link measurements correspond to the measurements made by the node a with a node k , for $k \neq b$, and between b and k , for $k \neq a$.

Another possible way to obtain distance between the nodes is to first localize the nodes, and subsequently, calculate the distance between the estimated coordinates. To this end, the localization approaches presented in the previous section can be applied. The method we present in Chapter 5 of this dissertation does not require localization as an intermediate step and calibration is also minimal.

CHAPTER 3

CORRELATED LINK SHADOW FADING IN MULTI-HOP WIRELESS NETWORKS

3.1 Abstract

Accurate representation of the physical layer is required for analysis and simulation of multi-hop networking in sensor, ad hoc, and mesh networks. Radio links that are geographically proximate often experience similar environmental shadowing effects and thus have correlated shadowing. This paper presents and analyzes a non-site-specific statistical propagation model which accounts for the correlations that exist in shadow fading between links in multi-hop networks. We describe two measurement campaigns to measure a large number of multi-hop networks in an ensemble of environments. The measurements show statistically significant correlations among shadowing experienced on different links in the network, with correlation coefficients up to 0.33. Finally, we analyze multi-hop paths in three and four node networks using both correlated and independent shadowing models and show that independent shadowing models can underestimate the probability of route failure by a factor of two or greater.

3.2 Introduction

Both simulation and analysis are critical to the development of multi-hop networks, including mesh, ad hoc, and sensor networks.¹ However, current physical layer models do not accurately represent radio channels in multi-hop wireless networks

¹This chapter first appeared in Piyush Agrawal and Neal Patwari, “Correlated Link Shadow Fading in Multi-Hop Wireless Networks,” *IEEE Transactions on Wireless Communications*, vol. 8, no. 8, 2009, and is reprinted with permission. © 2009 IEEE.

[92, 1]. As a result, there is a significant disconnect between simulation and analysis, and real world deployment. There is a significant interest in improving statistical models beyond the current state-of-the-art, in order to decrease the difference between simulation and analysis results and experimental deployment results.

Path losses between pairs of nodes are critical in any simulation or analysis of a multi-hop network. Path losses determine the connectivity and performance of multi-hop wireless networks. Path loss between an interferer and receiver determines the received interference power, which determines whether communication can exist during transmission of interference. In power control schemes, path losses between pairs of nodes determine the energy consumption required for communication between the nodes. In received signal strength (RSS) based localization, path losses determine the errors in range and position estimates of nodes.

This paper presents a non-site-specific statistical joint path loss model between a set of static nodes. Current statistical channel models used for multi-hop networks consider link path losses to be independent. This is a simplifying assumption, since shadow fading is determined by environmental obstructions, and geographically proximate links pass through similar obstructions. We hypothesize that links which pass through nearby parts of the environment have correlated shadowing losses. In this paper, we conduct extensive measurements to verify this hypothesis.

Non-site-specific path loss models are critical for multi-hop network analysis and simulation. Site-specific models use building floor plans or maps of the particular deployment area to predict path losses in the network, and have been critical for deployment planning for cellular systems and large WLAN deployments [93, 94]. However, site-specific models are not valuable for determining the statistical performance of a wireless network across the ensemble of possible deployments. Non-site-specific path loss models, often referred to simply as statistical path loss models, help system designers understand how network performance improves or degrades based on design decisions, in general environments.

3.2.1 Single-Link Path Loss Model

Radio propagation measurement and modeling for a single radio link has been reported extensively over the past century [17, 18, 19, 20]. In general, when there is no site-specific knowledge of the environment, the ensemble mean received power, $\bar{P}(d)$ (dBm), at a distance d from the transmitter, is [18, 19],

$$\bar{P}(d) = P_T - \Pi_0 - 10n_p \log_{10} \frac{d}{\Delta_0}, \quad (3.1)$$

where P_T is the transmitted power in dBm, n_p is the path loss exponent, and Π_0 is the loss experienced at a short reference distance Δ_0 from the transmitter antenna. This model incorporates the free space path loss model when $n_p = 2$, and extends to practical (obstructed) multipath environments when $n_p > 2$.

On a particular link, received power will vary from the ensemble mean because of *fading*. The measured received power for the link between transmitter i and receiver j can be written as,

$$P_{i,j} = \bar{P}(d_{i,j}) - Z_{i,j}, \quad (3.2)$$

where, $d_{i,j}$ is the distance between nodes i and j , and $Z_{i,j}$ is the fading loss. In general, shadow fading, narrowband or frequency-selective fading, and antenna and device losses all contribute to $Z_{i,j}$. Much research in antennas and propagation, and in RFIC design, have developed models for losses due to narrowband fading, antenna and device losses. Two antennas spaced closer than a wavelength do experience correlated small-scale fading, and a large body of research has explored those correlations [95].

This paper models the correlations among shadow fading on the various links in a network. Shadow fading, also called medium-scale fading [18], describes the loss experienced as the signal passes through or diffracts around major obstructions in its path from the transmitter to the receiver. These obstructions include walls and furniture indoors, and buildings, terrain, and trees outdoors.

We hypothesize that shadowing losses on different links are correlated when those links are geographically proximate. Since shadowing is central to the analysis in this paper, we separate total fading loss $Z_{i,j}$ into two components,

$$Z_{i,j} = X_{i,j} + Y_{i,j}, \quad (3.3)$$

where $X_{i,j}$ represents the shadow fading loss, and $Y_{i,j}$ represents all other (non-shadowing) losses.

3.2.2 Application in Multi-Hop Networking Research

In the multi-hop networking simulation and analysis literature, two path loss models are used:

1. The circular coverage model: $Z_{i,j} = 0$ for all links, and thus the coverage area is a perfect circle, as shown in Figure 3.1(a).
2. The i.i.d. log-normal shadowing model: For all links (i,j) , random variables $Z_{i,j}$ (in dB) are independent and identically distributed Gaussian with zero mean and variance σ_Z^2 , as shown in Figure 3.1(c).

We argue that the two models are at opposite extremes, and both problematic. Note that ‘realistic coverage’ is commonly depicted pictorially as a coverage area with random range as a function of angle [21, 22], as in Figure 3.1(b), and neither fading model produces such a random shape. It is easy to recognize that the deterministic, circular coverage areas are unrealistic for wireless communications links. However, circular coverage has been a common assumption in ad hoc and sensor network research and has been used to generate foundational research results. It has been

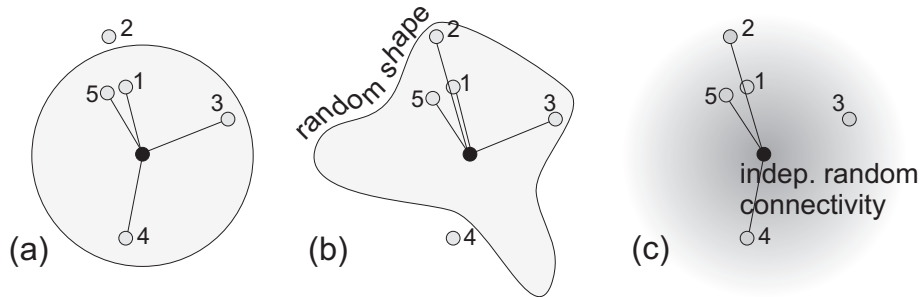


Figure 3.1. Graphical depiction of (a) circular coverage model, and (c) coverage in the i.i.d. log-normal shadowing model, compared to the common depiction of (b) in which coverage area is a random shape. In (a) and (b), nodes are connected if and only if they are within the gray area, while in (c), nodes are connected with probability proportional to the shade (darker is more probable).

shown that the majority of papers which require radio propagation models in their simulation use the circular coverage model [23].

In comparison, the i.i.d. shadowing model eliminates the concept of coverage area. Since the model has no spatial memory, even two nearly overlapping links would be represented as statistically independent. For example node 2 in Figure 3.1(c) may be connected while node 1 is not.

Recent research, including Hekmat and Van Mieghem [22] and Bettstetter and Hartmann [21], has studied connectivity in ad hoc networks using the i.i.d. log-normal shadowing model. Their analyses indicate that for a constant level of connectivity, node deployment density can be reduced when the variance of the shadowing is increased. This increase in connectivity is largely a result of the model's independence assumption. Since losses in links in the same direction from a transmitter are independent, if one link is disconnected because of high loss, another node in the same direction is likely to be connected.

In reality, if an obstacle in one direction from a transmitter strongly attenuates its signal, any receiver behind the obstacle is likely to experience high fading loss. For example, if the environment in Figure 3.2 causes severe shadowing, it is likely to cause additional path loss on both links a and b . In contrast, the i.i.d. log-normal shadowing model assumes that the shadowing across links a and b will be independent and thus exaggerate the connectivity. We quantify this argument in Section 3.7.

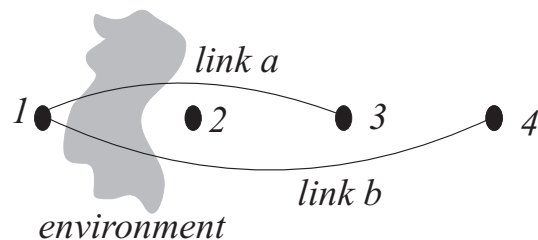


Figure 3.2. Example of factor in shadowing loss correlation. Because link a and link b cross the same environment, their shadowing losses tend to be correlated.

3.2.3 Correlation Limits Link Diversity

Diversity methods are common means to achieve reliability in unreliable channels. Multi-hop networking serves as a network-layer diversity scheme by allowing two nodes to be connected by any one of several multi-hop paths. All diversity schemes are limited by channel correlations. Correlations have been studied and shown to limit diversity gains in time, space, frequency and multipath diversity schemes [95, 18, 19].

Yet little research has addressed fading correlations among links in sensor, mesh, and ad hoc networks. This paper presents an investigation into quantifying the correlation in the shadow fading experienced on the different links of a multi-hop network, as well as a statistical joint path loss model which represents correlations in link shadowing. This investigation is based on extensive experimental measurements, using full link measurements of an ensemble of deployed networks to estimate and test for statistical correlations. Further, we quantify the effect that such correlation has on source-to-destination path statistics. We show for a simple three node network that the probability of path failure can be double or more what would be predicted by the i.i.d. log-normal shadowing model.

3.3 Related Research

Shadow fading correlations have been measured and shown to be significant in other wireless networks. For example:

1. In digital broadcasting, links between multiple broadcast antennas to a single receiver have correlated shadowing which affects the coverage area and interference characteristics [46].
2. In indoor WLANs correlated shadowing is significant (with correlation coefficients as high as 0.95), and strongly impacts system performance [47].
3. In cellular radio, correlation on links between a mobile station (MS) and multiple base stations (BSs) significantly affects mobile hand-off probabilities and co-channel interference ratios [48, 49, 50].

In cellular radio, the model of Gudmundson [62] is used to predict shadowing correlation for the link between a mobile station MS to a BS over time as the MS moves. In Section 3.4, we address the inability of this model to be directly applied to model the correlations among links in multi-hop networks. Wang, Tameh, and Nix [63] extended Gudmundson’s model to the case of simultaneous mobility of both ends of the link, for use in MANETs, and relate a sun-of-sinusoids method to generate realizations of the shadowing process in simulation. Both works use “correlated shadowing” to refer to the correlation of path loss in a *single link* over time, while the present work studies the correlation of *many disparate links* at a single time.

In [61], RSS measurements in a single network were used to quantify fading correlations between two links with a common node. Those results could not be complete because a single measured network does not provide information about an ensemble of network deployments. The present study uses the data from two campaigns each consisting of multiple measured networks to examine many pairs of links with the identical geometry, both with and without a common node.

Finally, we note that the performance of other RSS-based applications in wireless networks depends on accurate joint path loss models. Cooperative localization in sensor and ad hoc networks uses signal strength to estimate node coordinates. The error performance of such estimators is dependent on the statistical model for path losses in the network. All previous analytical studies of location estimation bounds assume independence of links [71, 73, 74, 72, 6], but new work shows that bounds change when correlated shadowing is taken into account [15]. Further, because multiple links will measure the shadowing caused by an attenuating object, the location of an attenuating object can be estimated. We have shown that tomographic imaging can be used to estimate and track the location of a moving RF attenuator such as a person [15]. Accurate RF tomographic imaging requires a non-site-specific statistical model which relates the attenuation field to the shadowing losses measured on links. This paper presents such a model, and more critically, provides experimental measurements which justify such a model.

3.4 Motivation

The present effort to model the shadowing correlation is motivated by the fact that no existing correlated link shadowing model is valid for arbitrary pairs of links in ad hoc networks. Yet shadowing correlation plays a very important role in determining the realistic performance of a network. To date, there have been two relevant statistical models for shadowing correlations:

1. The model of Gudmundson (1991), which predicts temporal shadowing correlations for the MS-BS path loss as the MS moves in a cellular network [62].
2. The model of Wang, Tameh and Nix (2006), an extension of Gudmundson's model, which predicts temporal shadowing correlations on a single link when there is mobility on both ends of the link [63].

In this section, we show that neither model can be applied to model shadowing correlation between arbitrary pairs of links in multi-hop networks.

Gudmundson's model has been widely applied to predict shadowing correlations in cellular networks where a mobile receiver (with a low antenna) communicates with a base station (with a high antenna). The model predicts the correlation in shadowing as the mobile receiver changes position with respect to the base station as shown in Fig. 3.3. For a mobile receiver going from position \mathbf{x}_i to \mathbf{x}_j , the shadowing correlation $R_X(\mathbf{x}_i, \mathbf{x}_j)$ is given as,

$$R_X(\mathbf{x}_i, \mathbf{x}_j) = \sigma_X^2 e^{-d_{ij}/D} \quad \text{where } d_{ij} = \|\mathbf{x}_i - \mathbf{x}_j\|, \quad (3.4)$$

and D is a distance constant, and σ_X^2 is the variance of shadow fading.

By design, the Gudmundson model does not apply to pairs of links that do not have a common end point. For example, consider a four node ad hoc network as shown in Fig. 3.4. The shadow fading on links c and f have no specified covariance in the model. In typical multi-hop networks with large numbers of nodes, such link pairs occur very commonly – most pairs of links do not share a common node.

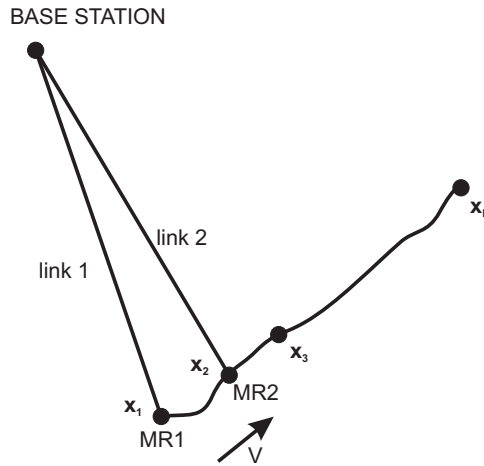


Figure 3.3. Example of the motion of mobile receiver and base station position in Gudmundson's model

3.4.1 Adaptation to Mobile-to-Mobile Link

Wang, Tameh, and Nix adapted the Gudmundson model to a more generalized setting of one link with two mobile nodes [63]. Let d_t and d_r be the distance moved the two mobile nodes between two time instants. According to [63], the correlation between the shadow fading between the two times is modified from (3.4) to be, $R_X(d_t, d_r) = \sigma_X^2 e^{-\frac{d_t + d_r}{D}}$.

However, the model is based on the assumption that the distances between the two nodes is large compared with d_t and d_r . The model cannot be directly applied to model the covariance of two arbitrary links. We might consider applying [63] to

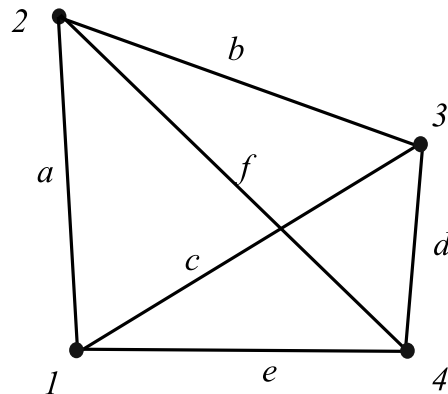


Figure 3.4. A simple four-node ad hoc network its six pairwise links.

two links if those two links share very nearby end points. For example, in Fig. 3.4, if $d_{23} \ll d_{12}$ and $d_{14} \ll d_{12}$, one might use [63] to model the correlation between the shadowing on links a and d .

In general, very few link pairs in ad hoc networks would meet the above criteria. For example, if d_{23} , d_{24} , d_{13} , d_{14} are of the same order of magnitude as d_{12} and d_{34} , then there is an ambiguity for which two distances should be used in the model of [63]. There seems to be no universally appropriate way to choose the two distances from the four available.

3.4.2 Adaptation to Multiple Links

In this section, we introduce what would be the direct application of the Gudmundson (1991) model to an arbitrary set of links in a multi-hop network and show that it does not provide a valid statistical joint path loss model. First, we define a direct, naïve application of (3.4) to a general multi-link network. For two links $a = (i, j)$ and $b = (k, l)$, the covariance between the shadowing on links a and b would be given by,

$$C(a, b) = \begin{cases} 0, & \text{if } i \neq k, i \neq l, j \neq k, \text{ and } j \neq l \\ \sigma_X^2 e^{-d_{ik}/D}, & \text{if } j = l \end{cases} \quad (3.5)$$

where d_{ik} is the distance between the non-common end points of the two links a and b .

Next, we prove by contradiction that such a model does *not* guarantee a positive semidefinite covariance matrix and thus is not a valid statistical model. Consider the four nodes and the six links between them depicted in Fig. 3.4. For simplicity, consider a subset of the links, the three links a , d , and e . The covariance matrix for the shadow fading experienced on these three links is given by (3.5) as,

$$C = \sigma_X^2 \begin{bmatrix} 1 & 0 & e^{-d_{24}/D} \\ 0 & 1 & e^{-d_{13}/D} \\ e^{-d_{24}/D} & e^{-d_{13}/D} & 1 \end{bmatrix} \quad (3.6)$$

The determinant of this covariance matrix is,

$$\text{Det}(C) = \sigma_X^2 (1 - e^{-2d_{13}/D} - e^{-2d_{24}/D}).$$

When d_{13} and d_{24} are low, $\text{Det}(C) < 0$. A negative determinant shows that C is not positive semidefinite and thus cannot be a valid covariance matrix. Thus the Gudmundson covariance model cannot be directly applied to arbitrary sets of links in a network.

3.4.3 Summary

In this section, we have explored application of the shadowing covariance models proposed in [62] and [63] to arbitrary sets of links in wireless networks. We have shown that neither can be applied directly to any general set of links. The Gudmundson model does not consider link pairs that do not have a common endpoint. The adaptation proposed in [63] when both the ends of a link are mobile cannot be applied directly to ad hoc networks as there would be an ambiguity in which two distances to use in the covariance function. We proved by counterexample that a naïve application of the Gudmundson model to model joint path losses in a multi-link network does not guarantee a valid covariance matrix. These arguments necessitate the development of new statistical path loss model which jointly models multiple links in a mesh, sensor, or ad hoc network.

3.5 Joint Path Loss Model

In this section, we propose a statistical joint path loss model for arbitrary sets of links in a wireless network. As described in Section 3.4, existing path loss models are not adequate to model correlations which exist in shadow fading between pairs of links in a network. We provide such a model in this section by connecting path losses in a network to a random shadowing environment of deployment. By connecting path losses to an environment, we preserve the physical relationships which exist between links in real-world deployments. By making the environment random, we preserve the non-site-specific nature of the model and allow it to be used in general-purpose simulation and analysis.

We start with the assumption that shadowing losses experienced on the links in a network are a result of an *underlying spatial loss field* $p(\mathbf{x})$. A spatial loss field quantifies the shadowing loss experienced by a link which passes through it –

shadowing on a link increases when its path crosses areas of high loss $p(\mathbf{x})$. First, we assume and justify a model for the spatial loss field. We then specify the functional relationship between the random spatial loss field $p(\mathbf{x})$ and path losses below in (3.9). Finally, we show how this model results in agreement with existing path loss models when considering a single link, and how it models correlated shadowing losses when considering multiple network links.

3.5.1 Spatial Loss Field

A statistical model for the spatial loss field $p(\mathbf{x})$ is required for the proposed joint path loss model. We first introduce such a field model and then justify our choices. We assume that the underlying spatial loss field $p(\mathbf{x})$ is an isotropic wide-sense stationary Gaussian random field with zero mean and exponentially-decaying spatial correlation. The covariance between $p(\cdot)$ at arbitrary positions \mathbf{x}_i and \mathbf{x}_j is given by,

$$\begin{aligned} E [p(\mathbf{x}_i)p(\mathbf{x}_j)] &= R_p(\mathbf{x}_i, \mathbf{x}_j) = R_p(\|\mathbf{x}_j - \mathbf{x}_i\|) \\ &= \frac{\sigma_X^2}{\delta} \exp\left(-\frac{\|\mathbf{x}_j - \mathbf{x}_i\|}{\delta}\right). \end{aligned} \quad (3.7)$$

where $\|\mathbf{x}_j - \mathbf{x}_i\|$ is the Euclidean distance between \mathbf{x}_i and \mathbf{x}_j , δ is a space constant and σ_X is the standard deviation of the shadow fading. One realization of the random field $p(\mathbf{x})$ is shown in Fig. 3.5.

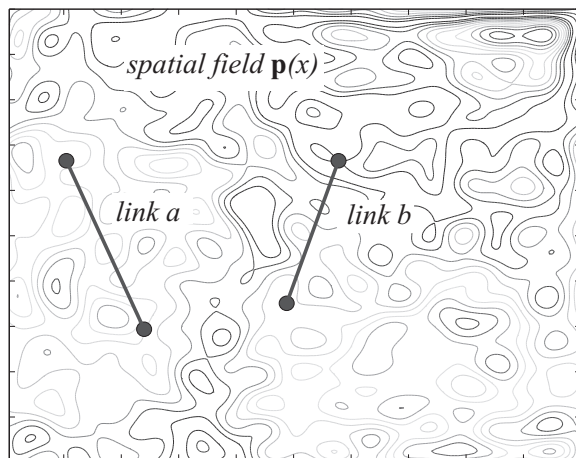


Figure 3.5. A link pair in an underlying spatial loss field $p(\mathbf{x})$.

The use of a zero-mean Gaussian random field is justified as follows.

1. A large-scale path loss equation such as (3.1) removes the mean shadowing loss when parameters Π_0 and n_p are estimated. Thus $Z_{i,j}$ is zero-mean.
2. Shadowing losses are often modeled as Gaussian when expressed in (dB). Our assumption of a Gaussian field results in this desired model property, as discussed below.

Two other assumptions about the statistical properties of $p(\mathbf{x})$ are justified below.

3.5.1.1 Isotropy

The assumption that the covariance between $p(\mathbf{x}_1)$ and $p(\mathbf{x}_2)$ is a function of $\|\mathbf{x}_2 - \mathbf{x}_1\|$ is valid when the field $p(\mathbf{x})$ is homogeneous and isotropic, which is suitable for many applications [96, 97]. A particular environment realization may have directional biases, but over an ensemble of environments, we would not expect anisotropy. We note that isotropic field models are the building blocks for more sophisticated non-isotropic and non-stationary fields which might be applied to future models for specific anisotropic environments.

3.5.1.2 Exponential Decaying Covariance

Many mathematically valid spatial covariance functions for isotropic fields are possible [98, 99]. We justify the use of the covariance function in (3.7) because of its basis in a Poisson spatial random process. Poisson processes are commonly used for modeling the distribution of randomly arranged points in space, and we suppose that attenuating obstructions can be modeled in such a fashion as well. Certainly, particular environments (*e.g.*, buildings in city blocks) have order which is not modeled in a Poisson point process, but a general statistical model should be neither specific to a particular type of environment nor overly complicated for analysis.

Analysis of Poisson point processes leads to an exponentially decaying covariance function. Assume that the attenuating field $p(\mathbf{x})$ is defined as the number of obstructions within a distance $R/2$ of point \mathbf{x} . When the obstructions are modeled as a 2-D

Poisson process, the covariance, $C(r)$, between two points separated by a distance r can be written as [99],

$$C(r) = \begin{cases} \sigma^2 [1 - \frac{2}{\pi} [S(r) + \sin^{-1}(\frac{r}{R})]] & r \leq R \\ 0 & r \geq R, \end{cases} \quad (3.8)$$

where $S(r) = \frac{r}{R} \sqrt{1 - \frac{r^2}{R^2}}$ and σ^2 is the variance of the attenuating field $p(\mathbf{x})$, when $r = 0$. The behavior of $C(r)$ in (3.8) is approximately equal to a function with exponential decay in r for low r [99]. We propose, for simplicity, to use an exponentially-decaying covariance function of (3.7) to describe the spatial loss field.

3.5.2 Shadowing Losses

We propose to model the shadowing on links $X_{m,n}$, for all pairs of nodes (m, n) , as a function of the spatial loss field $p(\mathbf{x})$. The correlation between shadowing losses on many links derives from the fact that all links' shadowing values are described as a function of the one spatial loss field. Specifically, each link's shadowing loss $X_{m,n}$ is a weighted integral of the spatial loss field,

$$X_{m,n} \triangleq \frac{1}{\|\mathbf{x}_n - \mathbf{x}_m\|^{1/2}} \int_{\mathbf{x}_m}^{\mathbf{x}_n} p(\mathbf{x}) d\mathbf{x}. \quad (3.9)$$

In short, (3.9) estimates the shadowing on an arbitrary link as a weighted line integral of the spatial loss field on which the link impinges. The units of $X_{m,n}$ are (dB); it is the shadowing loss caused by the link impinging on the spatial loss field $p(\mathbf{x})$.

A line integral along the path of the spatial loss field is an intuitive approximation for a path's loss, and has been used in many previous site-specific path loss models. In [100], the shadowing on an indoor-outdoor link at 5.85 GHz is modeled in a "partition-based model" as a sum of the losses caused by objects through which the straight line between the two nodes crosses. Site maps and floor plans are used to calculate the number of each kind of object for each link. The partition-based model reduces the standard deviation of model error to 2.6 dB, compared to a standard deviation of 8.0 dB using a purely distance-based path loss model. In [101], shadowing losses are also represented as a line integral for the purpose of extrapolating signal strength measurements beyond the points at which they have been measured. The model uses

a land use and terrain map to derive a piece-wise constant loss field (with units of dB attenuation per unit distance). The total path loss on a link is equal to the large scale path loss of (3.1) plus a line integral of the loss field. The difference in our proposed model is that the loss field is not a piece-wise constant function, and is statistical, rather than determined by a map.

The normalization in (3.9) is both necessary to explain physical behavior of links and intuitively acceptable. Consider an example of two different links: a short link of 5 m; and a long link of 500 m. When an attenuating object (*e.g.*, vehicle) drives into the line of the short link, it attenuates the signal. In relative terms, when the same vehicle drives into the line of the long link, it typically attenuates the signal less strongly. This is because the relative loss of diffracting or scattering over or around the vehicle is less, typically, for the long link. This is why the loss in a link cannot simply be a sum of all attenuation caused in the line-of-sight path – it must be a weighted integral that downweights loss for longer links. The reason the weight must be proportional to $d^{-1/2}$ is that this function of d makes the variance of shadowing constant vs. d , which is required for the model to have Property I, as described and proven below.

In summary, relevant site-specific models suggest that a line integral is an appropriate model for shadowing caused by major obstructions on a link. Weighting is suggested to agree with the intuition that individual attenuating objects are not as important for links with longer path lengths. Next, we prove that (3.9) agrees with known properties of shadowing loss on a single link, and then show that it leads to positive covariances between shadowing losses on multiple links.

3.5.2.1 Single-Link Properties

The proposed model agrees with two important empirically-observed link shadowing properties:

Prop-I The variance of dB shadowing on a link is approximately constant with the path length [18],[19],[80].

Prop-II Shadow fading losses (in dB) are Gaussian.

The model in (3.9) can be seen to have Prop-II, since $X_{m,n}$ is a scaled integral of a Gaussian field. The proposed model has Prop-I when $\|\mathbf{x}_j - \mathbf{x}_i\| \gg \delta$. We show this by considering $\text{Var}[X_a]$ for link $a = (i, j)$,

$$\text{Var}[X_a] = \frac{1}{\|\mathbf{x}_j - \mathbf{x}_i\|} \int_{\alpha=\mathbf{x}_i}^{\mathbf{x}_j} \int_{\beta=\mathbf{x}_i}^{\mathbf{x}_j} R_p(\|\beta - \alpha\|) d\alpha^T d\beta. \quad (3.10)$$

Using (3.7) as the model for spatial covariance, (3.10) is given by

$$\text{Var}[X_a] = \sigma_X^2 \left[1 + \frac{\delta}{\|\mathbf{x}_j - \mathbf{x}_i\|} e^{-\|\mathbf{x}_j - \mathbf{x}_i\|/\delta} - \frac{\delta}{\|\mathbf{x}_j - \mathbf{x}_i\|} \right], \quad (3.11)$$

and when $\|\mathbf{x}_j - \mathbf{x}_i\| \gg \delta$,

$$\text{Var}[X_a] \approx \sigma_X^2. \quad (3.12)$$

3.5.2.2 Joint Link Properties

Consider two links $a = (i, j)$ and $b = (k, l)$, as shown in Fig. 3.5, with shadowing X_a and X_b , respectively. The covariance of X_a and X_b is,

$$\text{Cov}(X_a, X_b) = \frac{\sigma_X^2}{\delta d_{i,j}^{1/2} d_{k,l}^{1/2}} \int_{C_{i,j}} \int_{C_{k,l}} e^{-\frac{\|\beta - \alpha\|}{\delta}} d\alpha^T d\beta. \quad (3.13)$$

where $d_{i,j} = \|\mathbf{x}_i - \mathbf{x}_j\|$ and, $C_{m,n}$ is the line between points \mathbf{x}_m and \mathbf{x}_n .

The solution to (3.13) is tedious to derive analytically. We use numerical integration to compute the value of ρ_{X_a, X_b} . Matlab calculation code for this purpose is available on the authors' website [102].

3.5.3 Total Fading Model

Since shadowing loss $X_{i,j}$ is only one part of the total fading loss $Z_{i,j} = X_{i,j} + Y_{i,j}$, we must also consider the model for non-shadowing losses $Y_{i,j}$. We note that shadow fading and non-shadow fading are caused by different physical phenomena, and thus $X_{i,j}$ and $Y_{i,j}$ can be considered as independent. The variance of total fading, $\text{Var}[Z_{i,j}]$, is thus,

$$\sigma_{dB}^2 \triangleq \text{Var}[Z_{i,j}] = \text{Var}[X_{i,j} + Y_{i,j}] = \text{Var}[X_{i,j}] + \text{Var}[Y_{i,j}]. \quad (3.14)$$

Non-shadow fading is predominantly composed of narrowband or small-scale fading, which can be well-approximated to have zero correlation over distances greater than a

few wavelengths. Since multi-hop networks typically have sensors spaced more than a few wavelengths apart, $\{Y_{i,j}\}_{(i,j)}$ are considered independent across link pairs in this paper. If multi-hop networks are designed with antennas spaced closer than a few wavelengths, this independence assumption could easily be replaced with a valid correlated small-scale fading model.

3.5.4 Analysis Using Proposed Model

In this section, we show how the model may be applied in simulation or analysis. In short, the vector of all link path losses $\{Z_{i,j}\}_{ij}$ in a deployed network can be modeled as a joint Gaussian random variables with zero mean and a given covariance matrix. Specifically, define $\mathbf{z} = [Z_{i_1,j_1}, \dots, Z_{i_N,j_N}]$, where $(i_1, j_1), \dots, (i_N, j_N)$ is a list of unique links in the deployed network and N is the total number of links in the deployed network. According to the model, the covariance matrix of \mathbf{z} is given by,

$$C_Z(\boldsymbol{\theta}) = C_X(\boldsymbol{\theta}) + \mathbb{I}_N \sigma_Y^2, \quad (3.15)$$

where \mathbb{I}_N is the $N \times N$ identity matrix, σ_Y^2 is the variance of non-shadow fading, *i.e.*, $\sigma_Y^2 = \sigma_{dB}^2 - \sigma_X^2$, and

$$C_X(\boldsymbol{\theta}) = [[\text{Cov}(X_{i_k,j_k}, X_{i_l,j_l})]]_{k,l}, \quad (3.16)$$

where $\text{Cov}(X_{i_k,j_k}, X_{i_l,j_l})$ is defined for arbitrary links in (3.13) as a function of the parameters δ and σ_X^2 . Note that the total fading values $\{Z_{i,j}\}$ are zero mean. Since we have assumed $\{Z_{i,j}\}$ to be multivariate Gaussian, the mean and covariance matrix completely determine the distribution as a function of $\boldsymbol{\theta}$.

In simulation, Gaussian random vectors with an arbitrary covariance matrix are generated by first generating i.i.d. Gaussian vectors and multiplying them by the square root of the covariance matrix. In analysis, Gaussian models are often convenient compared to more complicated distributional models. Analysis in [15] used the given joint path loss model to find an analytical lower bound for sensor localization variance. In this paper, we present a mix of analysis and simulation results in Section 3.7.

3.6 Experimental Validation

A statistical joint path loss model must be validated by measurements of the joint path loss across many deployed networks. In this section, we present two measurement campaigns, in a controlled indoor environment and in an uncontrolled outdoor environment, at 900 and 2400 MHz. We present the methods which we apply to the measurements to validate the proposed model, quantify link correlations, and estimate model parameters. The first part of this section describes the measurement campaigns, including descriptions of the environment, equipment, and measurement protocol. In the second part of this section, we present the statistical analysis of measurement data, including the estimation of the model parameters, the space constant δ and the variance of shadowing σ_X^2 .

3.6.1 Measurement Campaign Overview

For validation of the proposed joint path loss model, we have carried out two measurement campaigns. Each measured several realizations of wireless sensor networks, each network with several nodes and many measured links. In each network, the received signal strengths of all pair-wise links are measured and the results saved. In addition, in each deployment, the actual positions of all nodes are carefully determined and recorded. We believe that the time complexity of carrying out such measurements has in the past been a barrier to the study of link shadowing correlations in multi-hop wireless networks.

The two measurement campaigns presented in this section are carried out in different manners in order to achieve particular purposes. These purposes are:

1. *Controlled Measurement Campaign*: Study many realizations of networks with an identical node geometry in a controlled, repeatable experimental setup. Many identical-geometry measurements allow us to experimentally characterize correlation for particular geometries of pairs of links.
2. *Field Deployment Measurement Campaign*: Demonstrate shadowing correlations between links in natural, uncontrolled environments.

Campaign (1.) measured 15 network realizations, each with 16 nodes; campaign (2.) measured six network realizations, each with 16-19 nodes. In total, signal strength measurements on over 2700 different links were made and recorded. Campaigns (1.) and (2.) operated in the 902-928 MHz, and 2400-2483 MHz, U.S. ISM bands, respectively. For each link, measurements were repeated at 16 different center frequencies within the band of operation and repeated over time in order to average out narrow-band fading effects and changes due to motion in the environments. The large set of data allows us to validate the claim that shadowing losses are correlated between links, and to determine the parameters of the proposed joint path loss model.

3.6.2 Controlled Measurement Campaign

The first measurement campaign is designed to provide a random environment but yet provide a repeatable experimental procedure. In this campaign, we leave 16 nodes deployed in a grid geometry in a classroom and then, before each new measurement experiment, randomly vary the positions of obstructions within the room. Fifteen different random obstruction arrangements are created, corresponding to 15 realizations of a random environment.

This controlled experimental setup allows us to test many wireless networks with the identical node geometry, without the difficulty of finding that many different places which would allow nodes to be positioned in exactly the same geometry. Further, the experiment could readily be repeated by other researchers who want to measure link shadowing correlations, without access to the identical building used in this campaign.

The controlled measurement campaign begins by deploying nodes in an empty classroom in the Merrill Engineering Building at the University of Utah, in a 4x4 square grid of node locations with 4 ft (1.22 m) spacing between neighboring nodes. Nodes are placed on the floor at each grid point. Within this deployment area, we generate a *random environment* by randomly placing 10 cardboard boxes wrapped with aluminum foil. Foil-wrapped cardboard boxes represent metal obstacles which might be present in office environments. A Matlab script generates the random

location of these boxes within the area of deployment.

This first experiment uses Crossbow Mica2 wireless sensor devices [103], which operate in the 900-928 MHz band. Sensors are programmed with a TinyOS 1.x/NesC program to collect a large number of pairwise received signal strength (RSS) measurements. Sensors use a TDMA-based MAC protocol in which each wireless sensor broadcasts during an assigned slot to avoid interference with other sensors. Each broadcast contains the RSS values the sensor has measured during the most recent measurement period. One node overhears all broadcasts and logs the pairwise measurements over time. Nodes serially change frequency to 14 different center frequencies in the frequency band (902-928 MHz). The nodes are synchronized and programmed to frequency hop and measure RSS at each frequency. NesC code can be downloaded from the authors' website [102].

In summary, in this measurement campaign, we randomly change the environment while keeping a constant grid geometry of the network nodes. We will show that the large number of networks with an identical geometry allows the study of particular geometries of pairs of links to show particular cases of how geometries affect link shadowing correlation.

3.6.3 Field Deployment Measurement Campaign

The field deployment measurement campaign is carried out in two natural areas near Salt Lake City, Utah. These areas are Red Butte Canyon, an arid canyon area in the foothills of the Wasatch Mountain range (about 5,200 ft elevation), and Albion Basin, a high mountain valley at the top of Little Cottonwood Canyon, at an elevation of 10,000 ft. Measurements were conducted in summer, and at the low elevation, the vegetation consists of dry grasses, sage brush, and scrub oak. At the high elevations, the vegetation consists of many trees, including maples, pines, and willows, with a dense ground cover of flowering plants and shrubs. In both environments, terrain varies rapidly, with variation in ground height from 5-20 ft within a deployment area. We measure two network deployments in Red Butte Canyon and four deployments in Albion Basin.

In this campaign, measurements are carried out using a network of 19 Crossbow TelosB wireless sensor devices. These are 802.15.4-compliant radios which operate 2.4-2.48 GHz ISM band. Wireless sensors are kept at a height of 1 m using stands. After deployment, the coordinate of each sensor is carefully determined using a measuring tape and a compass. Such positioning measurements are overdetermined so that we can verify that sensor positions are determined accurately. The network geometry is random, depending on where it is possible to position the sensors within the varying terrain and vegetation. The sizes of network deployments range from 400 m² to 1800 m². A map of one such network deployment is shown in Fig. 3.6.

In this campaign, deployments are significantly larger in area than in the indoor campaign. Due to the range and the varying terrain and vegetation, we do not have fully connected networks. In particular, one eavesdropping node cannot reliably overhear all packet traffic from all nodes in the network. In these deployments, we use a protocol which forwards all measured data (over possibly multiple hops) to a root node for data collection purposes.

We accomplish data collection using a protocol which builds upon the TinyOS 2.0 “Collection Tree” protocol. Collection Tree creates a tree from the root node to each sensor based on a link quality indicator (LQI) metric [104]. First, deployed TelosB nodes perform a number of RSS measurements at a single frequency, and then average them. Next, all average RSS values are routed to the root node via Collection Tree and recorded on a laptop. Similar to the first campaign, nodes change center frequencies within the band of operation, and synchronize such that all nodes are transmitting and receiving on the same center frequency at the same time.

When one network deployment is finished measuring across all center frequencies and we have verified that full data have been recorded, we pick up the network, move up or down the canyon, redeploy in a new area, and redetermine sensor positions. The geometry of each network is unique because the area in which it is placed introduces unique limitations on where nodes can be positioned.

In summary, the field deployment measurement campaign allows the deployment of relatively large networks in random natural environments, each with a different

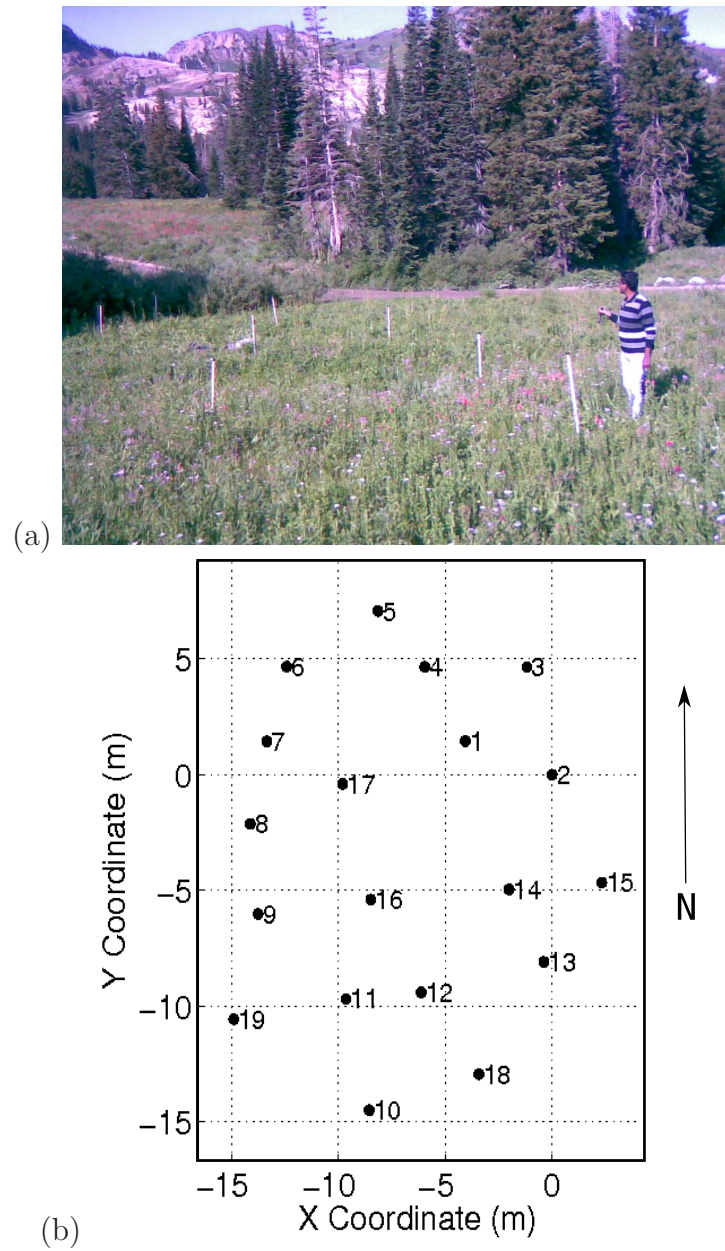


Figure 3.6. Figure (a) shows one realization of the network deployment at Albion Basin. The map constructed by such deployment of wireless sensors is shown in (b).

network geometry, and each in a naturally determined positioning of obstructions.

3.6.4 Statistical Analysis

With the large quantity of measured data, we hope to accomplish two main goals:

1. *Estimate* the parameters of the model in the two measurement campaigns, and
2. *Verify* that the shadowing on pairs of link are correlated and that the proposed model agrees with the measured correlations.

This subsection presents the analysis to accomplish both goals. Model parameter estimation includes:

1. *Large-scale path loss parameters*: n_p and $P_T - \Pi_0$ of (3.2), and
2. *Correlated shadowing parameters*, δ and σ_X^2 of (3.7).

Large-scale analysis determines the average path loss vs. distance; shadowing and other types of fading are what remain after large-scale path loss is removed. Thus large-scale path loss parameters are estimated first.

3.6.4.1 Estimation of Large-Scale Path Loss Parameters

For each realization of network, $m \in \{1, \dots, M\}$, where M is the total number of network realizations in each measurement campaign, the frequency-averaged RSS (in dB) between two nodes i and j , $P_{i,j}^{(m)}$, is represented by a distance-dependent path loss model (3.2), (3.3)

$$P_{i,j}^{(m)} = P_{T_j} - \Pi_0 - 10n_p \log \frac{d_{i,j}}{\Delta_0} - X_{i,j}^{(m)} - Y_{i,j}^{(m)}, \quad (3.17)$$

where $X_{i,j}^{(m)}$ is the shadow fading, $Y_{i,j}^{(m)}$ is the non-shadow fading, for the m th realization of link (i, j) , which has length $d_{i,j}$. Because $Y_{i,j}$ is an average of measurements across many different frequencies, we argue that it may be approximated as Gaussian (in dB), regardless of the underlying frequency-selective fading mechanism (*e.g.*, Rayleigh or Ricean). Shadow fading is typically modeled as Gaussian (in dB) [80], so we expect the total fading $Z_{i,j}^{(m)} = X_{i,j}^{(m)} + Y_{i,j}^{(m)}$ (in dB) to be Gaussian.

The model of (3.17) is a linear model for received power as a function of the log of the path length. Thus we use linear regression to estimate the ‘‘point’’ and ‘‘slope’’ of the linear model, which are $(P_T - \Pi_0)$ and n_p . In our analysis, we use $\Delta_0 = 1$ m. All nodes are set to the same transmit power and we monitor for equal battery voltages, so we expect transmit power P_T to be approximately constant across nodes.

3.6.4.2 Estimation of Correlated Shadowing Parameters

Once the large scale path loss model parameters n_p and $(P_T - \Pi_0)$ are determined, the next step is to estimate the parameters of correlated shadowing model introduced in Section 3.5. We define the parameter vector to be estimated as $\boldsymbol{\theta}$, where $\boldsymbol{\theta} = \left[\delta, \frac{\sigma_X^2}{\sigma_{dB}^2} \right]^T$.

From the residues of the large-scale path loss linear regression, the total fading loss $Z_{i,j}^{(m)}$ for each link (i, j) and the overall variance of $Z_{i,j}^{(m)}$, *i.e.*, σ_{dB}^2 , are determined. Then, we define $\mathbf{z}^{(m)} = \left[Z_{i_1, j_1}^{(m)}, \dots, Z_{i_N, j_N}^{(m)} \right]$, where $(i_1, j_1), \dots, (i_N, j_N)$ is a list of unique measured links in the network and N is the total number of links in the deployed network. According to the model, $\mathbf{z}^{(m)}$ is zero-mean with covariance matrix given by (3.15).

We use maximum likelihood estimation for estimating parameter $\boldsymbol{\theta}$. In other words, we find $\boldsymbol{\theta}_{MLE}$ which maximizes the conditional likelihood function given by (3.18),

$$\begin{aligned} f(\mathbf{z}|\boldsymbol{\theta}) &= \prod_m f(\mathbf{z}^{(m)}|\boldsymbol{\theta}) \\ &= \prod_m \frac{1}{(2\pi)^{N/2} |C_Z(\boldsymbol{\theta})|^{1/2}} \exp \left[-\frac{1}{2} \mathbf{z}^{(m)T} C_Z^{-1}(\boldsymbol{\theta}) \mathbf{z}^{(m)} \right], \end{aligned} \quad (3.18)$$

where $|\cdot|$ denotes the determinant of the matrix and \cdot^T denotes the transpose. Equivalently, $\boldsymbol{\theta}_{MLE}$ can be found by finding the maximum of the log likelihood function $l(\mathbf{z}|\boldsymbol{\theta}) = \log f(\mathbf{z}|\boldsymbol{\theta})$,

$$l(\mathbf{z}|\boldsymbol{\theta}) = \sum_m \left[-k - \frac{1}{2} |C_Z(\boldsymbol{\theta})| - \frac{1}{2} \mathbf{z}^{(m)T} C_Z^{-1}(\boldsymbol{\theta}) \mathbf{z}^{(m)} \right]. \quad (3.19)$$

where $k = \frac{N}{2} \log(2\pi)$ is a constant.

For lack of an analytical solution to the maximization of (3.19), we use a brute force approach. The log likelihood $l(\mathbf{z}|\boldsymbol{\theta})$ is computed for a wide range of $\boldsymbol{\theta}$, specifically, $\delta \in [0.1, 0.9]$ in increments of 0.01, and $\sigma_X^2/\sigma_{dB}^2 \in [0.1, \dots, 0.9]$ in increments of 0.01. The value of $\boldsymbol{\theta}_{MLE}$ for the controlled measurement campaign is found to be $\boldsymbol{\theta}_{MLE} = [0.30, 0.41]^T$, and for the field deployment measurement campaign, $\boldsymbol{\theta}_{MLE} = [0.57, 0.55]^T$.

3.6.4.3 Discussion

The two measurement campaigns are summarized in Table 3.1. The first parameter δ of the proposed model is the distance constant in the correlated random spatial loss field $p(\mathbf{x})$. It describes the separation at which the correlation between two points in that spatial loss field have correlation coefficient of e^{-1} . Loosely, we can describe it as a measure of the ‘size’ of attenuating obstructions in the environment. Comparing the controlled and field deployment measurement campaigns, the average sizes of obstructions in the indoor controlled campaign (boxes) are smaller than in the field deployment campaign (terrain and vegetation). Thus, we would expect the parameter δ to be greater in field deployment campaign compared to the controlled campaign, and in fact, the δ parameter in the field deployment campaign is almost double.

The second parameter σ_X^2/σ_{dB}^2 represents the relative contribution of shadowing, $X_{i,j}$, to total fading, $Z_{i,j}$. It is a function of the type of environment. Indoor environments have a higher angular spread of arriving multipath, due to more significant

Table 3.1. Summary of two measurement campaigns

Measurement Campaign	Controlled	Field Deployment
Environment	Indoor classroom	Outdoor canyon
# Network Realizations	15	6
# Nodes	16	16-19
Freq. Band	900-928 MHz	2.4-2.48 GHz
Est. δ	0.30	0.57
Est. σ_X^2/σ_{dB}^2	0.41	0.55

reflections, compared to the outdoor environments, so narrowband fading will be more significant. The analysis from the measurement campaigns concludes that for the outdoor field deployment measurement campaign, the contribution of shadowing to total fading is 55%, compared to 41% in the indoor controlled measurement campaign.

3.6.5 Verification

The repeated geometries in the controlled measurement campaign allow us to look at specific geometries of links in more detail. First, we use the measurements to verify that the shadowing on many realizations of specific *link pair geometries* do in fact show statistically significant correlations. Second, we show that the proposed correlated link shadowing model does suggest correlation coefficients similar to those estimated from measurements.

We refer to a *link pair geometry* as any pair of links with the same coordinates of endpoints within a translation and rotation. For example, consider link pair geometry #1 in Table 3.2. Any two links which have a common endpoint, extend in the same direction from that endpoint, and have one link of length one unit and the other link of length two units, have link pair geometry #1. Many such link pair geometries are shown in Table 3.2. Since we have 15 realizations of identical-geometry networks, and many pairs of links within each network which have an identical link pair geometry, we verify from a large set of realizations that shadowing values are correlated. Let $\{Z_{a_i}, Z_{b_i}\}$ be a set of measured total fading pairs, where $(a_1, b_1), \dots, (a_P, b_P)$ are the pairs of measured links which have a particular link pair geometry. Then we compute the experimental correlation coefficient $\hat{\rho}$ between $\{Z_{a_i}\}$ and $\{Z_{b_i}\}$.







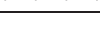



















Using a statistical test for correlation [105, pp. 427-431], we test between the two hypotheses:

$$H_0 : Z_a \text{ and } Z_b \text{ have } \rho = 0,$$

$$H_1 : Z_a \text{ and } Z_b \text{ have } \rho \neq 0.$$

In hypothesis testing, H_0 is the null hypothesis. We assume H_0 is true, unless experimental evidence shows beyond a reasonable doubt that H_0 is not true. If $\rho = 0$, this does not mean that every link pair geometry would measure $\hat{\rho} = 0$.

Table 3.2. Link geometry and correlation coefficients (observed, proposed model)

	Geometry	Correlation ρ			Geometry	Correlation ρ	
		Meas- ured	Prop. Model			Meas- ured	Prop. Model
1		0.33***	0.31	14		-0.04	0.09
2		0.21***	0.25	15		0.12***	0.18
3		0.23***	0.35	16		0.08*	0.12
4		0.05	0.06	17		0.12***	0.18
5		0.17***	0.29	18		0.03	0.17
6		-0.05	0.01	19		0.21***	0.22
7		-0.01	0.00	20		-0.02	0.13
8		-0.10**	0.01	21		0.23***	0.26
9		-0.03	0.09	22		0.00	0.08
10		0.04*	0.15	23		0.08**	0.22
11		0.14***	0.15	24		0.12	0.23
12		0.17***	0.15	25		0.08	0.00
13		0.05	0.11	26		0.03	0.04

p -value, <i>i.e.</i> , $P[\text{getting measured } \rho H_0]$		
*** $p < 0.005$	** $p < 0.01$	* $p < 0.05$

The measurements are random, and in fact, the event $\{\hat{\rho} = 0\}$ has probability zero. Instead, the hypothesis test says that when the measured $|\hat{\rho}|$ exceeds a particular threshold (which is a function of the number of measurements and desired probability of false alarm), it means that H_0 is very unlikely to have been true. The threshold is determined by the desired probability of false alarm, p , so that only in rare cases would the test decide H_1 if H_0 was actually true. We report in Table 3.2 the cases for which the test decides H_1 given three different false alarm rates p of 0.05, 0.01, and 0.005. In Table 3.2 tests which are statistically significant at these three false alarm rates are denoted with a *, **, and ***, respectively. There are 10 link geometries shown which have a p -value of less than 0.005; it is extremely unlikely that fading on these pairs of links is uncorrelated. We note that link pair geometries which

have greater “overlap” or “proximity” have higher correlation in shadow fading. This is intuitive because a greater overlap means a larger similarity in the environment through which the two links pass.

The proposed model is shown to have positive shadowing correlations between link pairs which do show significant shadow fading correlations. Table 3.2 lists the correlation coefficient computed from the correlated shadowing model (using the parameters $\delta = 0.30$ and $\sigma_X^2/\sigma_{dB}^2 = 0.41$ estimated from the controlled measurement campaign). The model-based correlation value ρ is not equal to the experimental correlation estimate $\hat{\rho}$, but is often very close, and generally is high when the measured $\hat{\rho}$ is high. Measurements and model particularly agree well when the number of measurements for the particular link pair geometry is high; link pair geometry #1 is repeated many (32) times in each measured network, many more times than link pair geometry #5 (which is repeated 8 times in each measured network).

Further, we expect that (1.) since each measurement is random, the $\hat{\rho}$ computed from measurements is also random, and (2.) that our proposed model does not explain all facets of the environment which cause correlated shadowing. In particular, we note that a link pair geometry #8 records a statistically significant negative correlation coefficient, but that our proposed model only predicts non-negative shadowing correlations. Studying mechanisms which cause negative link shadowing correlations is a topic of future research.

In summary, the results from the controlled measurement experiment provide a large set of measurements from pairs of links with identical relative geometries. These data show that particular geometries of proximate link pairs show statistically significant correlation, in other words, it is highly unlikely that link pairs of these geometries have uncorrelated shadow fading. We can quantify these correlations and the proposed method provides a statistical model to explain these correlations.

3.7 Application of Joint Model

Correlated shadowing is important because it has a major impact in mesh, ad hoc, and sensor networks. It is something experienced in deployed multi-hop networks

which is not, in state-of-the-art statistical channel models, represented in simulation or analysis of such networks. As discussed in Section 3.2.2, existing statistical and deterministic path loss models have been applied in networking research. We show in this section that the impact of correlated shadowing on end-to-end performance statistics in deployed multi-hop networks is significant. In this section, we give two examples of the differences between performance results when comparing the output of an i.i.d. shadowing model with the output of a correlated shadowing model. In general, for arbitrary larger deployments, we expect the effects of correlated shadowing to be even more significant, but we analyze two simple networks in this section for clarity of explanation.

To simplify the analysis we assume,

1. Packets are received if and only if the received power is greater than a receiver threshold γ , and
2. No packets are lost due to interference.

These assumptions do not limit the results in this section. In fact, performance in interference is also affected by joint path losses between the interfering transmitter and the two communicating nodes, and thus is also impacted by correlated shadowing.

We denote the *normalized received power above the threshold* for a link (m, n) , as $\beta_{m,n}$,

$$\beta_{m,n} = \frac{P_{m,n} - \gamma}{\sigma_{dB}} \quad (3.20)$$

where γ is the threshold received power, $P_{m,n}$ is received power given in (3.2) and σ_{dB} is the standard deviation of total fading in the network. Link (m, n) , by assumption, is connected if and only if $\beta_{m,n} > 0$. An important system parameter is the expected value of $\beta_{m,n}$,

$$\bar{\beta}_{m,n} \triangleq E[\beta_{m,n}] = \frac{\bar{P}(d_{m,n}) - \gamma}{\sigma_{dB}} \quad (3.21)$$

where $\bar{P}(d_{m,n})$ is given in (3.1). Intuitively, $\bar{\beta}_{m,n}$ is the number of standard deviations, σ_{dB} , of link margin we have in link (m, n) . If we design the multi-hop network with higher $\bar{\beta}_{m,n}$, we will have a higher robustness to the actual fading in the environment

of deployment. For example, one could set the internode distance to ensure that $\bar{\beta}_{m,n} = 2$, and then link (m, n) would only be disconnected if total fading loss was two standard deviations more than its mean.

3.7.1 A Three-Node Multi-Hop Path

Consider the simple multi-hop path shown in Fig. 3.7(a), which represents a part of a typical multi-hop network. In this example, $\|\mathbf{x}_i - \mathbf{x}_j\| = \|\mathbf{x}_j - \mathbf{x}_k\|$. For node i to transmit information to node k , the message packet can take two routes. One is the direct link (i, k) and the other is a two hop path through a relay node j , *i.e.*, through link (i, j) and then through link (j, k) . If for our particular deployment, the link (i, k) fails due to high shadowing, there is a chance that the message can still arrive via links (i, j) and (j, k) . This section shows that this ‘link diversity’ method is not as robust as would be predicted assuming independent link shadowing.

We define two events relating to the connectedness of links,

$$\begin{aligned} \mathcal{A} &= \{\text{Link } (i, k) \text{ is connected}\} = \{\beta_{i,k} > 0\} \\ \mathcal{B} &= \{\text{Link } (i, j) \text{ and link } (j, k) \text{ are both connected}\} \\ &= \{\beta_{i,j} > 0\} \cap \{\beta_{j,k} > 0\}. \end{aligned} \quad (3.22)$$

Then $\mathcal{A} \cup \mathcal{B}$ is the event that two nodes i and k can communicate, either directly or through an intermediate node j . The probability that node i and k cannot communicate is the *probability of path failure*,

$$1 - P[\mathcal{A} \cup \mathcal{B}] = 1 - (P[\mathcal{A}] + P[\mathcal{B}] - P[\mathcal{A} \cap \mathcal{B}]). \quad (3.23)$$

From (3.21) and (3.1), the relationship between $\bar{\beta}_{i,j}$, $\bar{\beta}_{j,k}$ and $\bar{\beta}_{i,k}$ for the simple three-node network is,

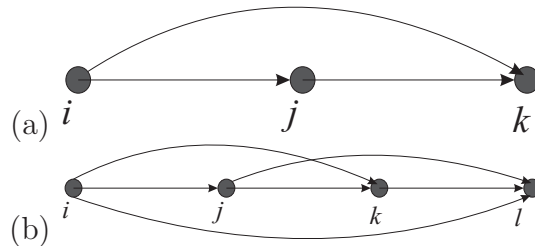


Figure 3.7. Example multi-hop networks of (a) three and (b) four nodes.

$$\bar{\beta}_{i,j} = \bar{\beta}_{j,k}; \quad \text{and} \quad \bar{\beta}_{i,k} = \bar{\beta}_{i,j} - \kappa. \quad (3.24)$$

where $\kappa = \frac{10n_p \log_{10} 2}{\sigma_{dB}}$. According to the definition (3.22), the probability of event \mathcal{A} is,

$$P[\mathcal{A}] = P[\{\beta_{i,k} > 0\}] = Q(-\bar{\beta}_{i,k}) = 1 - Q(\bar{\beta}_{i,j} - \kappa) \quad (3.25)$$

where $Q(\cdot)$ is the complementary CDF of a standard Normal random variable.

3.7.1.1 Case of i.i.d. Shadowing

Under the assumption that the shadowing across links in a network is i.i.d., the probability of event \mathcal{B} is

$$P[\mathcal{B}] = P[\{\beta_{i,j} > 0\} \cap \{\beta_{j,k} > 0\}] = (1 - Q(\bar{\beta}_{i,j}))^2. \quad (3.26)$$

From (3.26) and (3.23), the probability of path failure is

$$1 - P[\mathcal{A} \cup \mathcal{B}] = Q(\bar{\beta}_{i,j} - \kappa)Q(\bar{\beta}_{i,j})[2 - Q(\bar{\beta}_{i,j})]. \quad (3.27)$$

3.7.1.2 Case of Correlated Shadowing

From the correlation values reported in Table 3.2, we know that links (i, j) and (j, k) of Fig. 3.7(a) are nearly uncorrelated. Thus, the probability for event \mathcal{B} is approximately the same as in i.i.d. case. The probability $P[\mathcal{A} \cap \mathcal{B}]$ for the case of correlated shadowing is derived in the appendix. Combining the results from the appendix, (3.23), (3.24) and (3.26), the probability of path failure when shadowing on links is correlated is

$$1 - P[\mathcal{A} \cup \mathcal{B}] = Q(\bar{\beta}_{i,j} - \kappa) - (1 - Q(\bar{\beta}_{i,j}))^2 + P[\mathcal{A} \cap \mathcal{B}], \quad (3.28)$$

where

$$P[\mathcal{A} \cap \mathcal{B}] = \int_{\beta_{i,k} > 0} \left[Q \left(\frac{-\mu_1}{\sqrt{1 - \rho_{X_{i,j}, X_{i,k}}^2}} \right) \right]^2 e^{-\frac{(\beta_{i,k} - \bar{\beta}_{i,j} + \kappa)^2}{2}} d\beta_{i,k},$$

and, $\mu_1 = \bar{\beta}_{i,j} + (\beta_{i,k} - \bar{\beta}_{i,j} + \kappa)\rho_{X_{i,j}, X_{i,k}}$.

3.7.2 A Four-Node Multi-Hop Network

Next, consider the four-node link shown in Fig. 3.7(b). For this linear deployment we assume $\|\mathbf{x}_i - \mathbf{x}_j\| = \|\mathbf{x}_j - \mathbf{x}_k\| = \|\mathbf{x}_k - \mathbf{x}_l\|$. For node i to communicate with node l , the message packet can be routed in four different ways, as shown in Fig. 3.7(b).

An analytical expression for the probability of path failure is tedious, so instead we simulate the network shown in Fig. 3.7(b) in both the cases of correlated and i.i.d. link shadowing. We take 10^5 samples of the normalized received powers under both correlated shadowing and i.i.d. shadowing models. We then determine from the result the probability of path failure, *i.e.*, that there exists *no* connected path from node i to node l .

3.7.3 Discussion

We compare the probability of path failure between node i and node k for both the cases of i.i.d. and correlated link shadowing in Fig. 3.8. The analysis shows that when a multi-hop network is designed for $\bar{\beta}_{i,j} = 2, \forall(i, j)$, then the probability of path failure is 120% greater in correlated shadowing as compared to i.i.d. shadowing. Increasing the reliability of the network by designing it for higher $\bar{\beta}_{i,j}$ only increases the disconnect between the two models. It is only when we design the network for very unreliable links (*e.g.*, $\bar{\beta}_{i,j} = 0$, for which link (i, j) is connected half of the time) that the models have a similar result. Path connectivity is much more likely under the i.i.d. model than under the realistic correlated link shadowing model.

The four-node example shows that as paths become longer, it becomes increasingly important to consider correlated link shadowing. While the three-node network had a 120% increase in probability of path failure, the four-node network showed a 200% increase in the same probability. While Fig. 3.8 show the results up to $\bar{\beta}_{i,j} = 2.5$, higher values correspond to higher reliability links, and reliable networks will be designed with even higher link margins. When networks are designed for high reliability, the effects of ignoring link shadowing correlations are dramatic.

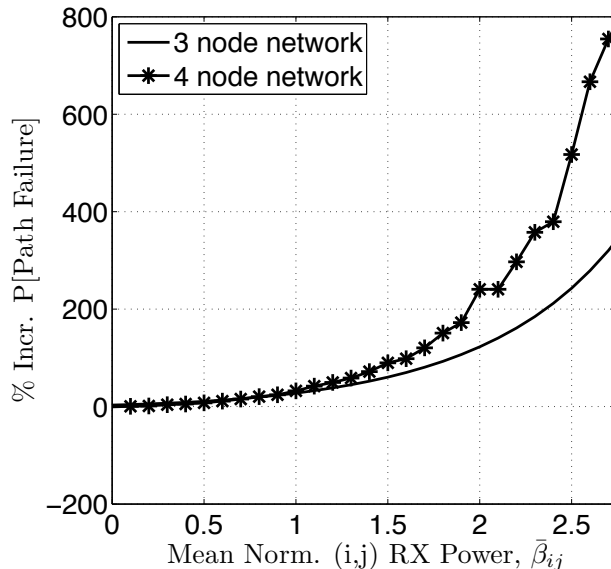


Figure 3.8. The percentage increase in P [link failure] for correlated, vs. i.i.d. shadowing, for three-node and four-node multi-hop network examples, as a function of $\bar{\beta}_{i,j}$.

3.8 Conclusion

We presented the need for statistical path loss models for multi-hop (sensor, ad hoc, and mesh) networks which model the correlation in shadow fading between proximate links. We discussed why existing correlated shadowing models do not apply to arbitrary geometries of links like those which exist in multi-hop networks. We present a new statistical joint path loss model that relates the shadow fading on different links in a multi-hop network to the random underlying spatial loss field. Two measurement campaigns are conducted to measure path losses in indoor and outdoor environments and in two different bands, 900 and 2400 MHz. The data sets demonstrate statistically significant shadowing correlations among particular geometries of link pairs and show that correlated shadowing can be measured in a repeatable experimental setup as well as in natural outdoor environmental sensor network deployments. Model parameters are given for these two campaigns. Finally, we analyze path connectivity statistics in simple multi-hop networks to show the importance of the consideration of shadowing correlation in reliable network design. Using the i.i.d. shadowing model, the probability of end-to-end path failure is under-

estimated by a factor of two or more.

Future work will test other ensembles of deployments in a wider variety of environments. We are working towards implementations of the simulation model for standard networking simulation environments such as `ns-2`. The effects of correlated shadowing will have impact on higher layer networking protocols and algorithms, and in interference and multiple-access control, and future work will quantify these effects.

3.9 Acknowledgments

The authors wish to thank Jessica Croft for her help with the field deployment measurement campaign.

3.10 Appendix

Here we present the derivation of the probability $P[\mathcal{A} \cap \mathcal{B}]$ for the case of correlated shadowing given in (3.28). From (3.20), we note that $\beta_{i,j}$, $\beta_{j,k}$ and $\beta_{i,k}$ are joint Gaussian random variables. Thus the conditional distributions, $f(\beta_{i,j}|\beta_{i,k} = b)$ and $f(\beta_{j,k}|\beta_{i,k} = b)$, are also Gaussian. From the measurement data the link pair (i, j) and (j, k) of Fig. 3.7 are observed to have very small or no correlation between them (see link pair geometry #4 in Table 3.2). Thus the joint distribution, $f(\beta_{i,j}, \beta_{j,k}|\beta_{i,k} = b)$, can be approximated as:

$$f(\beta_{i,j}, \beta_{j,k}|\beta_{i,k} = b) \approx f(\beta_{i,j}|\beta_{i,k} = b)f(\beta_{j,k}|\beta_{i,k} = b). \quad (3.29)$$

The joint distribution of $\beta_{i,j}$, $\beta_{j,k}$ and $\beta_{i,k}$, $f(\beta_{i,j}, \beta_{j,k}, \beta_{i,k})$, can be simplified using (3.29) and can be written as:

$$f(\beta_{i,j}, \beta_{j,k}, \beta_{i,k}) \approx f(\beta_{i,j}|\beta_{i,k} = b)f(\beta_{j,k}|\beta_{i,k} = b)f(\beta_{i,k}). \quad (3.30)$$

The probability $P[\mathcal{A} \cap \mathcal{B}]$ can be written in terms of joint distribution as,

$$\begin{aligned} P[\mathcal{A} \cap \mathcal{B}] &= P[\{\beta_{i,j} > 0\} \cap \{\beta_{j,k} > 0\} \cap \{\beta_{i,k} > 0\}], \\ &= \int_{\{\beta_{i,j} > 0\}} \int_{\{\beta_{j,k} > 0\}} \int_{\{\beta_{i,k} > 0\}} \\ &\quad f(\beta_{i,j}|\beta_{i,k})f(\beta_{j,k}|\beta_{i,k})f(\beta_{i,k})d\beta_{i,j}d\beta_{j,k}d\beta_{i,k}, \\ &= \int_{\beta_{i,k} > 0} [\mathcal{Q}(-\mu_1/\rho_1)]^2 e^{-\frac{(\beta_{i,k} - \bar{\beta}_{i,k})^2}{2}} d\beta_{i,k}, \end{aligned} \quad (3.31)$$

where $\mu_1 \triangleq E[\{\beta_{i,j}|\beta_{i,k}\}] = \bar{\beta}_{i,j} + (\beta_{i,k} - \bar{\beta}_{i,j} + \kappa)\rho_{X_{i,j},X_{i,k}}$ and $\rho_1 = \sqrt{1 - \rho_{X_{i,j},X_{i,k}}^2}$.

Note that for the link pairs geometry considered, $\rho_{X_{j,k},X_{i,k}} = \rho_{X_{i,j},X_{i,k}}$ which results in the square of Q(.) in (3.31).

CHAPTER 4

KERNEL METHODS FOR RSS BASED INDOOR LOCALIZATION

4.1 Abstract

This chapter explores the features and advantages of kernel-based localization. Kernel methods simplify received signal strength (RSS)-based localization by providing a means to learn the complicated relationship between RSS measurement vector and position. We discuss their use in self-calibrating indoor localization systems. In this chapter, we review four kernel-based localization algorithms and present a common framework for their comparison. We show results from two simulations and from an extensive measurement data set which provide a quantitative comparison and intuition into their differences. Results show that kernel methods can achieve an RMSE up to 55% lower than a maximum likelihood estimator.

4.2 Introduction

Knowledge of user's position is becoming increasingly important in applications that include medicine and health care [3], personalized information delivery [5, 9], and security.¹ Indoor localization algorithms have been proposed using various methods such as angle of arrival, time of flight and received signal strength (RSS), of which RSS-based algorithms are the most common.

In general, existing RSS-based indoor localization algorithms can be classified into three main categories: (1) model-based algorithms; (2) kernel-based algorithms; and (3) RSS fingerprinting algorithms. Kernel-based algorithms, the subject of

¹This chapter first appeared in Piyush Agrawal and Neal Patwari, "Kernel methods for RSS-based indoor localization," *Handbook of Position Location: Theory, Practice and Advances*, Eds. M. Buehrer and S. Zekavat, pp. 457-486, John Wiley and Sons, Inc., 2011, and is reprinted with permission.

this chapter, are a “middle-ground” between model-based and RSS fingerprinting algorithms.

Model-based algorithms [76, 36, 77, 75] use standard statistical channel models to provide a functional relationship between distance and RSS. Using this functional relationship, the location of a tag (unknown location device) is estimated from the RSS measured by in-range access points (APs) or anchors (known location devices) by first estimating the distances to the in-range APs using models, and then using methods of lateration to determine the coordinates. Some research [35, 84, 85] also proposes using statistical models to create an entire radio map as a function of position, in which the location of the tag is estimated directly from the RSS measured by the in-range APs.

RSS-fingerprinting methods [24, 83], on the other hand, work in two phases - an *offline* training phase and an *online* estimation phase. In the offline training phase, *RF signatures* are collected at some known locations in the deployment region, which are then stored in a database. An RF signature is a vector of RSS values measured by some predetermined APs. In the online estimation phase, a location is searched from the constructed database whose RF signature matches closely with the RF signature of the tag.

Statistical channel models, in most cases, are unable to capture the complicated relationship between RSS and location in indoor environments. They also typically assume that shadow fading on links are mutually independent, even though environmental obstructions cause similar shadowing effects to many links that pass through them, an effect called correlated shadowing [14, 15].

RSS-fingerprinting methods, on the other hand, do not assume any prior relationship between RSS and position, but the training phase consumes a significant amount of time and effort [24, 44]. To some extent, the training effort can be reduced via spatial smoothing [44, 87, 34], but this is possible only to distances at which the RSS is correlated. Some research has also suggested supplementing some of the measurements using predicted RSS using channel models [24]. Changes in the environment over time reduce the accuracy of the database, requiring recalibration.

In summary, model-based algorithms require the least training effort, but they rely heavily on the prior knowledge of the relationship between RSS and position. RSS-fingerprinting algorithms, on the other hand, are not based on any prior knowledge of the relationship between RSS and position, but require considerable training effort and time.

This chapter is an exploration of kernel-based algorithms, which provide the ability to mix the features of both model-based and RSS fingerprinting algorithms. Kernel-based algorithms encapsulate the complicated relationship between RSS and position, along with correlation in the RSS at proximate locations, in a *kernel*, which can be assumed as a parametrized “black box” that takes the measured RSS as inputs and gives a *measure* of position as output. In this chapter, we describe four different kernel-based RSS localization algorithms using a common mathematical framework and compare and contrast their performance (to each other, and to a baseline model-based algorithm, the maximum likelihood estimator) using a simulation example and using an extensive experimental study. These algorithms include LANDMARC [42], Gaussian kernel localization [43], radial basis function localization [44], and linear signal-distance map localization [45].

The experimental study described in this chapter demonstrates that all four of the kernel-based localization algorithms outperform the MLE in a real-world environment. In fact, the improvement in average RMSE is as high as 55% compared to the MLE. In this chapter, we explain this improved performance of the kernel-based algorithms by using several numerical and simulation examples, in which kernel methods are shown to enable the tag’s coordinate estimates to be robust to both shadowing and independent and identically distributed (i.i.d.) fading. The experimental evaluation also suggests that the complexities of the fading environment and the complicated nature of the large-scale deployment require more parameters than are available to typical model-based algorithms. In particular, in this chapter, we attempt to explain why the kernel-based algorithms perform better than model-based localization algorithms.

Standard kernel-based algorithms still require a training phase for calibration of

kernel parameters. In this chapter, we discuss methods to minimize the calibration requirements of kernel-based algorithms by performing training simultaneously while the system is online, using pairwise measurements between APs. Specifically, several APs are deployed at some known locations throughout the building. Each AP is a transceiver and can measure the RSS of packets from other APs (although we note that we do not limit ourselves to WiFi APs; we may use any standard which allows peer-to-peer communication). These pairwise measurements constitute the training data for calibration purposes.

Prior to discussing the four kernel methods for RSS-based localization algorithms, we present a common mathematical framework for kernel-based localization algorithms in Section 4.3.2. The remainder of Section 4.3 discusses four kernel-based algorithms. To provide more intuitive understanding of the advantages of kernel methods, we present a simple numerical example in Section 4.4. In Section 4.5, we evaluate the algorithms using kernel methods on a real-world measurement data set collected in a hospital environment. Finally we conclude this chapter in Section 4.6.

4.3 Kernel Methods

Kernel methods are a class of statistical learning algorithms in which the complicated relationship between the input (*e.g.*, signal strength) and the output (*e.g.*, physical coordinates) is encapsulated using kernel functions. A kernel function is a potentially nonlinear and parameterized function of input variables. The parameters control the functional dependencies between input and output, in our case, between signal strength and physical coordinates. A key feature of statistical learning is that it estimates the parameters based on some known input/output pairs, also called *learning* from known data. Models using kernel methods are typically *linear* with respect to the parameters, which gives them simple analytical properties, yet are nonlinear with respect to the input variables, *e.g.*, received signal strength.

In this section, we present an overview of coordinate estimation using statistical learning with kernel methods. We begin our discussion in this section by defining our problem statement and then proceed to present a general mathematical framework

for coordinate estimation using kernel methods.

4.3.1 Problem Statement

In this chapter, we consider signal strength-based tag localization. Specifically, we wish to find a two-dimensional tag coordinate, $\hat{\mathbf{x}}_t$, given the known two-dimensional reference coordinates of N APs, $\mathbf{x}_i, \forall i \in \{1, \dots, N\}$, their pairwise RSS measurements, $s_{i,j}, \forall i \neq j, i, j \in \{1, \dots, N\}$, and the RSS measured by N reference APs for a signal transmitted by a tag, $s_{i,t}, \forall i \in \{1, \dots, N\}$. Also, let notation \mathbf{s}_j indicate the RSS vector for AP j , where $\mathbf{s}_j = [s_{1,j}, \dots, s_{N,j}]^T$. Similarly, let notation \mathbf{s}_t indicate the RSS vector for a tag t , where $\mathbf{s}_t = [s_{1,t}, \dots, s_{N,t}]^T$.

Note that even though we consider a two-dimensional coordinate estimation here, the same methodology can readily be extended to a three-dimensional case. Before we proceed further, we clarify our notation for the signal strength $s_{i,j}$. A measurement, $s_{i,j}$, represents the dB signal strength measured by a AP i for the signal transmitted by AP j . Similarly, subscript t indicates that the measurement is for a tag (with an *a priori* unknown location).

The measurement $s_{i,i}$, which corresponds to the RSS measured by co-located APs, is unavailable. In practice, even if two APs are located at the same position, the RSS measured between them is non-zero, *i.e.*, $s_{i,i} \neq 0$, and depends on the transmit power of the APs [45]. Some localization algorithms require the value of $s_{i,i}$ to be known; thus in this paper, we assume when necessary that $s_{i,i} = -33$ dBm [45].

We do not assume full connectivity between links. Consequently, we define set $H(j)$ to be the set of APs which are in direct communication range of AP j . Set $H(j)$ does not include the AP j and $H(j) \subset \{1, \dots, N\}$. Similarly, $H(t)$ is the set of APs that are in direct communication range of tag t .

An AP k that is not in the set $H(j)$, is *not* in the direct communication range of AP j and would not measure any RSS from AP j . It does not necessarily mean that AP k does not receive any signal from AP j . Rather, it simply means that the signal power from AP j was so low that AP k could not demodulate its signal. This “non-measurement” of RSS by AP k is known as the “censored data” problem in statistics. We know this RSS value is low, but we do not know the value of

$s_{k,j}$. How should an algorithm represent $s_{k,j}$ for $k \notin H(j)$ in its RSS vector \mathbf{s}_j ? Most kernel-based approaches have not addressed this censored data issue, and have simply assumed full connectivity between APs. One algorithm estimates the non-measured RSS values using expectation-maximization [106]. In this article, we will provide for each kernel method a means to address non-measured RSS.

4.3.2 General Mathematical Formulation

In the framework of kernel methods, a function of the coordinate estimate of a tag, $\mathbf{f}(\hat{\mathbf{x}}_t)$, can be expressed as,

$$\mathbf{f}(\hat{\mathbf{x}}_t) = \sum_{i \in \tilde{H}(t)} \boldsymbol{\alpha}_i \phi_i(\mathbf{s}_t) + \boldsymbol{\alpha}_0 \quad (4.1)$$

where $\boldsymbol{\alpha}_i, \forall i \in \tilde{H}(t)$ is the *coordinate weight* of AP i , $\tilde{H}(t)$ denotes the set of APs that contribute to the kernel and $\phi_i(\cdot)$ is known as the *kernel function* corresponding to AP i . The parameter $\boldsymbol{\alpha}_0$ is known as the *bias* parameter which compensates for any fixed offset in the data [107]. In this section, we will show how the parameters, $\{\boldsymbol{\alpha}_i\}_{i \in \tilde{H}(t)}$ and $\boldsymbol{\alpha}_0$, are optimized and estimated, and how the kernel functions $\{\phi_i(\cdot)\}_{i \in \tilde{H}(t)}$ are chosen, for different algorithms and techniques in the literature.

The parameters $\{\boldsymbol{\alpha}_i\}_{i \in \tilde{H}(t)}$ are sometimes called “weights,” in particular when predetermined functions are used as kernel functions $\phi_i(\cdot)$, *e.g.*, Gaussian functions. However, these parameters represent the coordinates of the APs in “location space.” Typically, these parameters are functions of the AP coordinates and are optimized to match the information given by the AP pairwise RSS measurements and their coordinates. The coordinate estimate of the tag, $\hat{\mathbf{x}}_t$, is determined by taking the inverse \mathbf{f}^{-1} of $\mathbf{f}(\hat{\mathbf{x}}_t)$. Figure 4.1 shows the operation of coordinate estimation using kernel methods.

Algorithms in the class of kernel-based localization differ in the methods of optimization of $\mathbf{f}(\hat{\mathbf{x}}_t)$. Some algorithms set the kernel functions with predetermined functions and optimize the parameters $\{\boldsymbol{\alpha}_i\}_{i \in \tilde{H}(t)}$ based on pairwise RSS measurements [45, 44, 108]. In contrast, other algorithms set the parameters $\{\boldsymbol{\alpha}_i\}_{i \in \tilde{H}(t)}$ with

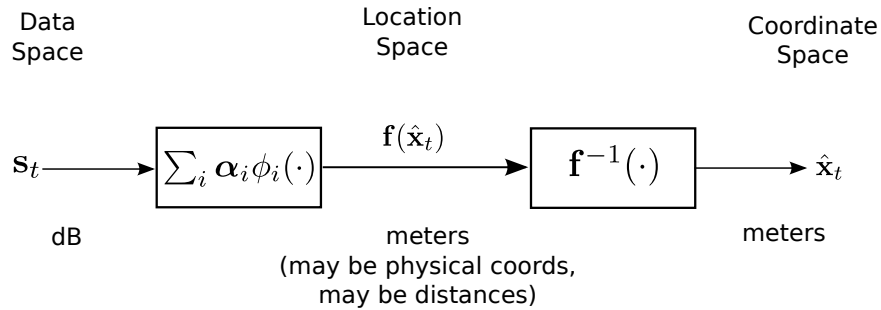


Figure 4.1. Flow chart showing the localization operation using kernel methods.

some functions of the physical coordinates of a set of APs and optimize the kernel functions using their pairwise RSS measurements [42, 43].

4.3.2.1 Determination of Kernel Parameters

Typically, the kernel functions $\phi_i(\cdot)$ belong to a class of parametric nonlinear functions. Determination of kernel parameters is not a trivial task and has been extensively studied in the statistical learning literature [109]. A common technique used for their estimation is cross-validation [25]. For the purposes of cross-validation of localization algorithms, we use the data set collected between APs. In this case, the AP measurement data set is divided into two groups, one group containing $(N - 1)$ APs and the other group containing one “left out” AP, where N is the total number of APs. Thus, there are N ways of dividing the data set. In cross-validation, we estimate the location of the left-out AP as if its coordinate was unknown. The location error can be determined after coordinate estimation, because every AP coordinate is, in fact, known. The average location error is computed by averaging over all left-out APs. The location error is a function of the kernel parameters. By repeating this procedure across a range of candidate values of the parameters, we can optimize the kernel parameters for the particular environment. This method is also called leave-one-out (LOO) cross-validation.

In general, existing RSS-based localization algorithms can be formulated in the framework of (4.1) by selection of:

- The function of coordinate estimates, $\mathbf{f}(\cdot)$,

- Set of APs that contribute to the kernel, $\tilde{H}(t)$,
- Coordinate weights, $\{\alpha_i\}_{i \in \tilde{H}_t}$,
- Kernel functions, $\phi_i(\cdot)$, and,
- Bias parameter, α_0 .

In the remainder of this section, we show how the mathematical framework of (4.1) can be applied to different positioning algorithms. In particular, we select four different algorithms from the RSS-based localization literature and show how the developed framework is applied for each algorithm.

4.3.2.2 Example Framework

Consider an example wireless network with four APs deployed at known locations $\mathbf{x}_i, \forall i \in \{1, 2, 3, 4\}$ as shown in Fig. 4.2. Also, consider a tag whose actual location (in m) is $\mathbf{x}_t = [3, 2]^T$. The coordinates (in m) of the four APs are $\mathbf{x}_1 = [0.5, 0.5]$; $\mathbf{x}_2 = [0.5, 3.5]$; $\mathbf{x}_3 = [3.5, 3.5]$; $\mathbf{x}_4 = [3.5, 0.5]$. Let us assume that all the APs are in direct communication range of the other APs and the tag, *i.e.*, $|H(t)| = |H(j)| = 4, \forall j \in \{1, 2, 3, 4\}$. Using the known locations of the APs, their pairwise RSS measurements are generated using a log-distance path-loss model. A brief description of log-distance path-loss model is given in Section 4.4. An instance of these pairwise RSS measurements is tabulated in Table 4.1. Each row of Table 4.1 represents the RSS measured by the four APs for the signal transmitted by the corresponding device. For example, the RSS values in the first row represents the RSS measured by the deployed APs when AP-1 was transmitting. Similarly, the APs' RSS measurements for the tag are generated, an instance of which is tabulated in the last row of Table 4.1.

For the purpose of this example, the values of various parameters are tabulated in Table 4.2.

The goal in this example is to estimate the location of the tag, $\hat{\mathbf{x}}_t$, using (1.) the known location of four APs, $\{\mathbf{x}_1, \mathbf{x}_2, \mathbf{x}_3, \mathbf{x}_4\}$, (2.) their pairwise RSS measurements $s_{i,j}, \forall i \neq j, i, j \in \{1, 2, 3, 4\}$, tabulated in Table 4.1, and (3.) the RSS measured by

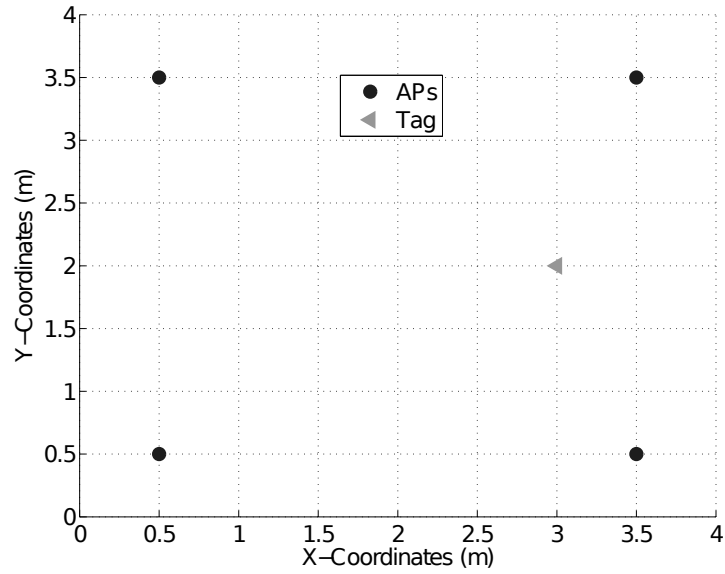


Figure 4.2. Position of APs and tags.

Table 4.1. Table showing an example RSS values (in dBm) measured by APs.

	Rx APs			
	AP 1	AP 2	AP 3	AP 4
Tx AP 1	n/a	-72	-62	-81
Tx AP 2	-70	n/a	-59	-85
Tx AP 3	-60	-65	n/a	-63
Tx AP 4	-59	-77	-72	n/a
Tag	-72	-69	-61	-60

Table 4.2. Log-normal path-loss parameter description and values used in the running example framework.

parameter	Description	Value
n_p	Path-loss exponent	4
σ_{dB}	Fading std. deviation	6.0 dB
Π_0	Reference RX Power (at 1 m)	-50 dBm

the four APs for a signal transited by the tag, $\mathbf{s}_{i,t}, \forall i \in \{1, 2, 3, 4\}$, tabulated in the last row of Table 4.1.

We will revisit this example wireless network throughout this section when we consider each localization algorithm in detail.

4.3.3 LANDMARC Algorithm

LANDMARC [42] is an RSS-based localization algorithm in which a tag's coordinate estimate is given by a weighted average of the coordinates of k closest APs that can hear the tag's transmission. In this section, we present how the LANDMARC algorithm can be expressed as a kernel method. Because LANDMARC is intuitive and can be explained with a single weighted average, it helps to demonstrate the concepts of kernel algorithms in an intuitive manner, and shows how simple a kernel-based algorithm can be.

In LANDMARC, a tag's estimated coordinate is written, using $\mathbf{f}(\hat{\mathbf{x}}_t) = \hat{\mathbf{x}}_t$, $\boldsymbol{\alpha}_i = \mathbf{x}_i$, $\boldsymbol{\alpha}_0 = \mathbf{0}$, and

$$\phi_i(\mathbf{s}_t) = \frac{1/\|\mathbf{s}_t - \mathbf{s}_i\|^2}{\sum_{j \in \tilde{H}(t)} 1/\|\mathbf{s}_t - \mathbf{s}_j\|^2} \quad (4.2)$$

Applying these relations in (4.1), we have,

$$\hat{\mathbf{x}}_t = \sum_{i \in \tilde{H}(t)} \mathbf{x}_i \frac{1/\|\mathbf{s}_t - \mathbf{s}_i\|^2}{\sum_{j \in \tilde{H}(t)} 1/\|\mathbf{s}_t - \mathbf{s}_j\|^2} \quad (4.3)$$

Here, $\tilde{H}(t)$ is the set of k APs that are closest to the tag. In LANDMARC, "closeness" is quantified by the Euclidean distance between the RSS vector of AP i , \mathbf{s}_i , and the RSS vector of the tag, \mathbf{s}_t , *i.e.*, $E_i = \|\mathbf{s}_t - \mathbf{s}_i\|$. We define the vector \mathbf{E} as,

$$\mathbf{E} = [E_1, \dots, E_N]^T \quad (4.4)$$

The set of APs $\tilde{H}(t)$ in (4.2) - (4.3) is the set of k AP indices with the k smallest E_i in the vector \mathbf{E} . In LANDMARC, k is a variable parameter which determines the number of APs that contribute in the kernel. Any non-measured RSS in vectors \mathbf{s}_t or \mathbf{s}_i , as discussed in Section 4.3.1, is replaced by the minimum RSS observed over the duration of the experiment minus one.

The only parameter that needs to be estimated in LANDMARC is the set of APs that contribute in the kernel, $\tilde{H}(t)$, which in turn depends on the parameter k . If $k = 1$, then we choose the AP which is “closest” (smallest E_i) to the tag as the coordinate estimate of the tag. Similarly, if $k = 2$, then the two ‘closest’ APs are considered and parameters are determined using (4.2). Unfortunately, there is no analytical solution for the optimal value of k , although it can be determined experimentally for a given environment or by using the cross-validation approach described in Section 4.3.2.

The above argument implicitly assumes that the optimal value of k is less than the number of neighbors of a tag, *i.e.*, $k < |H(t)|$, where $H(t)$ denotes the set of one-hop neighboring APs which hear the transmission from the tag. A question that arises is what would be the set $\tilde{H}(t)$ when k is greater than the number of one-hop APs, $H(t)$. A naive approach for this situation would be to place an upper threshold on the value of k . In other words, $k' = \min\{k, |H(t)|\}$, where k' is the actual number of neighbors used for a particular tag t .

Example 4.1 (Revisit Example Framework) *Consider the wireless network of Fig 4.2. Estimate the tag’s coordinate, $\hat{\mathbf{x}}_t$, using the LANDMARC algorithm.*

Solution: Let us assume $k = 3$. Using (4.4) and the definition of E_i , we can compute the Euclidean distance vector (in dBm) as,

$$\mathbf{E} = [44.36, 43.86, 30.71, 33.58]^T.$$

The set of APs $\tilde{H}(t)$ in (4.2) and (4.3) is the set of three AP indices with the smallest E_i in vector \mathbf{E} . Thus, $\tilde{H}(t) = \{2, 3, 4\}$. The values kernel function, $\phi_i(\cdot)$, corresponding to each AP $i \in \tilde{H}(t)$, is computed using (4.2),

$$\phi_2(\mathbf{s}_t) = 0.21, \quad \phi_3(\mathbf{s}_t) = 0.43, \quad \phi_4(\mathbf{s}_t) = 0.36$$

Using these kernel values and the known AP coordinates, $\{\mathbf{x}_2, \mathbf{x}_3, \mathbf{x}_4\}$, in (4.3), the LANDMARC coordinate estimate of the tag, $\hat{\mathbf{x}}_t$ (in m), is computed as,

$$\hat{\mathbf{x}}_t = [2.9, 2.4]^T.$$

Compared to the actual tag location, the LANDMARC coordinate estimate has an error of 0.44 m.

4.3.4 Gaussian Kernel Localization Algorithm

The Gaussian kernel localization algorithm is an RSS-based localization algorithm proposed by Kushki *et al.* [43]. Similar to LANDMARC, in the Gaussian kernel localization algorithm, the coordinate estimate of a tag is the weighted average of coordinates of the closest APs. However, the weights are determined by a Gaussian kernel, which gives a measure of distance between the RSS vector of the tag and the RSS vectors of the APs. Any stationary kernel function could be used in place of the Gaussian kernel to determine the weights. The authors chose to use the Gaussian kernel because it is widely used and studied in the literature. As presented by the authors, this algorithm uses the AP measurements over time, for time $\tau = 1, \dots, T$, denoted by $\mathbf{s}_i^{(\tau)}$. In this section, we briefly describe the various aspects of this algorithm and how it fits into the framework developed in Section 4.3.2.

In the Gaussian kernel positioning algorithm, the coordinate estimate of the tag, $\hat{\mathbf{x}}_t$, is written as in (4.1) with $\mathbf{f}(\hat{\mathbf{x}}_t) = \hat{\mathbf{x}}_t$, $\boldsymbol{\alpha}_i = \mathbf{x}_i$, $\boldsymbol{\alpha}_0 = \mathbf{0}$, $\tilde{H}(t) = H(t)$, and,

$$\phi_i(\mathbf{s}_t) = \frac{1}{T(\sqrt{2\pi\sigma^2})^d} \sum_{\tau=1}^T \exp\left(\frac{-\|\tilde{\mathbf{s}}_t - \tilde{\mathbf{s}}_i^{(\tau)}\|^2}{2\sigma^2}\right), \quad (4.5)$$

where σ is a parameter called ‘width’ of the kernel. The notation $\tilde{\mathbf{s}}_t$ represents the ‘reduced’ \mathbf{s}_t , the RSS vector of the tag, and is given as, $\tilde{\mathbf{s}}_t = [s_{t,i_1}, \dots, s_{t,i_d}]^T$, where i_1, \dots, i_d is a list of the elements in $H_d(t)$, a set of d predetermined APs. Similarly, $\tilde{\mathbf{s}}_i^{(\tau)}$ represents the reduced RSS vector for AP i at a particular time instant $\tau, \forall \tau \in \{1, \dots, T\}$. The estimation of the AP set $H_d(t)$ will be discussed below in the ‘‘Estimation of Parameters’’ subsection.

Simplifying, (4.1) reduces to,

$$\hat{\mathbf{x}}_t = \sum_{i \in H(t)} \mathbf{x}_i \phi_i(\mathbf{s}_t). \quad (4.6)$$

The kernel functions, $\{\phi_i(\dots)\}$, of (4.5) may be normalized [43]. Normalization avoids the situation where there are ‘‘holes’’ in the RSS space, regions of $\tilde{\mathbf{s}}_t$ where the sum in

(4.5) has a low value. This would lead to fewer predictions at those regions of the RSS space [110]. In other words, normalization makes sure that the resulting kernel covers the whole range of RSS values measured by APs. The normalized kernel functions, $\phi_i(\mathbf{s}_t)$ can be represented as,

$$\phi_i(\mathbf{s}_t) = \frac{1}{C} \left[\frac{1}{T(\sqrt{2\pi}\sigma^2)^d} \sum_{\tau=1}^T \exp \left(\frac{-\|\tilde{\mathbf{s}}_t - \tilde{\mathbf{s}}_i^{(\tau)}\|^2}{2\sigma^2} \right) \right], \quad (4.7)$$

where

$$C = \sum_{i \in H(t)} \phi_i(\mathbf{s}_t)$$

The Gaussian kernel localization algorithm requires estimation of the following parameters:

1. Width of the kernel, σ ,
2. A predetermined set of d APs, $H_d(t)$.

Neighboring APs would report correlated RSS measurements. It is suggested that including all neighbors leads to redundancy as well as biased estimates [43]. One can minimize this effect by selecting a subset of d APs, $H_d(t)$, from the set of neighboring APs, $H(t)$, which have minimum redundancy. This set $H_d(t)$ is found to be the set which has minimum divergence. Let, $V_{i,j}$ denote a vector time series of RSS measured by AP i for a signal transmitted by AP j , *i.e.*, $V_{i,j} = [s_{i,j}^{(1)}, \dots, s_{i,j}^{(T)}]$. The set of d APs, $H_d(t)$, is selected such that,

$$H_d(t) = \underset{H_p(t) \subset H(t): |H_p(t)|=d}{\operatorname{argmin}} \sum_{h_i, h_j \in H_p(t)} |h_i - h_j|, \quad (4.8)$$

where

$$|h_i - h_j| = \min_k \Delta(V_{i,k} - V_{j,k}),$$

where $\Delta(V_{i,k} - V_{j,k})$ is the *divergence* between two time series $V_{i,k}$ and $V_{j,k}$ and given by [43],

$$\Delta(V_{i,k} - V_{j,k}) = \frac{1}{8} (\mu_{i,k} - \mu_{j,k})^2 \left[\frac{\sigma_{i,k} + \sigma_{j,k}}{2} \right]^{-1} + \frac{1}{2} \log \frac{0.5(\sigma_{i,k}^2 + \sigma_{j,k}^2)}{\sigma_{i,k}\sigma_{j,k}} \quad (4.9)$$

where $\mu_{i,k}$ and $\mu_{j,k}$ are the means and $\sigma_{i,k}$ and $\sigma_{j,k}$ are the standard deviations for the time series $V_{i,k}$ and $V_{j,k}$, respectively. Although other divergence measures exist in the

literature, the divergence represented in (4.9) is commonly used when the distribution of the time series is Gaussian.

Another parameter to be determined is σ , the kernel width parameter. Note that the kernel width parameter, σ is a global parameter which depends on the pair-wise measurements of the APs and is independent of the RSS measurement of the tag. In our evaluation in Section 4.5, σ is determined using the cross-validation approach described in Section 4.3.2.

Example 4.2 (Revisit Example Framework) *Let's return to the example wireless network of Fig. 4.2. Estimate the tag's coordinate, $\hat{\mathbf{x}}_t$, using the Gaussian kernel localization algorithm.*

Solution: Note that the Gaussian kernel localization algorithm uses the AP measurements over time, which is used to determine the subset of APs that have minimum redundancy in their measured RSS. Our example framework cannot provide information about this redundancy because of the pairwise i.i.d. nature of RSS simulation model used in this example. For the purposes of this example, let us assume the set $H_d(t) = \{1, 2, 4\}$.

The next parameter we need to determine is the width of the kernel, σ , which is estimated using the cross validation approach described in Section 4.3.2. Based on the experimental evaluation in Section 4.5, the value of the kernel width is found to be $\sigma = 30$ dB.

Using the RSS values from Table 4.1 along with $H_d = \{1, 2, 4\}$, $\sigma = 30$ dB, and $T = 1$ in (4.7), the values of normalized kernel functions, $\phi_i(\dots)$, corresponding to AP $i, \forall i \in \{1, 2, 3, 4\}$, are determined to be:

$$\phi_1(\mathbf{s}_t) = 0.16, \quad \phi_2(\mathbf{s}_t) = 0.16, \quad \phi_3(\mathbf{s}_t) = 0.42, \quad \phi_4(\mathbf{s}_t) = 0.27.$$

Using these values of the kernel functions and their corresponding coordinates in (4.6), the estimated tag coordinate, $\hat{\mathbf{x}}_t$, (in m) is:

$$\hat{\mathbf{x}}_t = [2.6, 2.2]^T.$$

Compared to the actual tag coordinate, the Gaussian kernel-based coordinate estimate has an error of 0.5 m.

4.3.5 Radial Basis Function Based Localization Algorithm

In the statistical learning literature, radial basis functions have been widely used as the kernel functions $\phi_i(\cdot)$. Radial basis functions were introduced for the purpose of *exact* function interpolation. Given a set of training inputs and their corresponding outputs, the purpose of radial basis function interpolation is to create a smooth function that fits training data exactly [107].

Functions of this class have a property that the basis functions depends only on the *radial distance* (typically Euclidean) from a center $\boldsymbol{\mu}_i$, such that,

$$\phi_i(\mathbf{s}_t) = h(\|\mathbf{s}_t - \boldsymbol{\mu}_i\|),$$

where $h(\cdot)$ is a radial basis function. Typically, the number of basis functions and the position of their centers, $\boldsymbol{\mu}_i$, are based on the input data set $\{\mathbf{s}_i\}_{i=1,\dots,N}$. A straightforward approach is to create a radial basis function centered at every $\{\mathbf{s}_i\}_{i=1,\dots,N}$.

In the context of tag localization, the use of radial basis functions was proposed by Krumm *et al.* [44]. Primarily, the authors of [44] introduced interpolation using radial basis functions as a way to reduce the calibration effort of RADAR positioning [24] at the same time maintaining an acceptable location error. Specifically, the authors construct an interpolation function using radial basis functions that gives the location of a tag t , $\hat{\mathbf{x}}_t$, as a function of its RSS vector \mathbf{s}_t .

Using the same notation as in Section 4.3.1, the coordinate estimate of a tag, $\hat{\mathbf{x}}_t$, using radial basis functions can be written in our common framework using $\mathbf{f}(\hat{\mathbf{x}}_t) = \hat{\mathbf{x}}_t$, $\tilde{H}(t) = 1, \dots, N$, along with

$$\boldsymbol{\alpha}_0 = \frac{1}{N} \sum_{j=1}^N \mathbf{x}_j, \quad (4.10)$$

and,

$$\phi_i(\mathbf{s}_t) = \exp\left(\frac{-\|\mathbf{s}_t - \mathbf{s}_i\|^2}{2\sigma_{RBF}^2}\right), \quad (4.11)$$

where N denotes the total number of deployed APs, and σ_{RBF} is the width of the kernel. Applying these relations in (4.1), we have,

$$\hat{\mathbf{x}}_t = \sum_{i=1}^N \alpha_i \phi_i(\mathbf{s}_t) + \alpha_0, \quad (4.12)$$

The parameters $\{\alpha_i\}_{i \in \{1, \dots, N\}}$ are estimated. Unlike LANDMARC and the Gaussian kernel positioning algorithm, in which $\alpha_i = \mathbf{x}_i$ is the *actual* AP location, in the radial basis function localization algorithm, the parameters $\{\alpha_i\}_{i \in \{1, \dots, N\}}$ are “artificial” coordinates for each AP set such that $\hat{\mathbf{x}}_t$ in (4.12) minimizes the location error for all training measurements.

There are two parameters that need to be estimated in the radial basis function based localization algorithm:

- Coordinate weights, $\{\alpha_i\}_{i \in \{1, \dots, N\}}$, and,
- Width of the radial basis function kernel, σ_{RBF} .

We begin with the estimation and optimization of coordinate weights $\{\alpha_i\}_{i \in \{1, \dots, N\}}$. Specifically, the coordinate weights $\{\alpha_i\}_{i \in \{1, \dots, N\}}$ are the coordinates in “location space.” There is no need to make them equal to the coordinates of APs. In radial basis function localization, these parameters are optimized such that the information given by the AP pairwise RSS measurements best matches the known AP locations. Substituting the AP pairwise RSS measurements and their corresponding coordinates in (4.12) and expressing them in matrix, we get,

$$\mathbf{Z} = \Phi \mathbf{A}, \quad (4.13)$$

where \mathbf{A} is the coordinate weight matrix $\mathbf{A} = [\alpha_1, \dots, \alpha_N]^T$, and \mathbf{Z} is a matrix whose i^{th} row, \mathbf{z}_i , is given as,

$$\mathbf{z}_i = [\mathbf{x}_i - \alpha_0]^T,$$

and Φ is the kernel design matrix whose i, j element, $\Phi(i, j)$, is given as,

$$\Phi(i, j) = \phi_i(\mathbf{s}_j) = \exp\left(\frac{-\|\mathbf{s}_j - \mathbf{s}_i\|^2}{2\sigma_{RBF}^2}\right) \quad (4.14)$$

An optimal solution can be found by using the method of *least-squares* [111]. Within the framework of least squares, the coordinate weight matrix, $\mathbf{A} = [\boldsymbol{\alpha}_1, \dots, \boldsymbol{\alpha}_N]^T$, can be estimated as,

$$\mathbf{A} = (\boldsymbol{\Phi}^T \boldsymbol{\Phi})^{-1} \boldsymbol{\Phi}^T Z, \quad (4.15)$$

The term

$$\boldsymbol{\Phi}^\dagger = (\boldsymbol{\Phi}^T \boldsymbol{\Phi})^{-1} \boldsymbol{\Phi}^T$$

in (4.15) is known as the *pseudo-inverse* of the matrix $\boldsymbol{\Phi}$. The pseudo-inverse is a generalized matrix inverse for nonsquare matrices [112].

The other parameter that needs to be estimated is the radial basis function kernel width, σ_{RBF} . Estimation of this parameter, similar to the estimation of kernel width for Gaussian kernel position algorithm described in Section 4.3.4, is done via cross-validation.

Example 4.3 (Revisit Example Framework) *Consider the wireless network of Fig. 4.2. In this example, we will estimate the tag's coordinate, $\hat{\mathbf{x}}_t$, using the radial basis function based localization algorithm.*

Solution: The first step is to estimate the value of parameter σ_{RBF} , which is estimated using cross-validation as explained in Section 4.3.2. Based on the experimental evaluation in Section 4.5, the value (in dB) of kernel width is found to be $\sigma_{RBF} = 30$ dB.

Using the AP pairwise RSS from Table 4.1, the kernel design matrix, $\boldsymbol{\Phi}$, is determined using (4.14) as,

$$\boldsymbol{\Phi} = \begin{bmatrix} 1 & 0.20 & 0.35 & 0.18 \\ 0.20 & 1 & 0.27 & 0.06 \\ 0.35 & 0.27 & 1 & 0.24 \\ 0.18 & 0.06 & 0.24 & 1 \end{bmatrix}$$

The next step is to determine the coordinate weight matrix, \mathbf{A} using (4.15). In our example, $\boldsymbol{\alpha}_0 = [2, 2]^T$, using (4.10). The coordinate weight matrix \mathbf{A} is determined to be

$$\mathbf{A} = \begin{bmatrix} -2.24 & -2.28 \\ -1.81 & 1.43 \\ 2.43 & 2.32 \\ 1.43 & -1.74 \end{bmatrix},$$

in which row i corresponds to the coordinates of the APs i in “location space”, $\boldsymbol{\alpha}_i^T$. Using the estimated values of $\{\boldsymbol{\alpha}_1, \boldsymbol{\alpha}_2, \boldsymbol{\alpha}_3, \boldsymbol{\alpha}_4\}$, the coordinate estimate of the tag according to radial basis function based localization algorithm is computed from (4.12) as,

$$\hat{\mathbf{x}}_t = [2.8, 2.1]^T$$

Compared to the actual tag location, the radial basis function-based coordinate estimate has an error of 0.25 m.

4.3.6 Linear Signal-Distance Map Localization Algorithm

The linear signal-distance map localization algorithm differs from the kernel-based localization algorithms discussed so far in which the physical coordinate of a device (tag/AP) is ‘directly’ expressed as a weighted nonlinear function of the RSS vector \mathbf{s}_t . In other words, the function of coordinate estimate, $\mathbf{f}(\hat{\mathbf{x}}_t)$, in (4.1) was the coordinate estimate itself, *i.e.*, $\mathbf{f}(\hat{\mathbf{x}}_t) = \hat{\mathbf{x}}_t$. In the linear signal-distance map algorithm, $\mathbf{f}(\hat{\mathbf{x}}_t)$ is the log of the distance between $\hat{\mathbf{x}}_t$ and each AP in $H(t)$, *i.e.*,

$$\mathbf{f}(\hat{\mathbf{x}}_t) = [\log \|\hat{\mathbf{x}}_t - \mathbf{x}_{i_1}\|, \dots, \log \|\hat{\mathbf{x}}_t - \mathbf{x}_{i_n}\|]^T$$

where $\{i_1, \dots, i_n\} = H(t)$ [45]. In this algorithm, we first estimate $\mathbf{f}(\hat{\mathbf{x}}_t)$, and then use the estimated $\mathbf{f}(\hat{\mathbf{x}}_t)$ and the known coordinates of the APs to position the tag, using methods like multilateration. Specifically, multilateration can be viewed as inverse \mathbf{f}^{-1} function. In this section, we present a mathematical formulation of this algorithm in the framework of kernel methods developed in Section 4.3.2.

A key aspect of this localization algorithm is determining the relationship between the pair-wise RSS measurements between the APs and their geographical distances. Let the log-distance estimate between a tag, t , and AP, k , be represented by $\delta_{k,t}$, such that the estimated log-distance vector of the tag to the in-range APs, $H(t)$, be

represented by $\boldsymbol{\delta}_t = [\delta_{1,t}, \dots, \delta_{|H(t)|,t}]$. Following the same notation of Section 4.3.1 and using (4.1), the estimated log-distance vector of the tag, $\hat{\boldsymbol{\delta}}_t$, is given by,

$$\mathbf{f}(\hat{\mathbf{x}}_t) = \hat{\boldsymbol{\delta}}_t = \sum_{i=1}^N \boldsymbol{\alpha}_i \phi_i(\mathbf{s}_t), \quad (4.16)$$

where $\boldsymbol{\alpha}_i \in \mathbb{R}^{|H(t)|}$, N denotes the total number of deployed APs, $\tilde{H}(t) = \{1, \dots, N\}$ and,

$$\begin{aligned} \boldsymbol{\alpha}_0 &= \mathbf{0}, \\ \phi_i(\mathbf{s}_t) &= \mathbf{e}_i^T \mathbf{s}_t \end{aligned} \quad (4.17)$$

where \mathbf{e}_i is a column vector whose j^{th} element, $\mathbf{e}_i(j)$, is given as,

$$\mathbf{e}_i(j) = \begin{cases} 1, & \text{if } i = j \\ 0, & \text{otherwise} \end{cases} \quad (4.18)$$

Note that $\boldsymbol{\alpha}_i$ is a column vector of the same length as $\boldsymbol{\delta}_t$. Once the log-distance to every known location AP in the set $H(t)$ is estimated, the coordinate of the tag can be determined using techniques like multilateration.

From (4.16), we can observe that the log-distance estimate of between a tag and AP is a *linear* function of the raw RSS. The basis for this linearity comes from existing radio propagation models such as the log-distance path-loss model [19]. A typical log-distance path-loss model represents the received power P_r at a distance d from the transmitter as,

$$P_r = \Pi_0 - 10n \log_{10} d.$$

So, one might represent the log-distance as

$$\log_{10} d = \frac{\Pi_0 - P_r}{10n} \quad (4.19)$$

which shows that the log-distance is linear with respect to the received signal strength P_r . Technically, (4.19) is affine while (4.16) is linear, however, (4.19) shows some motivation for the formulation of log-distance as linear with RSS.

In the linear signal-distance map algorithm the only parameters that need to be estimated are the coordinate weights $\{\boldsymbol{\alpha}_i\}$, $\forall i \in \{1, \dots, N\}$. A least-squares

approach is used. As in the radial basis function localization algorithm, let the coordinate weight matrix, \mathbf{A} , be represented as, $\mathbf{A} = [\boldsymbol{\alpha}_1, \dots, \boldsymbol{\alpha}_N]^T$. The least squares solution gives the estimate of coordinate weight matrix as,

$$\mathbf{A} = (S^T S)^{-1} S^T \log(D), \quad (4.20)$$

where S denotes the signal strength matrix such that,

$$S = [\mathbf{s}_{i_1}, \dots, \mathbf{s}_{i_n}], \quad \text{where } \{i_1, \dots, i_n\} = H(t)$$

and, D is the Euclidean AP distance matrix, whose i, j element is the Euclidean distance between AP i and AP j , $\|\mathbf{x}_i - \mathbf{x}_j\|$, and $\log(D)$ is element-wise logarithm on elements of the matrix D .

Example 4.4 (Revisit Example Framework) *Consider the wireless network of Fig. 4.2. The goal of this example is to estimate the coordinate of the tag, $\hat{\mathbf{x}}_t$ using the linear signal-distance map localization algorithm.*

Solution: As in the previous examples, we start with the estimation of parameters.

Using known coordinates of the APs, the distance matrix D is:

$$D = \begin{bmatrix} 0 & 3.0 & 4.2 & 3.0 \\ 3.0 & 0 & 3.0 & 4.2 \\ 4.2 & 3.0 & 0 & 3.0 \\ 3.0 & 4.2 & 3.0 & 0 \end{bmatrix}.$$

Note: Typically, before taking the logarithm of matrix D , the diagonal is replaced by a small positive value ϵ , in order to avoid taking logarithm of zero. It has been recommended in [45] to take the value of $\epsilon = d_{min}/e$, where d_{min} is the minimum value of the off-diagonal elements of the matrix D . In our example, $d_{min} = 3.0$ m and, hence, $\epsilon = 1.1$ m.

The RSS matrix S in (4.20) is constructed from Table 4.1. Using the matrices S and D , the coordinate weight matrix \mathbf{A} is determined using (4.20) as,

$$A = \begin{bmatrix} -0.032 & 0.001 & 0.015 & -0.004 \\ -0.005 & -0.025 & -0.006 & 0.002 \\ 0.014 & 0.003 & -0.031 & 0.009 \\ -0.006 & 0.006 & -0.006 & -0.021 \end{bmatrix},$$

in which row i corresponds to the optimized coordinates of AP i in the “data space”, α_i^T . Using the estimated values of $\{\alpha_1, \alpha_2, \alpha_3, \alpha_4\}$ in (4.16), the estimated log-distance of the tag to the four APs, $\hat{\delta}_t$ is:

$$\hat{\delta}_t = [1.48, 1.11, 0.75, 0.84]^T.$$

Using this estimated log-distance to the APs, the coordinate estimate of the tag is determined using methods of multilateration, which are discussed in the other chapters of this book. Instead, in this example, we use a simple grid search method in which distances are computed between each grid point and the four APs. The grid point which gives the least squared error with the estimated distances to the four APs, $\hat{\delta}_t$, is the desired coordinate of the tag. Using this method, the coordinate estimate of the tag is computed as,

$$\hat{\mathbf{x}}_t = [3.5, 2.1]^T$$

Compared to the actual tag coordinate, the linear signal distance map-based coordinate estimate has an error of 0.51 m.

4.3.7 Summary

This section first presented a mathematical framework for localization using kernel methods. Next, we showed through four RSS-based localization algorithms, how the common framework, represented in (4.1), can be applied to different positioning algorithms. The various parameters and their differences and similarities are presented in Table 4.3.

4.4 Numerical Examples

For the purposes of obtaining an intuitive understanding of the advantages of kernel methods in localization algorithms, we show some numerical examples. Specifically, we compare the coordinate estimation of kernel-based localization algorithms, in an example setting, with that of a maximum likelihood coordinate estimation (MLE) using the log-normal shadowing model. Before we proceed with the example, we briefly describe the MLE algorithm.

Table 4.3. Table summarizing the similarities and dissimilarities of LANDMARC (LM), Gaussian kernel (GK), radial basis function (RBF) and linear signal-distance map (SDM) localization algorithms.

	LM	GK	RBF	SDM
$\mathbf{f}(\hat{\mathbf{x}}_t)$	$\hat{\mathbf{x}}_t$	$\hat{\mathbf{x}}_t$	$\hat{\mathbf{x}}_t$	$\hat{\boldsymbol{\delta}}_t$
$\boldsymbol{\alpha}_i$	Actual AP coords, \mathbf{x}_i	Actual AP coords, \mathbf{x}_i	Optimized Coords in “Loc. space”	Optimized Coords in “Data space”
$\phi_i(\mathbf{s}_t)$	Unitless weight determined by (4.2)	Unitless weight determined by (4.5)	Unitless weight determined by (4.11)	RSS (dBm) from tag to AP i
$\boldsymbol{\alpha}_0$	$\mathbf{0}$	$\mathbf{0}$	Centroid of all deployed APs	$\mathbf{0}$
$\tilde{H}(t)$	Top k APs	All APs	All APs	All in-range APs
length of \mathbf{s}_t	N	d using (4.8)	length N	length N

4.4.1 Maximum Likelihood Coordinate Estimation

A commonly used statistical model for radio propagation is the log-distance path-loss model, in which the shadowing is modeled as log-normal (*i.e.*, Gaussian if expressed in dB). Within this model, the dB RSS between devices i and j is represented as [19],[18],

$$s_{i,j} = \Pi_0 - 10n_p \log_{10} \|\mathbf{x}_i - \mathbf{x}_j\| + X_{i,j} \quad (4.21)$$

where Π_0 represents the RSS at a reference distance of one meter, n_p represents the path-loss exponent, and $X_{i,j}$ (in dB) is the fading error, modeled as a Gaussian random variable with a standard deviation (in dB) of σ_{dB} .

4.4.1.1 Estimating Coordinate from RSS

Given the path-loss model parameters in (4.21), the coordinate of the tag can be estimated by maximizing the likelihood of \mathbf{s}_t or minimizing the negative log-likelihood. The negative log-likelihood of \mathbf{s}_t is given by (4.22),

$$L(\mathbf{s}_t | \mathbf{x}_t, n_p, \Pi_0) = C + \frac{1}{2\sigma_{dB}^2} \sum_{j \in H(t)} [s_{t,j} - (\Pi_0 - 10n_p \log_{10} \|\mathbf{x}_t - \mathbf{x}_j\|)]^2 \quad (4.22)$$

where C is a constant. Note that the negative log-likelihood equation (4.22) assumes that the shadowing on links are mutually independent. This is a simplifying assumption as it has been observed that geographically proximate links exhibit correlated shadowing [14].

The maximum likelihood coordinate estimate of the tag, $\hat{\mathbf{x}}_t^{MLE}$, can be determined by minimizing the negative log-likelihood function of (4.22),

$$\hat{\mathbf{x}}_t^{MLE} = \underset{\mathbf{x}_t}{\operatorname{argmin}} \sum_{j \in H(t)} [s_{t,j} - [\Pi_0 - 10n_p \log_{10} \|\mathbf{x}_t - \mathbf{x}_j\|]]^2 \quad (4.23)$$

In the likelihood equation of (4.22), the path-loss parameters n_p and Π_0 were assumed to be known. These parameters can be estimated using the pair-wise RSS measurements between APs and their known locations. Specifically, a linear regression is performed on the pair-wise RSS measurements and log-distances, computed using the known locations, to give the path-loss parameters n_p and Π_0 [73].

4.4.1.2 Implementation Details

Due to the lack of an analytical solution to (4.23), the minimum is computed by using a *brute-force* grid search over possible coordinates of \mathbf{x}_t . The deployment area is divided into a grid of predetermined size, which determines the resolution of the coordinate estimate. At each grid point the value of negative log-likelihood, $L(\mathbf{s}_t | \mathbf{x}_t, n_p, \Pi_0)$, is determined by using (4.22). The grid point which has the minimum negative log-likelihood is the MLE coordinate estimate of the tag, $\hat{\mathbf{x}}_t^{MLE}$.

The maximum likelihood coordinate estimation of (4.23) suffers from computational disadvantage. Compared to the coordinate estimation of (4.1) using kernel methods, there is no closed form solution for minimizing the the negative log-likelihood of (4.23). Typically, for real-time implementation, one must use numerical optimization methods [73].

4.4.2 Description of Comparison Example

In this section, we illustrate through example the advantages of kernel-based position estimation over model-based estimation. Consider a simple network of four APs placed at the corners of a square with a wall separating them, as shown in

Fig. 4.3. We consider two tag positions, one at the center of the network and the other at the edge. Using this AP placement, we generate RSS values using (4.21) where $X_{i,j}$ includes the wall loss if the line between transmitter and receiver crosses through the wall. Specifically, the RSS, $s_{i,j}$, between devices i and j is computed using (4.21) with $n_p = 2$ and $X_{i,j}$ given as,

$$X_{i,j} = \begin{cases} L_w + Y_{i,j}, & \text{if link } (i,j) \text{ passes through the wall} \\ Y_{i,j}, & \text{otherwise} \end{cases} \quad (4.24)$$

where $Y_{i,j}$ is the shadowing loss, modeled as a zero mean i.i.d. Gaussian in dB random variable, *i.e.*,

$$Y_{i,j}[dB] \sim \mathcal{N}(0, \sigma_{dB}^2)$$

and L_w is the additional loss incurred when passing through a wall. The channel parameters used for generating the RSS vectors are tabulated in Table 4.4.

Note that the channel parameters given in Table 4.4 are assumed to be *a priori* unknown to the MLE algorithm. The path-loss parameters, n_p and Π_0 in (4.23), are estimated using the pairwise RSS measurements between the APs and their

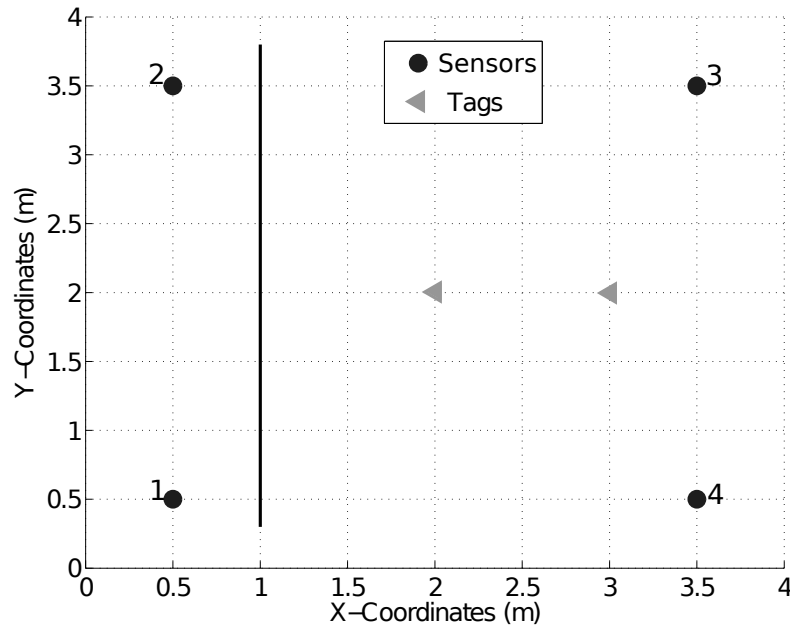


Figure 4.3. Position of APs and tags. There is a wall separating the network, represented by a black vertical line.

Table 4.4. Parameter description and values used in the simulation of network. The values are assumed to be *a priori* unknown to the localization algorithm.

parameter	Description	Value
n_p	Path-loss exponent	2
L_w	Loss across wall	5.0 dB
σ_{dB}	Fading std. deviation	0 dB and 6.0 dB
Π_0	Reference RX Power	-40 dBm

known locations. Specifically, a linear regression is performed on the pair-wise RSS measurements and log-distances, determined using the known locations of the APs [73, 61]. In determining the path-loss, the most recent RSS measurement between the AP pair is used.

Example 4.5 *Consider the scenario when the shadowing standard deviation, $\sigma_{dB} = 0$. A noise variance of zero dB is practically not possible, but, nevertheless, it helps in understanding the effects of shadowing on coordinate estimation, with no other fading losses. Links that pass through the wall suffer an additional loss of L_w dB due to transmission through the wall.*

Solution: The coordinate estimates for different kernel algorithms discussed in the previous section are shown in Fig. 4.4. In addition to kernel-based algorithms, we plot the coordinate estimate using MLE, described in Section 4.4.1. For a fair comparison between algorithms, we keep the set of the APs that contribute to the kernel, for different algorithms, the same and equal to four, *i.e.*, $|\tilde{H}(t)| = 4$ for all algorithms.

We also studied the performance of the coordinate estimation algorithms when different sets of APs contribute to the kernel. We observed that 1.) the Gaussian kernel and 2.) the radial basis function based algorithms have the best performance when all the in-range APs contribute to the kernel. However, for the LANDMARC localization algorithm, the best AP set $\tilde{H}(t)$ depends on the relative location of the

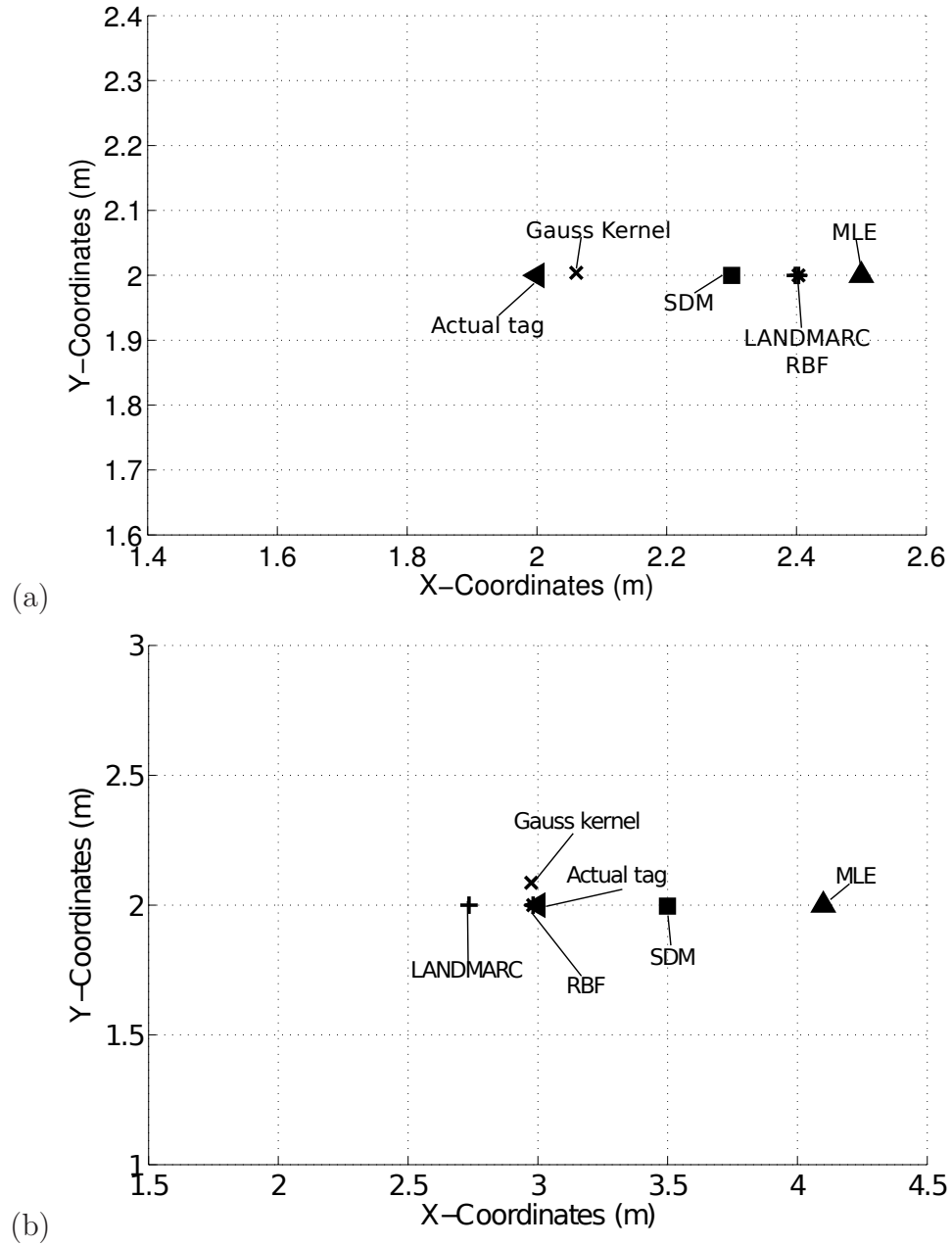


Figure 4.4. Plot showing the coordinate estimates for different localization algorithms along with the position of the tag. In (a) the tag is at the center of the network and in (b) the tag is at the edge of the network.

tag in the network. For tags located at the center of the network, (*e.g.*, Fig. 4.4(a)), taking all in-range APs as the set $\tilde{H}(t)$ performs best. On the other hand, for tags located on the edge of the network, taking the top three APs as the set $\tilde{H}(t)$ performs the best.

We observe that the kernel-based algorithms for coordinate estimation perform better compared to the MLE. One can also observe that the MLE coordinate estimates have errors in the direction away from the wall. This is intuitive, because the presence of a wall between an AP and a tag would lower the RSS of the transmitting tag. Consequently, the log-normal propagation model would predict that the tag is further away from the AP, which is behind the wall. For example, in Fig. 4.3, APs 1 and 2 are behind the wall for the two tag locations and these APs would think the tag is further away from them. Consequently, the coordinate estimate would point in the direction away from the wall. Statistically, the coordinate estimate of the tag is said to have a bias, pointing away from the wall. More bias analysis is performed in the next example.

This example clearly demonstrates the effect of shadowing and how kernel-based methods can overcome these effects. Specifically, shadowing due to walls or obstacles causes a reduction in RSS from the mean RSS. General propagation models, like the one in (4.21), would account this loss to the loss suffered because of distance, in order to minimize the error $X_{i,j}$. Consequently, even in the absence of noise variance, the estimates are biased in the direction away from the source of obstruction. Kernel-based algorithms, on the other hand, “learn” to adapt to this loss because they have more freedom in the parameters than a pure model-based approach and thus, overcome the limitations of the model. Kernel methods interpolate the RSS and the physical coordinate using the AP pair-wise RSS measurements and AP known coordinates.

Example 4.6 *In this example, in addition to the wall loss of Example 4.5, the effect of shadowing variance is added in the path-loss equation (4.24), i.e., $\sigma_{dB} > 0$. Independent Monte Carlo trials are run and the coordinate of the tag is estimated in*

each trial. A one standard deviation covariance ellipse and bias performance of the location estimates is then determined. The one-standard deviation covariance ellipse is a useful representation of the magnitude and variation of the coordinate estimates [113].

Solution: The covariance ellipse along with the bias performance is shown in Fig. 4.5 and Fig. 4.6. In the Fig. 4.5, the tag is located at the center of the network (at $[2, 2]^T$ m) and in the Fig. 4.6, the tag is located at the edge of the network (at $[3, 2]^T$ m).

One of the most important lessons learned from this example is that the kernel-based localization algorithms perform better than the MLE in terms of average RMSE. This can be easily observed in Fig. 4.5 and Fig. 4.6, where the MLE coordinate estimates, Fig. 4.5(e) and Fig. 4.6(e), suffer from both high bias and high variance. The performance improvement for kernel-based localization algorithms can be explained as follows. In the kernel-based methods, the estimated coordinate of a tag is a weighted average of some function of the coordinates of the APs that are in range of the tag. These weights are distinct for the distinct APs and each AP maintains a table of its weights for all the other APs in the network. The determination of the weights is different for different algorithms. Consequently, the APs that are on a particular side of the wall would have lower weights for the APs that are on the other side. For example, in Fig. 4.5 and Fig. 4.6, APs 1 and 2 have lower weights assigned to them by AP 3 as compared to the weight assigned to AP 4.

On the other hand, maximum likelihood coordinate estimation algorithm assumes a *common* statistical channel model for all the links in the network. Consequently, when minimizing the overall error, the path-loss exponent, which signifies the slope of the decay in RSS with respect to log-distance, is higher, similar to Example - 1. Since all the links are weighted equally, this causes a high bias in the maximum likelihood coordinate estimates, pointing away from the wall.

In summary, the advantage of the kernel-based localization algorithms over MLE is that in the kernel-based algorithms the APs which naturally have significantly

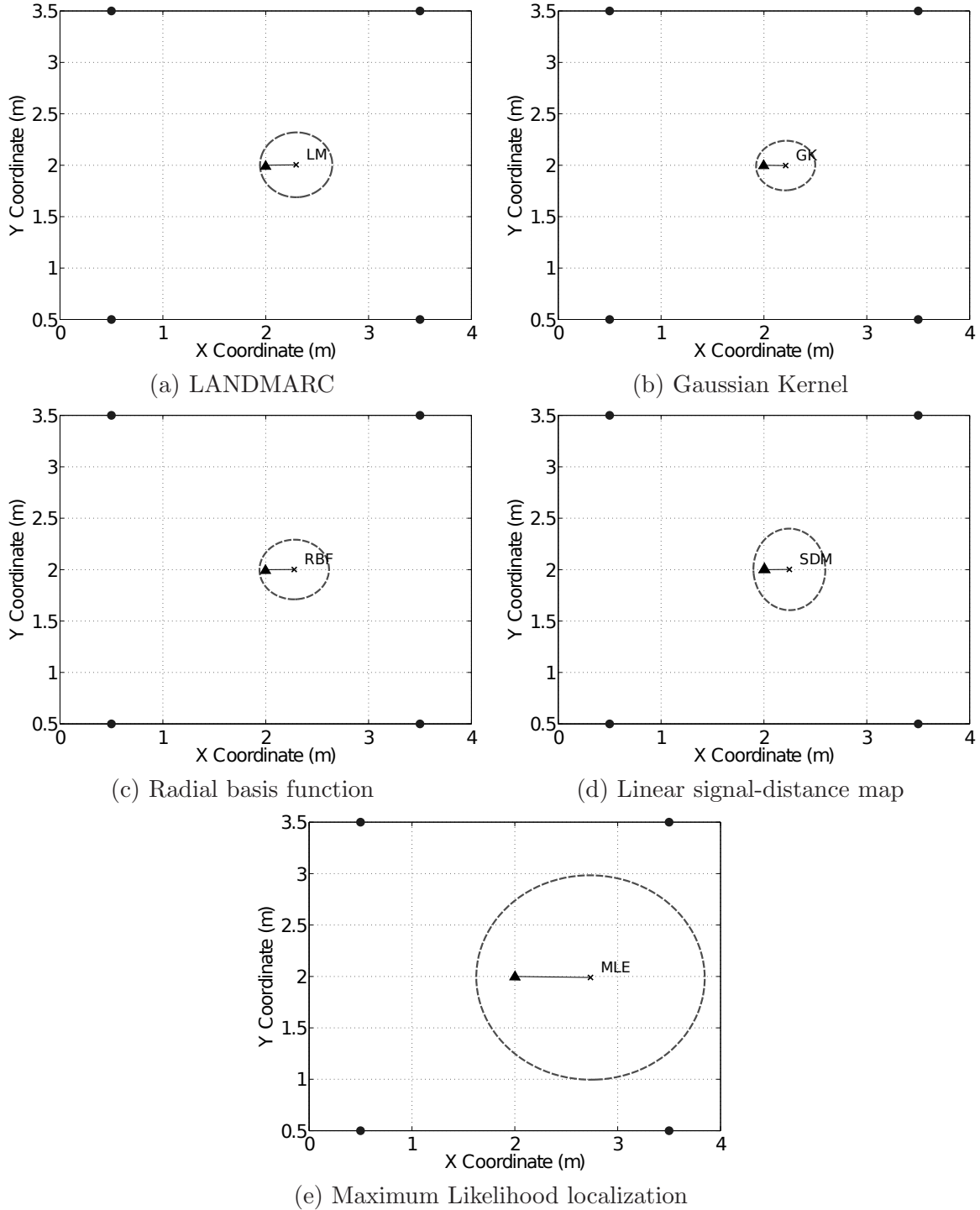


Figure 4.5. Bias plot showing the mean (×) of tag location estimates over 500 trials for different localization algorithms. Actual tag location (▲) is connected to the mean location estimate (—). Plot also shows 1- σ covariance ellipse (---) for the coordinate estimates. The APs (●) are at the corners of the grid. The tag is located at the center of the network.

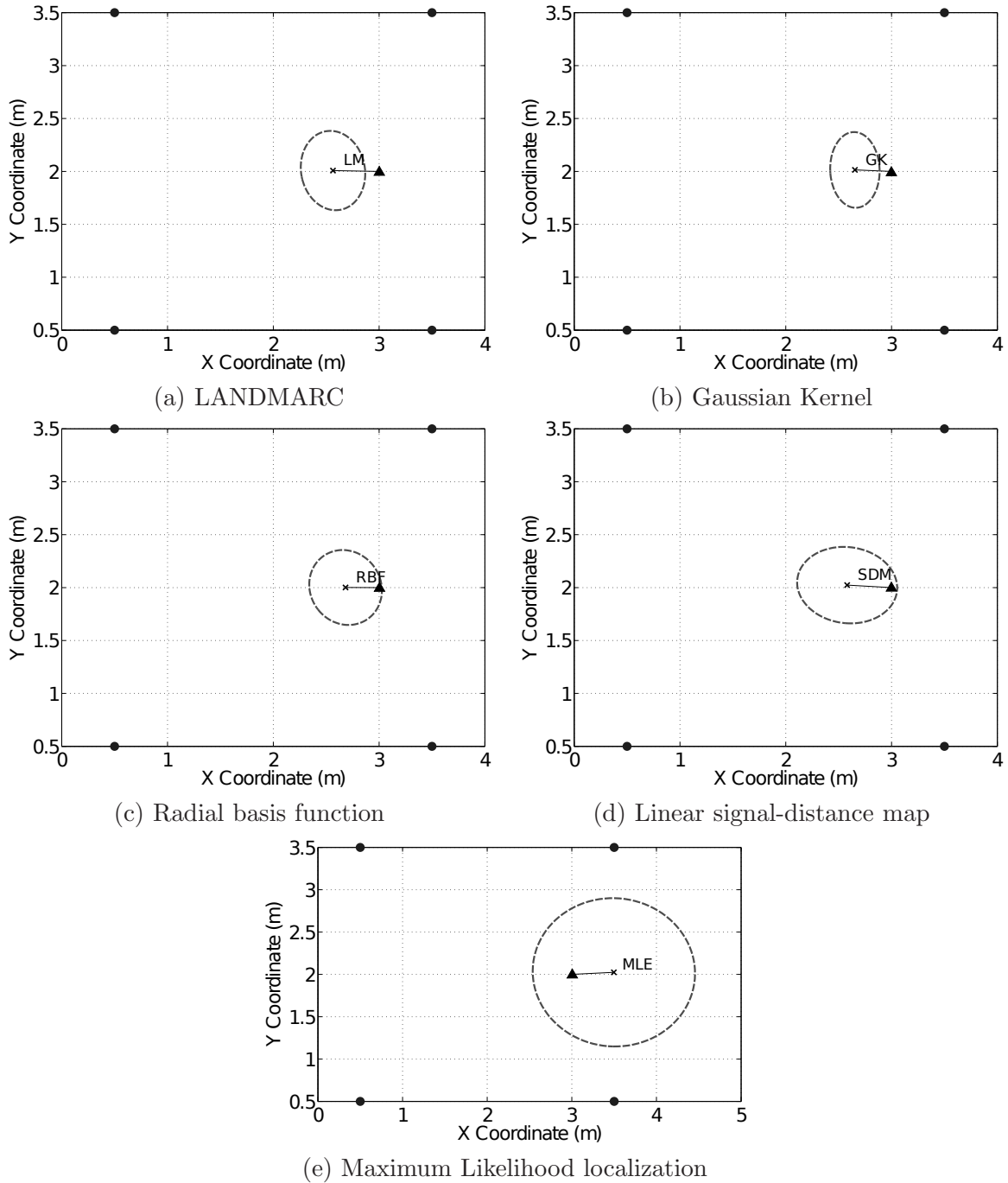


Figure 4.6. Bias plot showing the mean (\times) of tag location estimates over 500 trials for different localization algorithms. Actual tag location (\blacktriangle) is connected to the mean location estimate (—). Plot also shows $1\text{-}\sigma$ covariance ellipse (---) for the coordinate estimates. The APs (\bullet) are at the corners of the grid. The tag is located at the edge of the network.

different RSS values compared to the tag are weighted less compared to the other APs. On the other hand, in maximum likelihood coordinate estimation, all the in-range APs have equal weights when computing the likelihood ratio and thus, the APs which have significantly different RSS values compared to the tag dominate the coordinate estimates pushing the tag further away from its actual location.

4.5 Evaluation Using Measurement Data Set

In this section, we compare the performance of the different kernel-based localization algorithms introduced and formulated in the previous sections. Performance is quantified using two related measures:

- *Bias*: Bias is the difference between the average coordinate estimate (over many trials) and the actual coordinate. In this chapter, we show the bias using a bias plot, in which the actual coordinate and average coordinate estimate are plotted together for each tag. Bias is a consistent error in the coordinate estimate.
- *Root-mean squared error (RMSE)*: The RMSE is used to summarize both bias and variance effects. The “squared error” is the difference between the coordinate estimate and the actual location, squared, with units of m^2 . The RMSE is then the square root of the average squared error (averaged over all tags in the deployment). Bias and error variance are two components of RMSE. The two together, quantified by RMSE, provide a good summary metric for quantifying localization performance.

In the rest of this section, we describe the environment along with the processing of the experimental data and the evaluation procedure for each data set.

4.5.1 Measurement Campaign Description

The measurement data consists of the pairwise RSS measured between 224 known-location wireless APs deployed on a single floor of a hospital with an area of 16,700 square meters. These APs are wireless transceivers which operate in the 2.4 - 2.48 GHz frequency band and transmit at a constant power. The APs have a limited range, and as such, the network formed by the deployed APs is not fully connected.

Each AP has a limited set of neighboring APs to which it can hear and make RSS measurements. The RSS values were collected for a period of 10 minutes during which 40 RSS measurements were collected for each measurable link.

Since there are no “tags” in the measurement data, we simulate an unknown location tag using leave-one-out (LOO) procedure. In the LOO procedure, whenever we need to “create” a known-location tag, we “change” an AP into a tag for purposes of evaluation. We expect the RMSE for the leave-one-out procedure to be higher than would be seen in deployed systems with tags. APs are deployed purposefully to be spatially separated from one another, for purposes of achieving coverage with a small number of APs. So when one AP is converted to a tag, its nearest neighboring APs are relatively far from it, compared to the nearest neighbors of an actual tag that would be used in the system when no APs were “left out.”

4.5.2 Evaluation Procedure

It was mentioned in Section 4.5.1 that the measurement data consist of pairwise RSS between APs only. In order to simulate a tag measurement, we employ the leave-one-out approach. As mentioned before, an AP is assumed as a tag and its position is estimated based on the remaining APs in the deployment. When we refer to a “tag” in this section, we mean the left-out AP which is used as a known-location tag.

The RMSE for each particular tag is computed based on the RSS collected over a period of 10 minutes. This procedure is repeated for all the APs in the deployment. When reporting an average RMSE, we provide two numbers. First, we average over *all* the tag (left-out AP) locations. Second, we average over just the APs in what we consider to be the “sweet spot”, that is, APs in the middle of the largest section of the floor plan shown by (*) in Fig. 4.7. These APs should have lower bias because they are not at the edge of the building and therefore the edge of the network. The RMSE in the sweet spot provides intuition about location estimation in “good” areas, while the RMSE for all APs provides the average error result.

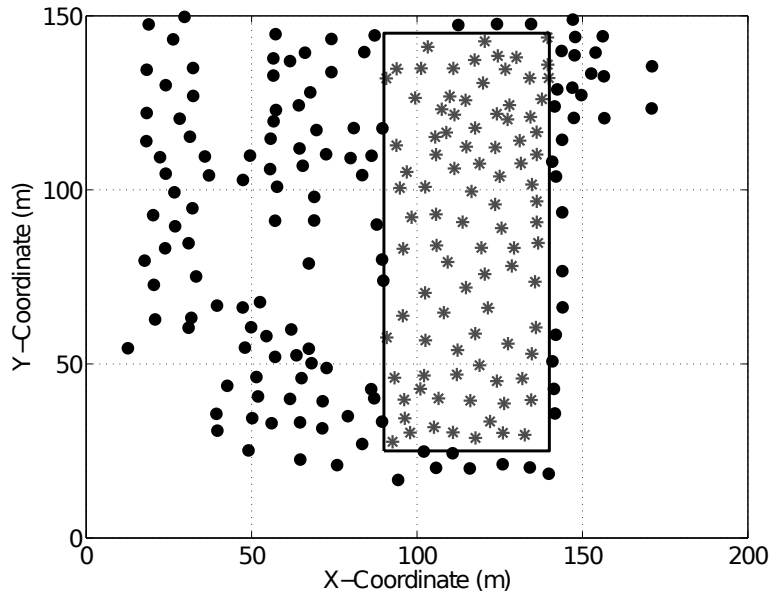


Figure 4.7. Coordinates of APs in the measurement analysis. The APs represented by (*) are said to be in “sweet spot” of the deployment.

4.5.3 Results

In this section, we present the results of applying the four kernel-based localization algorithms, discussed in Section 4.3, on the measurement data set. Specifically, we quantify the algorithms with the two related measures namely, 1.) bias, and 2.) root-mean squared error.

4.5.3.1 Bias Results

Figure 4.8 shows the bias plot for the four kernel-based localization algorithms and maximum-likelihood coordinate estimation. As mentioned before, bias is a consistent error in the coordinate estimates. In addition, we compute the average bias for each localization algorithm, which is shown in Table 4.5. We observe that the lowest bias is observed for the signal-distance map localization algorithm. Specifically, the average bias is 3.72 m. The coordinate estimates are more biased for the maximum-likelihood coordinate estimation algorithm, with an overall bias of 5.41 m and 5.01 m for the sweet spot region. Moreover, as one would expect, the average bias for the APs located in the sweet spot of the deployment region is lower compared to the overall

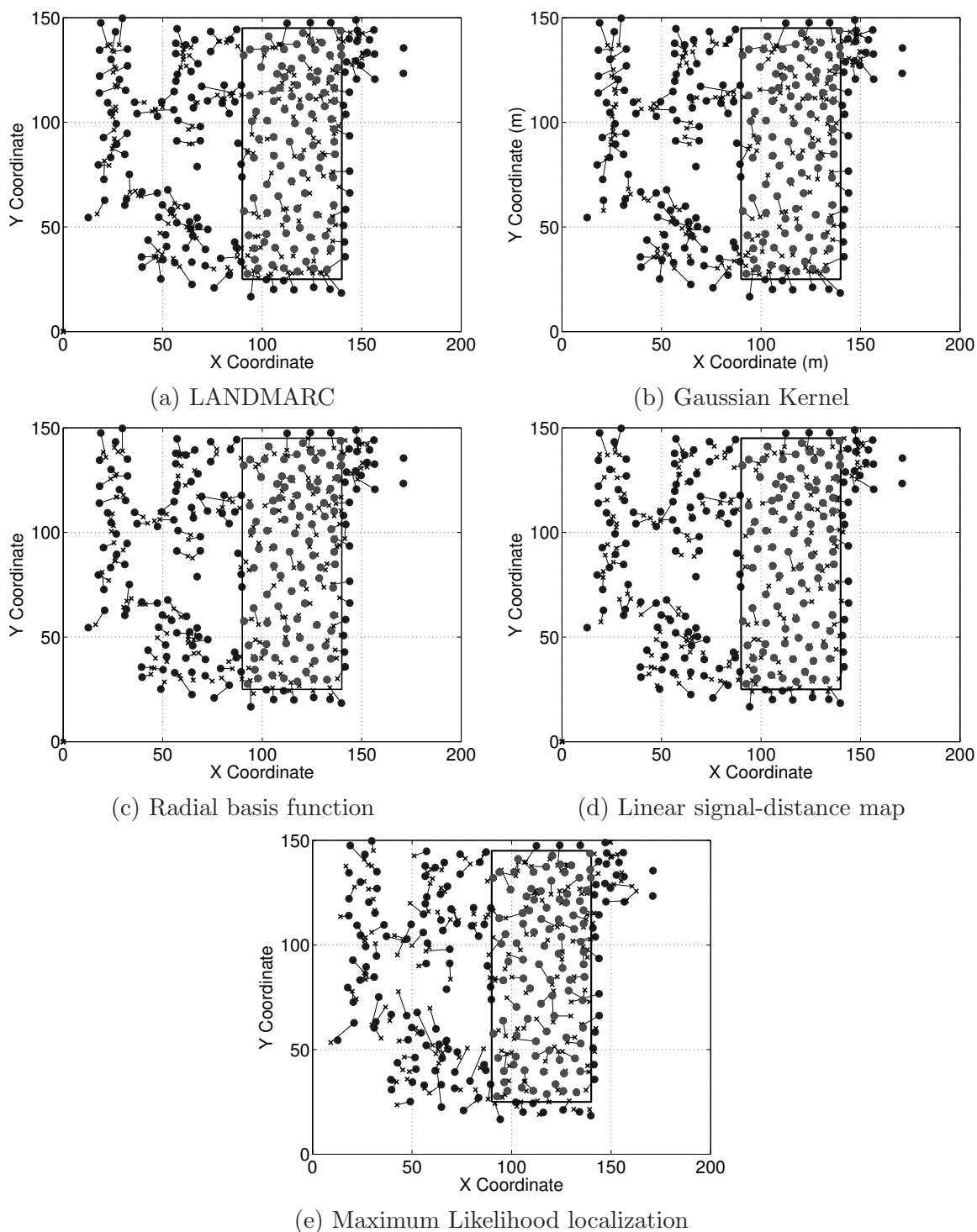


Figure 4.8. Bias plot showing the mean (\times) of location estimates of the APs when it is emulated as a tag. In all the plots, actual AP location (\bullet) is connected to the mean location estimate (---). The APs in “sweet spot” are marked with (\bullet) and are inside the box.

Table 4.5. Table showing the overall (O.A.) and sweet spot (S.S.) performance of different localization algorithms for the real-world measurement data.

Algorithm	Avg. bias (m)		Avg. RMSE (m)	
	O.A.	S.S.	O.A.	S.S.
LANDMARC	5.01	3.28	5.48	4.06
Gaussian Kernel	5.25	3.30	5.87	4.04
Radial basis function	4.16	2.75	4.87	3.53
Linear SDM	3.72	2.49	4.31	3.18
MLE	5.41	5.01	6.87	7.04

average bias.

4.5.3.2 RMSE Results

In most cases, the average RMSE provides a good metric for quantifying the localization performance. The average RMSE results for different localization algorithms are tabulated in Table 4.5. From the table, we observe that all the kernel-based localization algorithms perform better than the MLE, which is a pure model based approach. In fact, the linear signal distance map localization algorithm performs the best with an overall improvement of 37% over the MLE, while the improvement is 55% for the APs in the sweet spot region.

4.6 Discussion and Conclusion

This chapter explores the advantages and features of a class of statistical learning algorithms, called kernel methods, as used in RSS-based localization. Kernel methods provide a simplified framework for localization without any *a priori* knowledge of the complicated relationship between the RSS and position. Instead, these relationships are encapsulated in parametrized nonlinear functions. Algorithms based on kernel methods inherently account for spatial correlation in the RSS, which most model-based approaches fail to capture. Kernel methods do not rely solely on a database of training measurements, like RSS fingerprinting algorithms, which must be measured very densely in space. In this chapter, a calibration scheme is presented

which attempts to minimize the calibration requirements of kernel-based algorithms. Specifically, in this scheme, training is performed simultaneously while the system is online, using the AP pairwise measurements.

A simulation example of a simple four AP network is presented to provide better understanding of kernel methods. The results show that the kernel-based algorithms provide better location accuracy compared to the model-based algorithms, in terms of average RMSE. This is because kernel methods provide an adaptive weighting scheme for the APs. Within this weighting scheme, the APs that have significantly different RSS values compared to the tag are weighted less compared to the other APs.

An extensive experimental evaluation is performed for all the kernel-based algorithms and the MLE using a data set collected from a large hospital facility. These real-world experimental results indicate that all four kernel-based algorithms perform better than the MLE. In fact, the linear signal-distance map localization algorithm has the best performance in terms of average RMSE. The linear signal distance map localization algorithm has an overall RMSE reduction of 37% over the MLE, while the RMSE reduction is as high as 55% for the “sweet spot” areas of the deployment region. The complexities of the fading environment and the complicated nature of the large-scale real-world deployment require more parameters than are available to a single log-distance path-loss model. In particular, even though the linear signal-distance map localization algorithm assumes a linear with respect to log distance relationship for RSS, the parameters of the linear relationship are learned and adapted locally to the RSS measured at each AP.

Another perspective of this analysis is that spatial correlation in the RSS can be particularly useful in wireless localization. Typically, geographically proximate links would encounter similar environmental obstructions and the shadowing loss suffered on these links would be correlated. Better understanding of the area can be obtained when considering spatial correlations. Kernel methods are a strong candidate because the *kernel* in a kernel-based algorithm provides a spatial similarity measure. Additionally, kernel models are typically linear with respect to the parameters, allowing good analytical properties, yet are nonlinear with respect to the RSS measurements.

CHAPTER 5

NETWORK DISTANCE: DISTANCE ESTIMATION VIA MEASUREMENTS WITH NEIGHBORS

5.1 Abstract

Distance estimation between nodes is an important task for a large number of applications in wireless ad hoc networks, *e.g.*, localization and geographic routing. In order to estimate distance between two nodes a and b , most distance estimation algorithms use the direct link measurements made between a and b . In other words, the distance between a and b was estimated *only* from the measurements made between the nodes a and b . In this paper, we explore an alternate means of estimating distance, using the measurements made by a and b with the neighboring nodes. We call these measurements *indirect link measurements* and we call our estimator a *network distance estimator*. In this paper, we motivate *why* indirect link measurements contain relative information between the nodes and show, using an extensive measurement campaign, that distance estimates between the nodes are *more* accurate using indirect link measurements than using direct link measurements. In fact, based on our experimental data the improvement in distance estimates can be as high as 38% compared to the estimator that uses direct link measurements.

5.2 Introduction

A large number of applications of wireless ad hoc networks depend on the ability to estimate distance between pairs of radio devices. For instance, range-based localization algorithms determine the location of the sensor devices using the distance to a selected number anchor nodes [6]; many communication and routing protocols use the knowledge of the distance to neighboring devices for routing of data packets [28, 29, 30].

When estimating the distance between two nodes, a and b , most sensor localization systems use a *direct link measurement* between a and b , for example, the received signal strength (RSS) between a and b [6, 34, 35, 36], or just whether a and b communicate [31, 33, 32, 37, 38]. In this paper, we explore the capability to estimate range between two nodes a and b from indirect link measurements, that is, the measurements between nodes a and k , for $k \neq b$, and between b and k , for $k \neq a$. We find, surprisingly, that the indirect link measurements alone enable better range estimation between a and b than the direct measurement alone. The results should, when indirect link measurements are available, enable improved performance for range-based localization algorithms.

An advantage of a network distance estimator is that nodes a and b do not need to be capable of peer-to-peer communication. For example, two cell phones are not inherently capable of peer-to-peer measurements (without additional wireless network interfaces) and thus cannot directly measure RSS-based range between them. Network distance estimators provide an alternate to direct measurements - rather than measuring signals from the other device, one may instead measure the state of the RF environment at two locations, and use those to infer the distance between the two positions. In fact, a single device may use network distance to discover or estimate how far it has moved, perhaps as a (noisy) complementary measurement for an inertial measurement system.

Most sensor localization systems are either (1) RSS fingerprinting based methods [24, 42, 83] or (2) range-based methods which first estimate relative distance between pairs of nodes and then estimate positions [75, 76, 77]. We note that RSS fingerprinting methods use indirect link measurements to estimate each node's position, but cannot work without an extensive database of calibration measurements. The vast majority of range-based methods use solely direct link measurements to estimate the distance between pairs of nodes. Note that we include so-called "range-free" methods which use direct link measurements of connectivity in this latter category.

This paper proposes to estimate the range between two radios using indirect link measurements, but does not require a database of RSS fingerprints. In this sense, it

partially bridges the gap between RSS fingerprinting and range-based methods.

This work is motivated by analyses of correlated shadowing which indicated the usefulness of correlations in indirect link measurements [14, 15]. This work showed that there are correlations in the shadow fading measured on proximate links, links that travel through similar parts of space, and that those correlations actually reduce lower bounds on localization variance. To achieve lower variance in practice, we believe it is important to explicitly use the correlations in indirect link measurements to estimate the relative positions of nodes.

In this paper, not only do we show that indirect measurements contain relative location information, we also show that range estimates between two radios are *more accurate* using the indirect link measurements only compared to using the direct link measurements only. We certainly do not imply that a method should use one or the other; direct and indirect measurements provide two sources of range estimates which can be combined – but it is surprising to us that indirect measurements lead to *better* range estimates.

The paper is organized as follows. In section 5.3 we present the work related to range estimation from the literature. Next, in Section 5.4 we present the model for distance estimation using indirect link measurements. In Section 5.5 we present an intuition about the relationship between the proposed estimator and the geographic distance. Next, in Section 5.6 we present a brief overview of the range estimators that uses the direct link measurements. In Section 5.7, we describe our experimental set up and in Section 5.8 we present the experimental results. Finally, in Section 5.9 we apply the proposed estimator to localization.

5.3 Related Work

A number of techniques for range estimation have been proposed in the literature. When determining the distance between two devices a and b , most range estimation algorithms use the direct link measurements between a and b , for example, the RSS between a and b [6, 34, 35, 36], or just whether a and b communicate [31, 33, 32, 37, 38].

RSS-based range estimation algorithms use statistical channel models which relate

measured RSS and distance. The most commonly used channel model is the log-distance path loss model, which expresses the ensemble mean of the RSS in dB as linear with the log of distance [19, 80, 14]. Suppose that we want to estimate the distance between two devices a and b . Device a measures the RSS for the signal transmitted by b (similarly b measures the RSS for the signal transmitted by a), which we call the direct link RSS measurement. A standard estimator of distance is the maximum likelihood estimator (MLE) which calculates what distance is “most likely” given the direct link RSS measurement and the log-distance path loss model [6, 88, 73].

In indoor or cluttered environment, however, RSS measurements deviate from the model because they suffer from multipath fading, shadowing, and non-isotropic antenna gain patterns, all of which cannot be known *a priori* [14, 15, 89]. Consequently, systems relying exclusively on the measured RSS for distance estimation remain inaccurate estimators.

Another possible way to obtain distance between the nodes is to first localize the nodes, and subsequently, calculate the distance between the estimated coordinates. To this end, finger printing based methods [24, 42], and multi-hop localization methods [31, 32] can be applied. However, the downside is that multi-hop localization methods need a large number of anchor nodes and fingerprinting methods require a large amount of calibration effort. The method we present in this paper does not require localization as an intermediate step and calibration is also minimal.

5.4 Distance Estimation Model

In this paper, we consider estimation of distance d between two nodes a and b with two modalities of the indirect link measurements, packet reception rate (PRR), and binary connectivity, *i.e.*, whether or not a pair can communicate reliably. We generally call both measurements “connectivity” measurements, because the PRR can be seen as a continuous valued measure of the connectivity.

In this paper, we discuss two types of distances - the dissimilarity in measurement space, and the geographical distance. The “dissimilarity” is a quantification of how

“far apart” one node’s connectivity measurements are from a second node’s connectivity measurements. The dissimilarity is related to the geographical distance because two nodes that are near to each other will have similar connectivity measurements to other nodes in the network. These connectivity measurements are embedded as a vector of higher dimensional space. Such an embedding is called *Lipschitz embedding* [39, 40, 41]. Using the Lipschitz embedding, the important information about the distance between the two nodes can be captured by the dissimilarity measure in the embedding space. Our paper shows that using a nondecreasing function of the dissimilarity provides an estimate of the geographical distance between the nodes. We call the distance estimate using the nondecreasing function of the dissimilarity the *network distance estimate*.

5.4.1 Framework for Network Distance Estimation

Before we describe the framework for the network distance estimation, we define what we mean when two nodes are neighbors of one another. A node k is said to be a *neighbor* of a node a if the link (a, k) between the two nodes is connected *reliably*, that is the packet reception rate (PRR) on the link is greater than a threshold. In other words, we quantify the reliability of the link with the ratio of the number of packets a receiver node has received to the number of packets the transmitter node has sent during a given time window. Within an ideal model for a wireless link, two nodes have a PRR of one if they are within a communication range, and a PRR of zero if they are outside the communication range (disconnected link). However, in real-world radio communication, there is a wide range of distances at which $0 < \text{PRR} < 1$ [114, 115, 116].

Let \mathcal{H}_a represent the set of neighbors of device a excluding b and \mathcal{H}_b represent the set of neighbors of device b excluding a . Note that neither a nor b is a member of either set \mathcal{H}_a and \mathcal{H}_b , since a device cannot communicate with itself, and the a and b neighbor relationship is specifically excluded by definition, even if they can communicate. We refer to the set $\mathcal{K} = \mathcal{H}_a \cap \mathcal{H}_b$ as the set of *common neighbors*. The complementary set \mathcal{K}^c contains:

1. *non-common* neighbors, *i.e.*, $\mathcal{H}_a \otimes \mathcal{H}_b$, where \otimes indicates set of XOR neighbors - nodes which are neighbors of a or b but not both; and
2. *non-neighbors*, nodes that are neighbors of neither a nor b but are not a and b themselves.
3. Nodes a and b themselves.

Let $r_{a,k}$ denote the PRR for packets received by node a and transmitted by node k . Similarly, $r_{b,k}$ denotes the PRR measured by node b for the link (b,k) . We define the “dissimilarity” measure in the embedding space between the nodes a and b , $\delta_{a,b}$ as,

$$\delta_{a,b} = \sum_{k \in \mathcal{K}^c} |f(r_{a,k}) - f(r_{b,k})| - \sum_{k \in \mathcal{K}} f(r_{a,k})f(r_{b,k}), \quad (5.1)$$

where f is a nondecreasing function of the PRR. We hypothesize that the dissimilarity $\delta_{a,b}$ between the nodes a and b is useful for network distance estimation.

The function f in (5.1) transforms the packet reception rates to “weights” on the links between nodes. The weights are assigned based on the reliability of the links. The choice of the function f is, however, arbitrary. In this paper, we consider two types of function f :

1. τ -connectivity:

$$f(r) = \begin{cases} 1 & \text{if } r > \tau, \\ 0 & \text{Otherwise} \end{cases} \quad (5.2)$$

2. τ -PRR:

$$f(r) = \begin{cases} r & \text{if } r > \tau, \\ 0 & \text{Otherwise} \end{cases} \quad (5.3)$$

where $0 \leq \tau \leq 1$ is a threshold PRR.

When τ -connectivity is used, the function f assigns equal weights to all the links that have PRR greater than τ . Consequently, (5.1) simplifies to:

$$\begin{aligned} \delta_{a,b} &= \sum_{k \in \mathcal{H}_a \otimes \mathcal{H}_b} 1 - \sum_{k \in \mathcal{K}} 1, \\ \delta_{a,b} &= |\mathcal{H}_a \otimes \mathcal{H}_b| - |\mathcal{K}|, \end{aligned} \quad (5.4)$$

which is equivalent to using neighbor counts for determining the dissimilarity δ .

On the other hand if τ -PRR is used, it weighs the link to each node with the PRR measured on the particular link. Consequently, neighbors that are closer to the nodes are weighted more compared to the nodes that are far apart. Any PRR less than the parameter τ is truncated to zero.

5.4.2 Discussion

We call the first term in (5.1), $\sum_{k \in \mathcal{K}^c} |f(r_{a,k}) - f(r_{b,k})|$, the ‘‘XOR connectivity’’ between the nodes a and b . From the definition of the set \mathcal{K} , the set \mathcal{K}^c contains non-common neighbors. If a non-common neighbor node k has a link with node a with high reliability and does not have a connected link with node b , then one might infer that nodes a and b are distant. In general, the first term essentially denotes the ‘‘number’’ of non-common neighbors for the two nodes a and b .

In addition, the set \mathcal{K}^c contains nodes k such that the PRR on both the links (a, k) and (b, k) is less than the τ . In other words, links to these nodes k are highly unreliable and such nodes k are distant from both the nodes a and b . The definition of the weighing function f ensures that $f(r_{a,k}) = f(r_{b,k}) = 0$ and thus non-neighbors do not contribute to the XOR connectivity term.

We call the second term in (5.1), $\sum_{k \in \mathcal{K}} f(r_{a,k})f(r_{b,k})$, the ‘‘AND connectivity’’ of the nodes a and b . The similarity is caused by the common neighbors. For example, assuming a uniform deployment of nodes, if two nodes are closer to one another, they will have more common neighbors compared to the nodes that are distant. As the distance between the nodes increases, the number of common neighbors decreases, which makes the neighbor similarity to decrease.

5.4.3 Transforming Dissimilarity to Geographical Distance

As mentioned before $\delta_{a,b}$ gives an estimate of the dissimilarity between nodes a and b and does not represent the geographical distance. It gives an estimate of ‘‘how far’’ node b is from node a in a feature space. The feature space, in our analysis, is given by the connectivity information of neighbor set for nodes a and b .

In order to transform the dissimilarities to geographical distances, we suppose that we can define a non-decreasing function $g : \mathbb{R}^+ \rightarrow \mathbb{R}^+$ which transforms the network

distances δ into geographical distance d .

$$\hat{d} = g(\delta) \tag{5.5}$$

In the next sections we discuss the function g . In Section 5.5, we show that for distances less than the range of the nodes, the function g can be approximated by a polynomial of order one (affine function). In Section 5.8 we evaluate our choice for g using an extensive real-world measurement data set.

5.5 Expected Neighbors with Distance

In this section we show that the estimated dissimilarity δ has an approximate affine relationship with the geographical distance.

For the purposes of providing intuition about the relationship between dissimilarity and geographic distance, we use some ideal channel assumptions. Let us assume that sensors a and b have coverage radius R and are separated by distance d and other sensors are deployed as a Poisson point process. With sensors assumed distributed as a Poisson field, the expected number of other sensors (besides a and b) in an area is λA , where λ is the average density of sensors per unit area, and A is the area. (Note that in a Poisson field the existence of a and b does not affect the distribution of other sensors.) We consider Fig. 5.1 and find A_o , the area of overlapping coverage, and A_n , the area of single coverage either by a or b but not by both.

We can find the area A_o by doubling the area in the segment formed by the vertical line in Fig. 5.1. For example, consider the area in the left-most circle that is also to the right of the vertical line. The area in the segment is the the area in the sector of the circle, minus the area in sector to the left of the vertical line. The area in the sector is θR^2 . The area to be subtracted is two identical right triangles, each with area $\frac{d}{4}R \sin \theta$. Note that trig identities give us:

$$\begin{aligned} \theta &= \cos^{-1} \left(\frac{d}{2R} \right) \\ \sin \theta &= \frac{\sqrt{R^2 - d^2/4}}{R} \end{aligned} \tag{5.6}$$

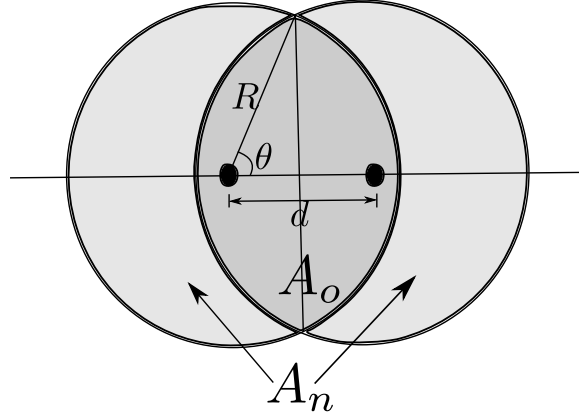


Figure 5.1. Two sensors (\bullet) and their coverage areas, including the area of coverage overlap.

Thus,

$$\begin{aligned} A_o &= 2R^2 \cos^{-1}\left(\frac{d}{2R}\right) - d\sqrt{R^2 - d^2/4} \\ \frac{A_o}{\pi R^2} &= 2/\pi \cos^{-1}\left(\frac{d}{2R}\right) - \frac{1}{\pi} \frac{d}{R} \sqrt{1 - \frac{d^2}{4R^2}} \end{aligned} \quad (5.7)$$

Using (5.7), the normalized area $A_n/(\pi R^2)$ is given as:

$$\frac{A_n}{\pi R^2} = 2 \left(1 - \frac{A_o}{\pi R^2}\right). \quad (5.8)$$

By Taylor's series expansion, the normalized overlap area, $\frac{A_o}{\pi R^2}$, from (5.7) can be written in a polynomial form as:

$$\frac{A_o}{\pi R^2} = 1 - \frac{4}{\pi} \frac{d}{2R} + \frac{1}{\pi} \left(1 - \frac{1}{3}\right) \frac{d^3}{(2R)^3} + \frac{1}{4\pi} \left(1 - \frac{3}{5}\right) \frac{d^5}{(2R)^5} \cdots$$

For nonzero area of overlap, the value of $\frac{d}{2R}$ is always less than one. Consequently, ignoring the higher order terms, we get

$$\frac{A_o}{\pi R^2} \approx 1 - \frac{2d}{\pi R}, \quad (5.9)$$

which gives the first order approximation of the area of overlap. Similarly, using (5.8), the first order approximation of the single coverage of non-overlap area is given as:

$$\frac{A_n}{\pi R^2} \approx \frac{4d}{\pi R}. \quad (5.10)$$

In Fig. 5.2, we plot the value of normalized areas of overlap and non-overlap for a range of values of $\frac{d}{R}$. Also shown in Fig. 5.2 is the first order approximation of the overlap and non-overlap area.

One may see from Fig. 5.2 that the area of overlap, A_o in (5.7), decreases nearly linearly for $d < R$. Similarly, the area of non-overlap, A_n in (5.8), increases nearly linearly for $d < R$. In addition, it can be seen from Fig. 5.2 that for $d < R$ (5.9) and (5.10) provides a good approximation to the true overlap area and true non-overlap area, respectively.

When τ -Connectivity is used, the weighting function f assigns equal weights to all the links and as such the dissimilarity $\delta_{a,b}$ is given by (5.4). Based on our assumption about the nodes being distributed as Poisson field, the expected value of $\delta_{a,b}$, $E[\delta_{a,b}]$ is given as:

$$E[\delta_{a,b}] = \lambda A_n - \lambda A_o.$$

Using (5.9) and (5.10) $E[\delta_{a,b}]$ can be approximated as

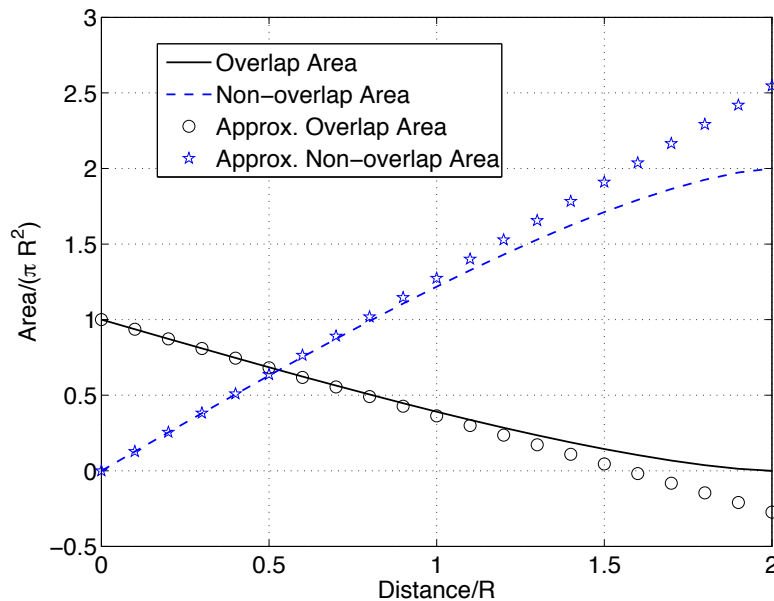


Figure 5.2. The normalized areas of overlap and of non-overlap (one or the other but not both) of two circles of radius R , when their centers are separated by distance d . The plot also shows the first order approximation.

$$E[\delta_{a,b}] \approx \lambda\pi R^2 \left(\frac{6d}{\pi R} - 1 \right).$$

We can normalize the $E[\delta_{a,b}]$ with $\lambda\pi R^2$, where $\lambda\pi R^2$ gives the average number of nodes that are in range of the deployed nodes. We define the normalized $E[\delta_{a,b}]$ as:

$$\frac{E[\delta_{a,b}]}{\lambda\pi R^2} \approx \frac{6d}{\pi R} - 1 \quad (5.11)$$

In Fig. 5.3, we plot the value of normalized $E[\delta_{a,b}]/(\lambda\pi R^2)$ for a range of values of $\frac{d}{R}$. We see that for $d < R$, the $E[\delta_{a,b}]/(\lambda\pi R^2)$ has an approximate affine relationship with $\frac{d}{R}$.

5.6 Prior Range Estimation Algorithms

In this section, we briefly describe distance estimation commonly used in the literature. We first describe algorithms that use direct link measurements *alone* for distance estimation. Next, we present an alternate algorithm, based on the localization algorithms from the literature, that uses the indirect link measurements *alone* for distance estimation.

We begin with the description of direct link distance estimation algorithms.

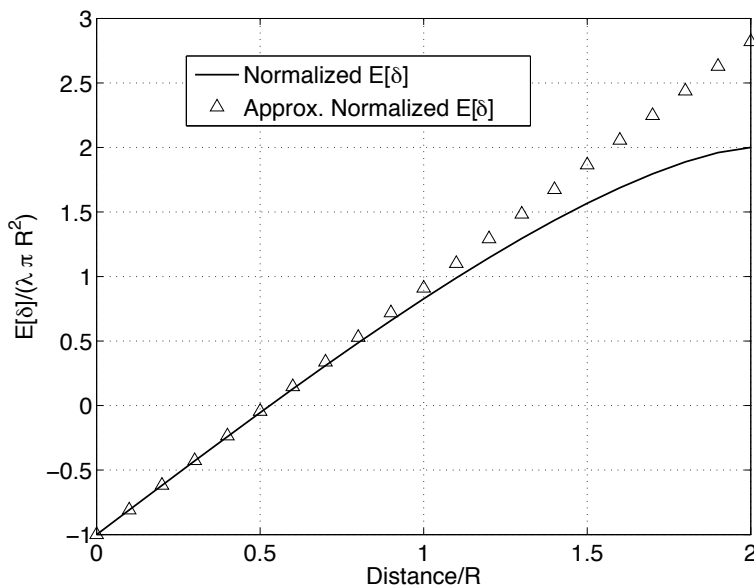


Figure 5.3. The normalized values of $E[\delta_{a,b}]/(\lambda\pi R^2)$ as a function of d/R . The plot also shows the first order approximation.

5.6.1 Direct Link Distance Estimation

In this section, we present a brief description of how traditionally distance is estimated using the direct link measurements between the nodes. There are two well known direct link measurement distance estimators that are commonly used in the literature, namely:

1. Constant per-hop (CPH) distance estimator,
2. RSS-based distance estimator.

In this section, we briefly describe how the distance is estimated in both distance estimators.

5.6.1.1 Constant Per-Hop (CPH) Distance Estimator

Constant per-hop distance estimator is one of the simplest estimators of the distance between two nodes. In this estimator, distance estimate between two nodes is determined based on the *number of hops* in the shortest path between them. For instance, if two nodes a and b are one-hop away (*i.e.*, directly connected), then the distance estimate between the two nodes is equal to a constant, ideally the average distance between all one-hop nodes in the network. If a node c is two hops away from the node a then the distance estimate between a and c is twice the one-hop distance constant. This type of distance estimator is commonly used in methods that use hop count information for distance estimation, *e.g.*, DV-hop [31].

5.6.1.2 RSS-based Distance Estimator

In addition to connectivity, which is used in the CPH distance estimator, the other common direct link measurement used in distance estimation is RSS [6, 88, 73]. One such estimator that uses RSS was introduced in Section 5.3 - the maximum likelihood estimator (MLE) of distance. The expression for the MLE distance estimator, $\hat{d}_{a,b}^{MLE}$, for the link (a, b) is given as [73]:

$$\hat{d}_{a,b}^{MLE} = \Delta_0 10^{\frac{\Pi_0 - \psi_{a,b}}{10n_p}}, \quad (5.12)$$

where $\psi_{a,b}$ is the RSS (in dB) measured on the link (a, b) , Π_0 is the RSS measured at a unit distance of Δ_0 and n_p is the path loss exponent. The RSS $\psi_{a,b}$ is the direct

link measurement between the nodes a and b and the MLE distance estimate $\hat{d}_{a,b}^{MLE}$ depends only on the direct link measurement $\psi_{a,b}$.

It is known that the estimator given by (5.12) is a biased estimator with a multiplicative bias factor [88]. A bias-corrected estimator of the distance is [88, 73]:

$$\hat{d}_{a,b}^{BC} = \frac{1}{C} \hat{d}_{a,b}^{MLE}, \quad (5.13)$$

where

$$C = \exp \left(0.5 \left(\frac{\sigma_{dB} \ln 10}{10n_p} \right)^2 \right),$$

is the bias correction and σ_{dB} is the standard deviation of RSS model error.

5.6.2 Neighbor Connectivity-based Distance Estimator

In this section, we describe an alternate estimator which uses indirect link measurements to estimate the distance between two nodes. We call this estimator *neighbor connectivity (NC)-based distance estimator*.

For every pair of node a and b , we define a connectivity matrix $C_{a,b}$, which represents the connectivity information of the nodes in a “neighborhood” set $\mathcal{S}_{a,b} = \mathcal{H}_a \cup \mathcal{H}_b \cup \{a, b\}$. Specifically, $C_{a,b}$ is a $|\mathcal{S}_{a,b}| \times |\mathcal{S}_{a,b}|$ matrix whose the (i, j) element $C_{a,b}(i, j) = 1$, if the i^{th} element of $\mathcal{S}_{a,b}$ is connected to the j^{th} element of $\mathcal{S}_{a,b}$; and ∞ , otherwise. In addition, since the emphasis is on an alternate estimator using the indirect link measurements, we do not consider nodes a and b to be connected in $C_{a,b}$.

The matrix $C_{a,b}$ can be viewed as connectivity information between the nodes a and b in a higher dimensional space, $\mathbb{R}^{|\mathcal{S}_{a,b}|}$. The distance between the nodes a and b is then determined by computing the Euclidean distance between the representation of the nodes in a lower dimensional space (*e.g.*, 2D or 3D). We use Isomap [117] to determine the 2D representation of the nodes a and b , \mathbf{x}_a and \mathbf{x}_b respectively, from the connectivity matrix $C_{a,b}$. Figure 5.4 shows the block diagram of the distance estimation in the neighbor connectivity-based distance estimator. The last block of normalization is needed because the coordinates \mathbf{x}_a and \mathbf{x}_b are the coordinates in an arbitrary embedding space.

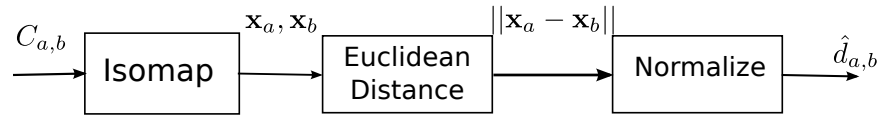


Figure 5.4. Block diagram showing the distance estimation in neighbor connectivity-based distance estimator.

5.7 Experimental Setup

In this section, we describe our measurement environment and the experimental setup.

5.7.1 Measurement Campaign Description

An extensive measurement campaign is performed in which 224 wireless nodes are deployed at known locations on a single floor of a hospital, spanning over an area of 16,700 square meters, as shown in Fig. 5.5. These nodes are IEEE 802.15.4 wireless transceivers which operate in the 2.4 - 2.48 GHz frequency band and transmit at a constant power. The nodes have a limited transmission range, and as such, the network formed by the deployed nodes is not a fully connected network. Each node has a limited set of neighbors. Measurements are made for a period of 10 minutes at 9:15 am on a weekday. During the experimental time each node transmits 40 times. Each time a node correctly demodulates a packet, it records its RSS and counts it has successfully received packets from that transmitting node. The packet reception rate (PRR) is calculated as the total number of received packets from that transmitter divided by 40. We also compute the average RSS over all successfully received packets from that transmitting node. The measurements are collected at a central server for analysis. In this measurement campaign, we know the actual locations of the nodes and, thus, we can determine the actual geographical distance d between every pair of nodes.

Note that for the purpose of determining network distance, the deployed nodes need not have the capability of measuring RSS. All we need is the connectivity information for the network distance. However, in this measurement campaign we have collected RSS measurements to compare the performance of connectivity-based

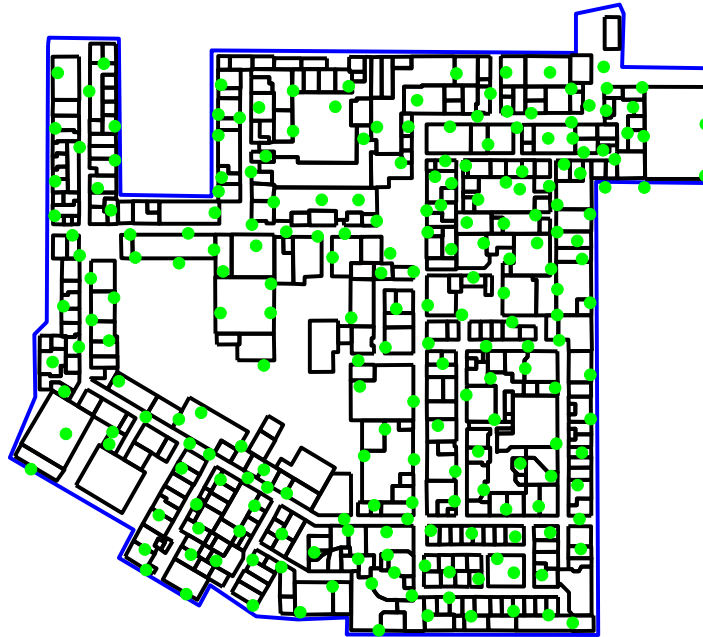


Figure 5.5. Coordinates of the sensors (\bullet) in the measurement campaign.

distance estimation to RSS-based distance estimation.

5.7.2 Experimental Procedure

The experimental procedure involves estimating the geographic distance between the pairs of nodes. For every link (a, b) , we compute the dissimilarity $\delta_{a,b}$ using (5.1) and the network distance estimate $\hat{d}_{a,b}$ using (5.5). We evaluate the performance of the distance estimation in terms of the mean square error (MSE) defined as:

$$MSE = \frac{1}{L} \sum_{a,b} \left(d_{a,b} - \hat{d}_{a,b} \right)^2, \quad (5.14)$$

where L represents the total number of links for which we are estimating the distance and $d_{a,b}$ and $\hat{d}_{a,b}$ represent the actual and estimated geographical distance between the nodes a and b , respectively. The MSE is an average error in m^2 and, consequently, represents the average “area error.” For applications like target tracking and localization, area error is often very indicative of the cost of the distance error – it

is proportional to the area which must be searched when looking for the object or person being located.

We do not propose that the network distance estimator will have the *same* accuracy for all links. As two nodes are further apart, as shown in Section 5.5, the dissimilarity δ changes slowly with distance, and thus we expect that the distance estimates based on δ will be less accurate. To study this effect, we introduce a parameter γ which we call the *PRR limit*. In other words, we will be estimating distance only for links with $\text{PRR} > \gamma$.

Intuitively, as the value of the PRR limit γ increases the number of links that have $\text{PRR} > \gamma$ would decrease. In Fig. 5.6, we plot the percentage of connected links that have a $\text{PRR} > \gamma$ for different values of γ . We observe from Fig. 5.6 that as γ increases, the percentage of connected links that have $\text{PRR} > \gamma$, in general, decreases. From Fig. 5.6 we observe that about 89% of the connected links have a $\text{PRR} > 0.1$ and 71% of the links have a $\text{PRR} > 0.6$, which also goes to suggest that, in our measurement data set, there are not many links with $0.1 < \text{PRR} < 0.6$.

In Fig. 5.7, we plot the average number of non-common and common neighbors

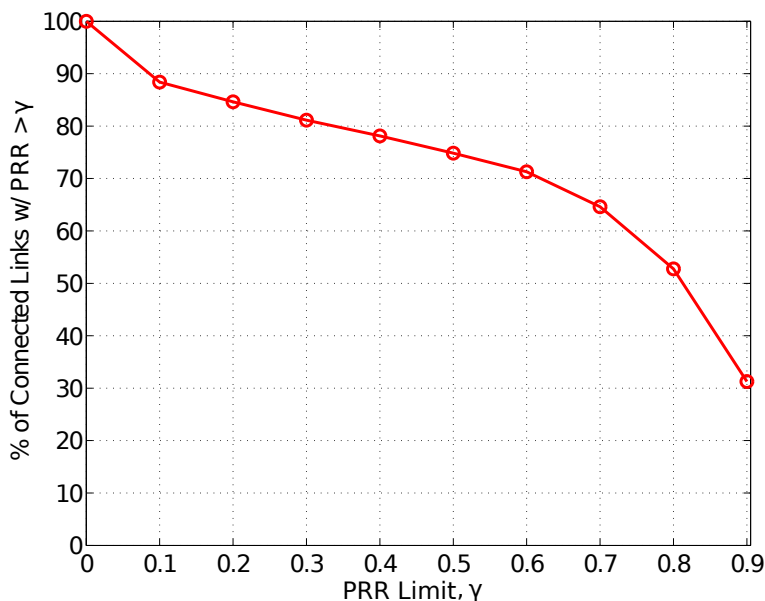


Figure 5.6. Percentage of connected links that have $\text{PRR} > \gamma$ for different values of γ .

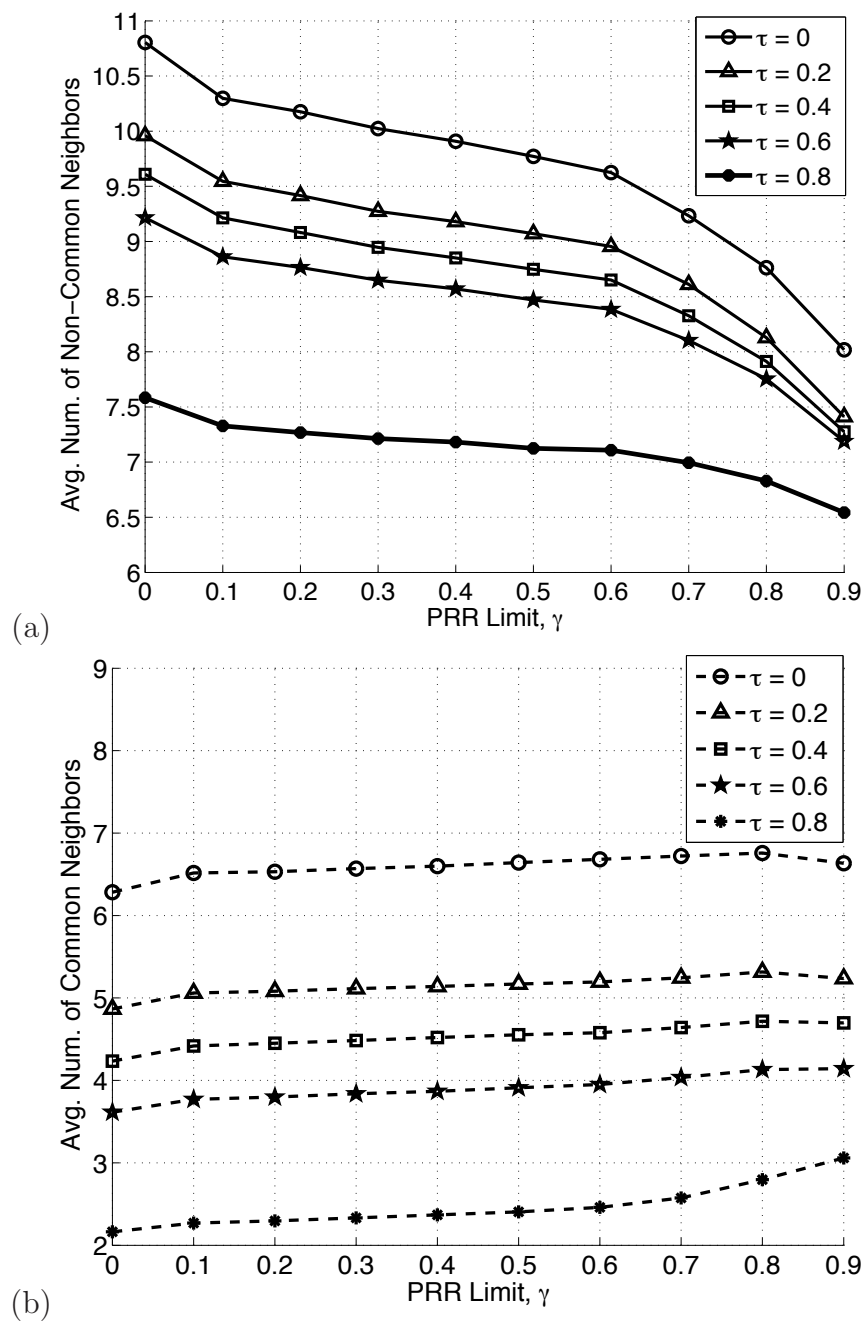


Figure 5.7. Average number of (a) non-common and (b) common neighbors of the pairs of nodes, such that the link between the nodes have $\text{PRR} > \gamma$, for different values of γ and τ .

of node pairs, which have $\text{PRR} > \gamma$ for different values of γ and τ . We observe from Fig. 5.7 that, in general, as the value of γ increases, the average number of non-common neighbors between the pair of nodes decreases. In addition, the average number of common neighbors between the pair of nodes increases. This signifies that as the value of PRR limit γ increases, the links for which we are estimating network distances, on average, becomes smaller.

We have already used τ in (5.2) and (5.3) as a threshold for connectivity and for the weight function f . In essence, τ is a parameter of our distance estimator which determines the set of neighbors for the nodes, which in turn affects the performance of the distance estimator. Increasing the number of links for which we estimate distance by increasing γ will also affect average performance, since the additional links may perform better or worse in our algorithm. By using γ as a separate parameter from τ , we may separately study the performance both as a function of parameter values and the number of links.

An advantage of studying network distance as a function of PRR limit γ is that it allows us to study and evaluate the performance of the network distance estimator for all one-hop links. In addition, it allows us to compare the performance of the network distance estimator with the direct link measurements-based estimators which estimates distances primarily for links that are one hop separated. However, as mentioned in Section 5.2, the network distance estimators can also be used in estimating distance in systems not capable of peer-to-peer communication. In order to study the performance of network distance estimator in such systems, we need a parameter different from γ .

To study network distance for systems, where peer-to-peer communication is not possible, we introduce a parameter $\rho_{a,b}$ for every link (a, b) which we call the *neighbor ratio* and defined as,

$$\rho_{a,b} = \frac{|\mathcal{H}_a \cap \mathcal{H}_b|}{|\mathcal{H}_a \cup \mathcal{H}_b|}, \quad (5.15)$$

where $0 \leq \rho_{a,b} \leq 1$. In other words, we will be estimating distance between nodes a and b that have $\rho_{a,b}$ greater than a threshold ρ . The motivation of using common neighbors in (5.15) is based on the observation of Section 5.5 that as two nodes are

further apart, the number of common neighbors decreases and at sufficiently large distance becomes zero.

5.8 Results

In this section, we investigate and evaluate the performance of the network distance estimator. In addition, in this section, we compare the performance of the network distance estimator with estimators that use *only* the direct link measurements and the network connectivity-based estimator described in Section 5.6.

The organization of this section is as follows. We first validate the affine approximation for the function $g(\cdot)$ in (5.5) using the one-hop link measurement data. Next, we analyze the performance of the network distance estimator as a function of the parameter τ and number of links. Then, we compare the performance of network distance estimator with the existing estimators described in Section 5.6 by estimating the distance for one-hop links. Next, we compare the performance of the network distance estimator for estimating the distances of nodes that are separated by two hops. Finally, we investigate the performance of the network distance estimator for systems in which peer-to-peer communication is not available.

5.8.1 Experimental Validation of Affine Approximation

We have proposed in Section 5.5 that the dissimilarity δ can be converted into network distance estimate \hat{d} using a polynomial function transformation. In addition, we have proposed that for one-hop distances (or distances less than or equal to the communication range of the nodes) the polynomial function can be approximated as an affine function, *i.e.*, a polynomial of order one.

In this subsection, we will evaluate the affine approximation of the relationship between the dissimilarity δ and geographic distance using the measurement data set. Specifically, using the measurement data set, we will demonstrate that the dissimilarity between the nodes that are one-hop away has an affine relationship with the actual geographic distance between the deployed nodes. For the purposes of analysis in this subsection, we will evaluate the distance of the one-hop links that have PRR limit $\gamma = 0.5$. In addition, the value of the parameter τ in (5.2) and (5.3)

is $\tau = 0.5$.

In Fig. 5.8, we plot the dissimilarity δ with respect to the actual geographical distance d . Figure 5.8(a) shows the plot when τ -connectivity is used as the weighting function, while Fig. 5.8(b) shows the plot of τ -PRR as weighting function. Also shown in both the figures is the least-squares linear regression line between δ and d .

To investigate further we determine the network distance estimate \hat{d} from δ for different polynomial orders. Particularly, for every order of the polynomial, we determine the polynomial coefficient values using the polynomial regression between

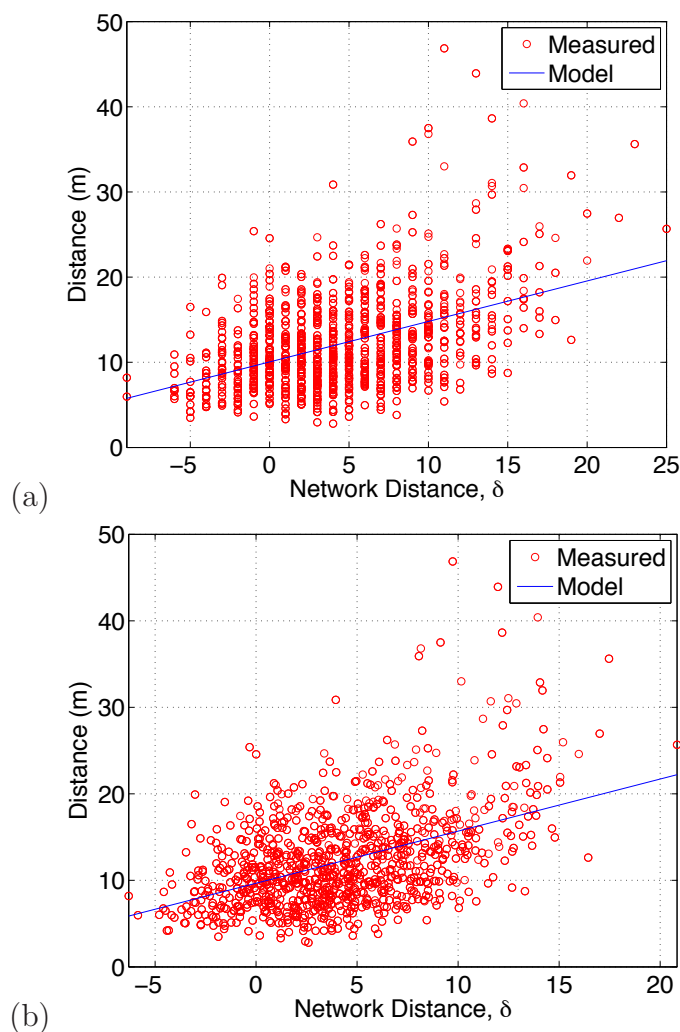


Figure 5.8. Scatter plot of δ computed with (a) τ -connectivity and (b) τ -PRR vs. actual geographical distance d (\circ). Also shown is the least-squares linear regression line (a) $d = 0.48\delta + 10.05$ and (b) $d = 0.60\delta + 9.67$.

the actual geographical distance d and the computed dissimilarity δ . Using these coefficient values, we transform the dissimilarity δ into network distance estimate \hat{d} . To measure the performance of each polynomial order, we compute the MSE between the actual geographical distance d and estimated network distance \hat{d} using (5.14) for different orders of the polynomial. In Fig. 5.9, we plot the relative MSE for different orders of the polynomial.

From Fig. 5.9 we see that the MSE for higher orders of the polynomial is almost the same as the MSE for the first order polynomial. In other words, Fig. 5.9 indicates that the relationship between the geographical distance and the dissimilarity can be well captured by a polynomial function of order one (an affine function). Increasing the order of the polynomial does not significantly reduce the MSE compared to the affine approximation. In addition, higher order polynomials increase the number of parameters, which may result in overfitting [107]. Thus, based on this experiment, we believe it best to model the relationship between the dissimilarity δ and geographical distance d as affine.

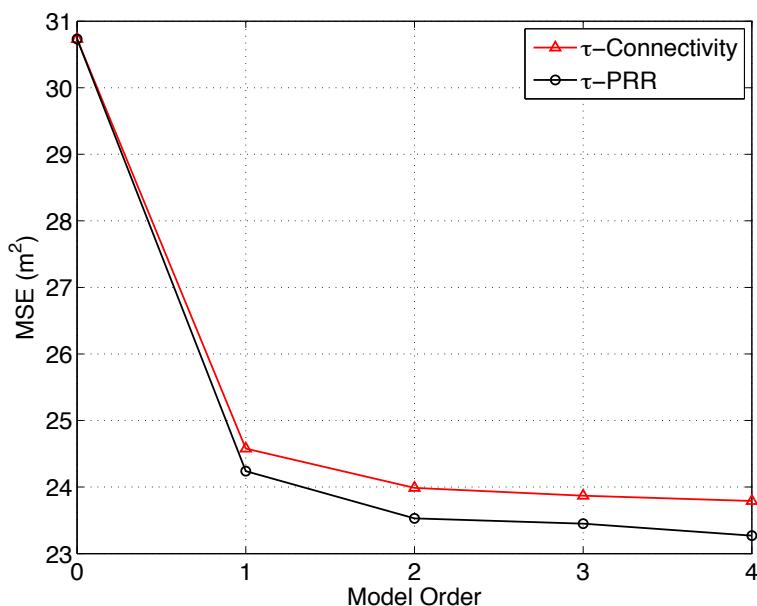


Figure 5.9. MSE vs. model order.

5.8.2 Analysis of Network Distance

In this section, we present an analysis of the network distance as a function of the parameter τ . In addition, in this section, we will investigate the performance of the network distance for different “kind” of links. We classify the links based on their PRR and choose the links using the tuning parameter γ . For instance, if $\gamma = 0$, then we are considering links between the node pairs that received a packet even once between them. On the other hand, links with $\text{PRR} > \gamma = 0.5$ corresponds to those links for which the receiver nodes received packets at least 50% of the time.

We divide the analysis of this section into two parts, namely

1. Analysis as a function of τ for a specific PRR limit, γ . This analysis would signify the dependence of the network distance on τ for the same set of links.
2. Next, we assume a fixed value of τ , and study the performance of the network distance for different kinds of links, *i.e.*, study how the performance varies when the link reliability changes.

5.8.2.1 Analysis as a Function of τ

We begin the analysis by first determining the links between the pairs of nodes that have $\text{PRR} > \gamma$. For these pairs of nodes, we determine the dissimilarity δ using (5.1) and then determine the network distance \hat{d} using (5.5) with $g(\cdot)$ an affine function. We determine the network distance \hat{d} for different values of τ . In Fig. 5.10 we plot the performance of the network distance estimates as a function of τ for $\gamma = 0.1, \gamma = 0.3, \gamma = 0.5, \gamma = 0.7$ and $\gamma = 0.9$. Figure 5.10(a) shows the plot with τ -Connectivity weighing function while Fig. 5.10(b) shows the plot when τ -PRR weighing function is used.

The performance curves in Fig. 5.10 shows that for high τ , the MSE increases, indicating the reduction in the performance. This is expected because when the value of τ increases, we essentially are reducing the number of contributing common and non-common neighbors in (5.1) while estimating the dissimilarity δ . In fact, Fig. 5.10 indicates that using the indirect link information from the so called “unreliable” neighbors can help in improving the network distance estimation.

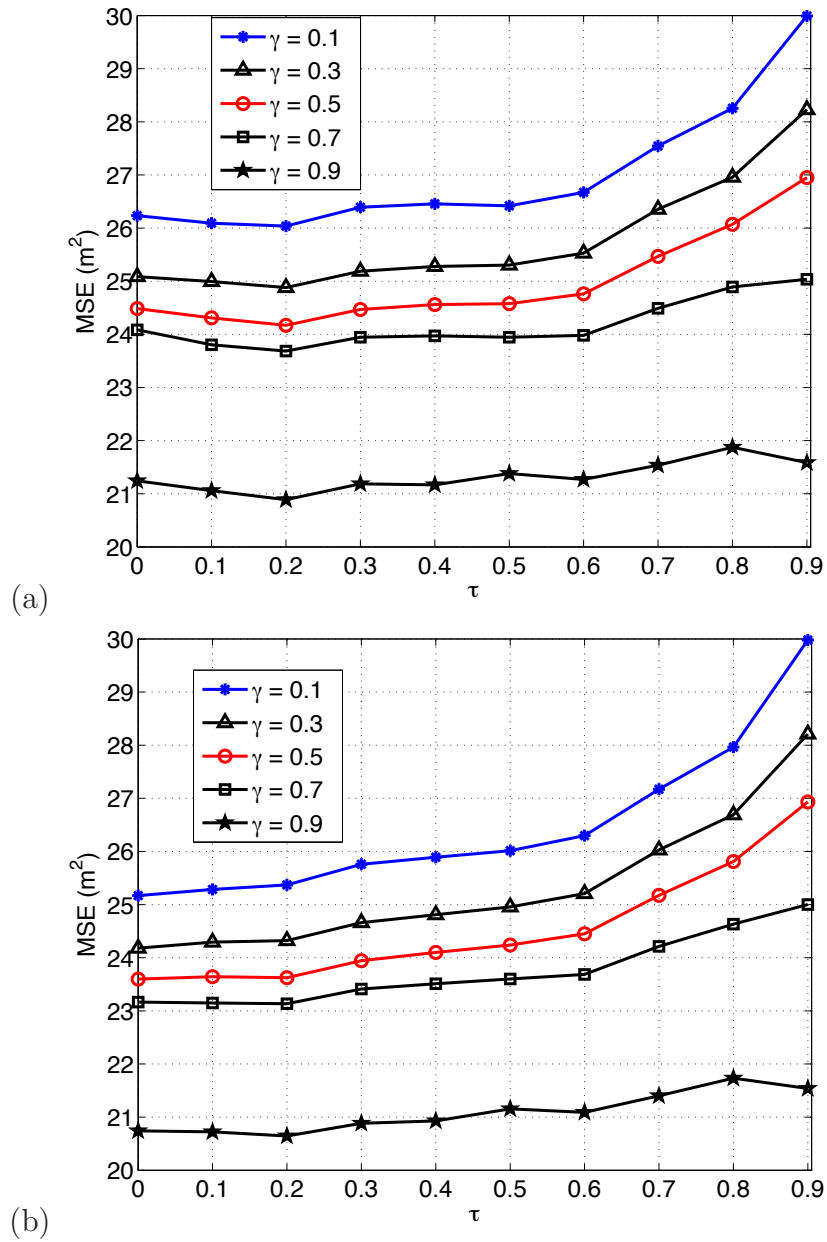


Figure 5.10. MSE of network distance estimate vs. τ for different values of the PRR limit γ . In (a) τ -Connectivity weighing function is used while in (b) τ -PRR weighing function is used.

Another observation that one can make is that when $\tau > 0.6$, the increase in the MSE is more steep compared to that when $\tau < 0.6$. To investigate this issue, we divide the PRR range into 10 equally spaced bins and determine the number of links in each bin. In Fig. 5.11, we plot the normalized number of links in each PRR bin, where the normalization is done such that the number of links in all the 10 bins sum to one. From Fig. 5.11, we observe that in the PRR range of $0 < \text{PRR} < 0.6$, there are not many links compared to the links with $\text{PRR} > 0.6$. Consequently, for $0 < \tau < 0.6$, ignoring links while computing the network distance does not seem to have a drastic effect on the MSE performance.

5.8.2.2 Analysis for Different Link Reliability

From Fig. 5.10 we also see that, for a particular value of τ , as the value of γ decreases the MSE increases. A decrease in γ signifies that we are estimating path lengths of the links that have low reliability (lower PRR) as well. For instance, when γ falls from 0.5 to 0.2, it means that in addition to the links that have a $\text{PRR} > 0.5$, we are estimating path lengths of the links that have a $0.2 < \text{PRR} < 0.5$. A lower

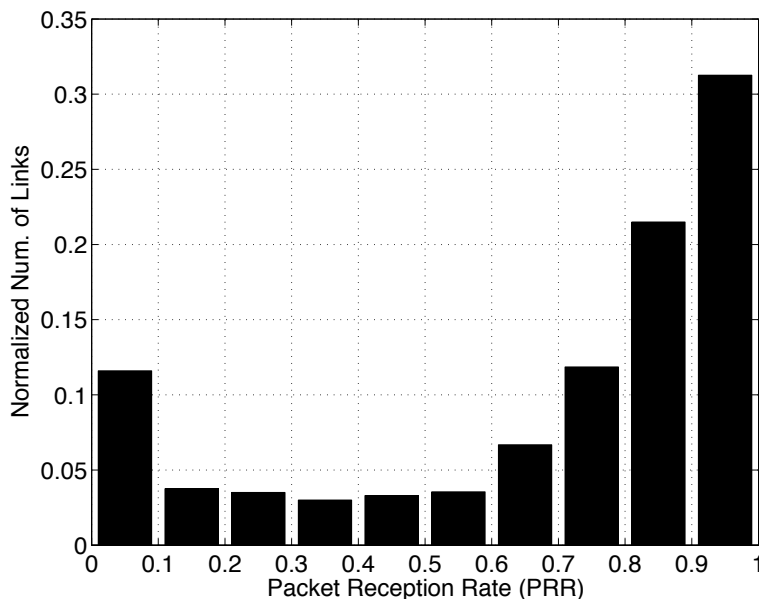


Figure 5.11. Normalized number of links in each PRR bin. The normalization is done such that the sum of the links in all the bins is one.

value of γ signifies that on average we are considering links that have a poor reception, which could be because of either increase in the fading or interference on the links or increase in the distance between the node pairs [114], [115]. This section is a study of the PRR limit γ on the performance of network distance estimator.

In Fig. 5.12 we plot the MSE of the network distance estimates for the links with $\text{PRR} > \gamma$ for a range of values of γ . While computing the network distance, we have assigned the value of $\tau = 0.2$.

From Fig. 5.12 we confirm that the MSE is a monotonically varying function of γ . In addition, we observe that there is a sharp decrease in the MSE when γ increases from $\gamma = 0$ to $\gamma = 0.1$. In fact, compared to $\gamma = 0$, when $\gamma = 0.1$, the MSE decreases by almost 30%. On the other hand, the decrease in MSE from $\gamma = 0.1$ to $\gamma = 0.9$ is about 18%, an average decrease of about 2.3% per step size of γ .

The results in Fig. 5.12 show that the performance of the network distance estimator is, in general, high for links that have high PRR. In our measurement campaign, we see that when we do not consider links with $0 < \text{PRR} < 0.1$, the MSE improves by 30%. On the other hand, when we remove the links with $0.6 < \text{PRR} < 0.7$, the

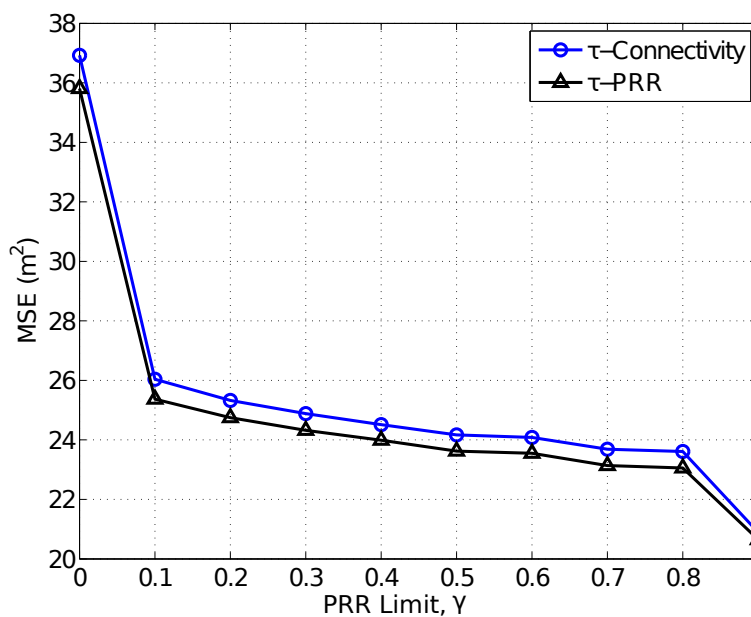


Figure 5.12. MSE vs. PRR limit γ .

MSE does not have a significant change.

5.8.2.3 Discussion

The analysis of this subsection shows that τ and γ have opposite effects on the network distance performance. The performance of network distance benefits when we consider the PRR on the “indirect” links for estimating the distance. On the other hand, the network distance estimates are not so accurate for nodes which have low “direct” link PRR.

The analysis of the performance of network distance estimator with respect to PRR limit γ shows that higher values of γ is desirable. However, setting a higher PRR limit would also mean that we are estimating distance for fewer links in the network, which is not desirable in applications like localization. However, from the analysis we find that a severe degradation in the performance occurs for links whose $0 < \text{PRR} < 0.1$. Consequently, for the rest of this section, we set $\gamma = 0.1$, *i.e.*, we consider links which have $\text{PRR} > 0.1$. Increasing γ does not offer a significant improvement in the performance, but decreases the number of links for which we estimate distances.

5.8.3 Comparison of Network Distance with Other Distance Estimators

In this subsection, we compare the performance of the network distance estimator with the prior distance estimators from the literature, briefly outlined in Section 5.6. Specifically, we compare the performance of the network distance estimator with

1. Neighbor connectivity (NC)-based distance estimator,
2. Constant per-hop (CPH) distance estimator,
3. RSS-based distance estimator.

5.8.3.1 Comparison with Neighbor Connectivity (NC)-based Distance Estimator

In Fig. 5.13, we compare the CDF curves of the squared error for network distance estimators with respect to the NC-based distance estimator. Following the curve for

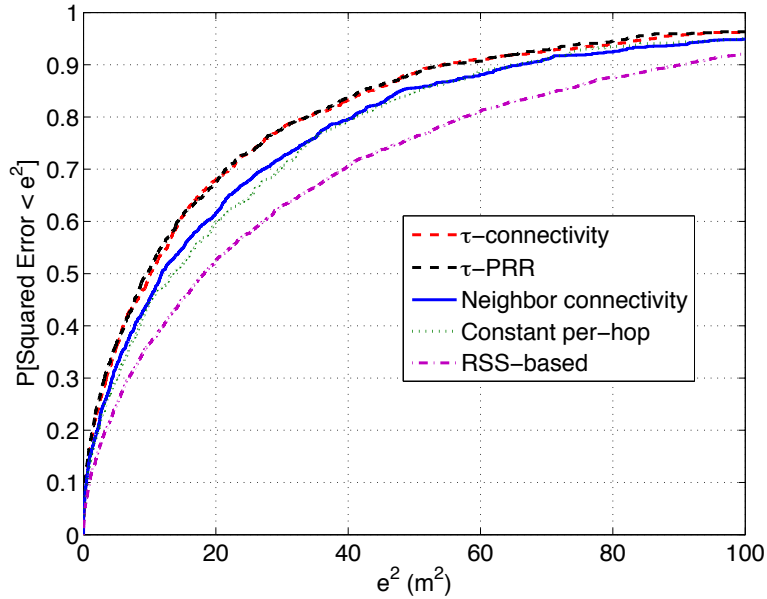


Figure 5.13. CDF plots of the squared errors for network distance estimators (τ -connectivity and τ -PRR), Neighbor connectivity (NC)-based distance estimator, constant per-hop (CPH) distance estimator and RSS-based distance estimator.

NC-based distance estimator, we observe that in NC-based distance estimator 90% of the squared errors lie below 64.23 m^2 . In comparison, the network distance estimators have 90% of the squared errors lying below 54.76 m^2 for τ -connectivity and 54.28 m^2 for τ -PRR, an improvement of about 15% compared to the NC-based distance estimator. The MSE results are tabulated in Table 5.1. In general, the τ -connectivity decreases the MSE by 20.5% compared to that of NC-based distance estimator. In addition, the τ -PRR decreases the MSE by 23% compared to the NC-based distance estimator.

5.8.3.2 Comparison with Constant Per-Hop (CPH) Distance Estimator

In Fig. 5.13, we show the performance comparison of the network distance estimators with respect to the CPH distance estimator. Figure 5.13 shows that in the CPH distance estimator, 90% of the squared errors in the distance estimates lie below 65.76 m^2 , an increase of about 17% compared to the network distance estimators. The

Table 5.1. Table showing the MSE of the distance estimates between nodes that are one hop separated for different algorithms.

Estimator	MSE (m ²)	% decrease from NC-based	% decrease from CPH	% decrease from RSS-based
τ -connectivity	26.01	20.5%	24.5%	36.5%
τ -PRR	25.30	22.7%	26.6%	38.2%
NC-based	32.71	-	-	-
CPH	34.46	-	-	-
RSS-based	40.96	-	-	-

MSE results are shown in Table 5.1. In general, in comparison with the CPH distance estimator, the network distance estimator using τ -connectivity decreases the MSE by 24.5%, while the decrease in MSE using the network distance with τ -PRR is 27%.

The constant average distance estimator is in a way linked to the network distance estimator. Specifically, the constant average distance estimator is equivalent to using a zero-order polynomial, *i.e.*, a constant, to transform the dissimilarity to network distance estimate \hat{d} . In other words, when using a zero-order polynomial for $g(\cdot)$, every distance estimate is the same. Since, in this subsection, we are estimating the distance of only the one-hop links, the distance estimate is constant for all links.

5.8.3.3 Comparison with RSS-based Distance Estimator

In Fig. 5.13 we compare the RSS-based distance estimator given by (5.13) with the network distance estimators. It can be seen that the network distance estimators, both τ -connectivity and τ -PRR, outperform the RSS-based direct link distance estimator. In fact, in the RSS-based distance estimator, 90% of the squared errors are less than 90.14 m², which is about 40% increase from the network distance estimators. In Table 5.1, we also show the MSE of the RSS-based distance estimator. In general, our network distance estimators reduce the MSE by as much as 38%.

5.8.4 Distance Estimation Between Two-Hop Nodes

In many applications one needs to determine the distance between the nodes that are not connected. One such application is multi-hop localization, where we need to estimate distances to other nodes or anchors which are not in direct communication range.

A commonly used way of determining the distance between two nodes a and b , which are not in the communication range of each other, is to approximate the geographical distance between the nodes with the distance along the shortest path between the nodes a and b [31, 38, 33, 118]. However, the shortest-path distance approximation does not work well for nodes that are far away, *i.e.*, spanning over multiple hops. Also, the errors in the distance estimation accumulate over multiple hops. In general, it has been found that the shortest-path approximation works well for nodes that are separated by two hops [37]. In this section, we will evaluate the performance of the network distance for estimating the distance between the nodes that are two hops away.

An important feature for the network distance estimators is that if we need to estimate the distance between nodes that are two hops separated, we need not use the shortest-path approximation. This is because while estimating the network distance we do not use direct link measurements. Network distance estimators use the indirect link measurements *i.e.*, measurements with the neighbors of the nodes a and b . So even for nodes a and b that are separated by two hops, there are nodes that are common, and non-common, neighbors to a and b .

5.8.4.1 Validation of Affine Approximation for Two-Hop Links

We first begin with demonstrating that even for estimating the distances between the nodes that are separated by two hops, the affine relationship between dissimilarity and geographical distance holds. This can be seen in Fig. 5.14 which shows the scatter plot of the dissimilarity δ with the actual geographical distance between the nodes that are two hops apart. Also shown in Fig. 5.14 is the polynomial regression line for both the τ -Connectivity and τ -PRR weighing functions. Similar to the analysis

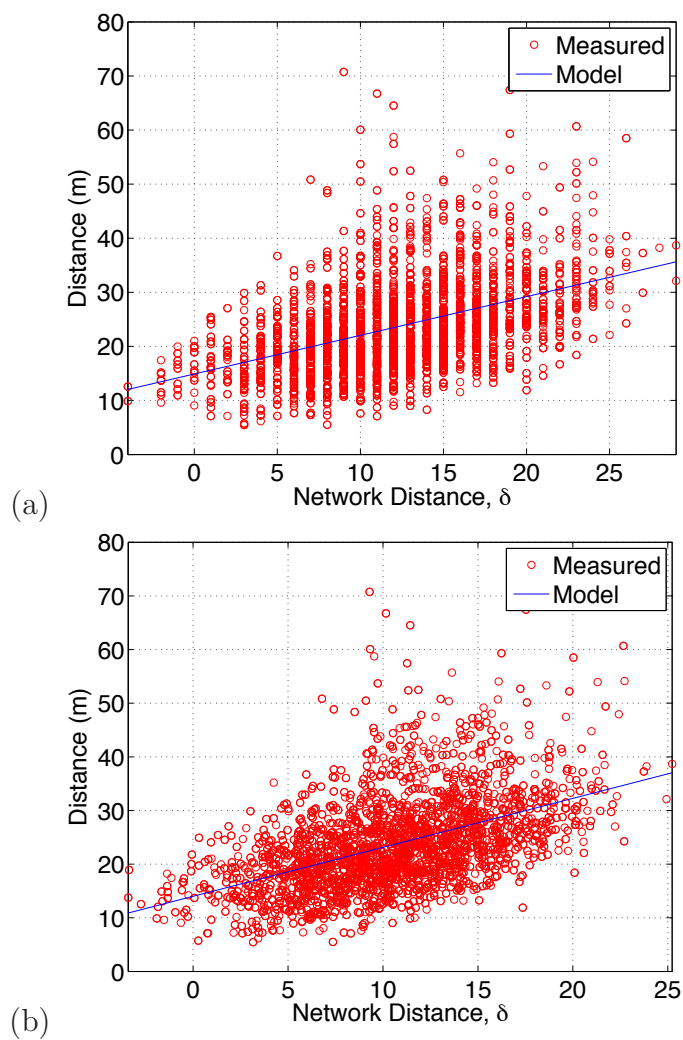


Figure 5.14. Scatter plot of δ computed with (a) τ -Connectivity and (b) τ -PRR vs. actual geographical distance d (\circ). Also shown is the least-squares linear regression line (a) $d = 0.72\delta + 14.90$ and (b) $d = 0.91\delta + 14.02$.

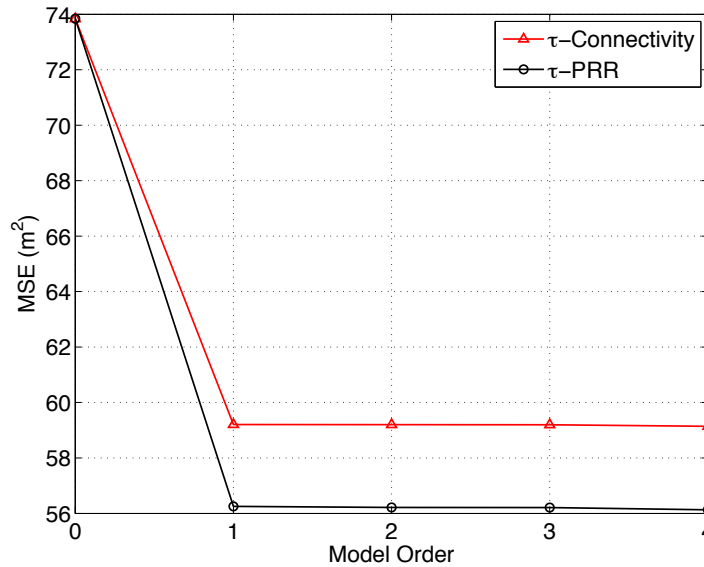


Figure 5.15. MSE vs. model order for computing distance between nodes that are two hops away.

of Section 5.8.1, we assume $\tau = 0.5$ and $\gamma = 0.5$ for the plots in Fig. 5.14.

In addition, in Fig. 5.15 we plot the MSE between the network distance estimate using δ for different polynomial orders. We can see from Fig. 5.15 that for higher order polynomial (*i.e.*, orders greater than one), the MSE does not change significantly. Thus, we can say that the first order approximation (affine approximation) between dissimilarity and geographical distance holds true even for two-hop distance estimation.

5.8.4.2 Comparison with Other Distance Estimators

In this section, we compare the performance of the network distance estimators for the two-hop links with the direct-link estimators, presented in Section 5.6. Before we begin the comparison with direct-link estimators, we plot the performance of the network distance estimators as a function of τ . As in Section 5.8.2, we assume the links which have a PRR > 0.1 as connected. In Fig. 5.16, we plot the MSE of the network distance estimators for estimating distance between nodes that are two hops separated as a function of τ .

As with the one-hop links, the network distance estimators benefit from low values

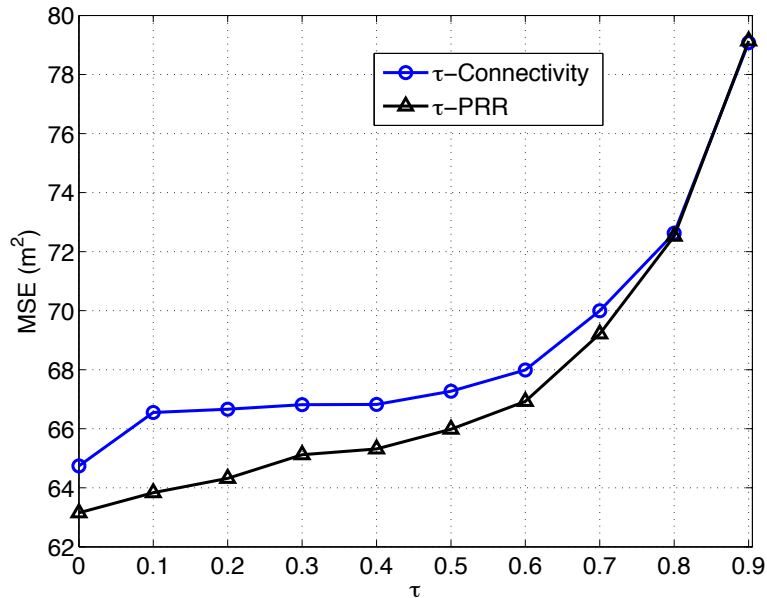


Figure 5.16. MSE of network distance estimates vs. τ for links that have PRR > 0.1 .

of τ . Compared to the one-hop links (Fig. 5.10), where the minimum MSE occurs at $\tau = 0.2$, for the two-hop links the minimum MSE occurs at $\tau = 0$. The reason for the decrease in the value of optimum τ is that the nodes that are separated by two hops would, in general, have fewer common neighbors. Consequently, with the increase in the value of τ , there would be fewer common neighbors, compared to the non-common neighbors. Consequently, the dissimilarity δ for such nodes would be predominantly given by the non-common neighbors, which would be in the saturation region (Fig. 5.2 for $\text{Distance}/R > 1$).

In Fig. 5.17 we compare the network distance estimators with the prior estimators outlined in Section 5.6. In the constant per-hop distance estimator and RSS-based distance estimator, the distance between the two-hop nodes is approximated by the sum of the distance along the shortest-path between the two nodes.

We can see from Fig. 5.17 that the network distance estimators perform consistently better than all the prior distance estimators including the constant per-hop distance estimator, the RSS-based distance estimator and the neighbor connectivity (NC)-based distance estimator. Specifically, we observe that in constant per-hop

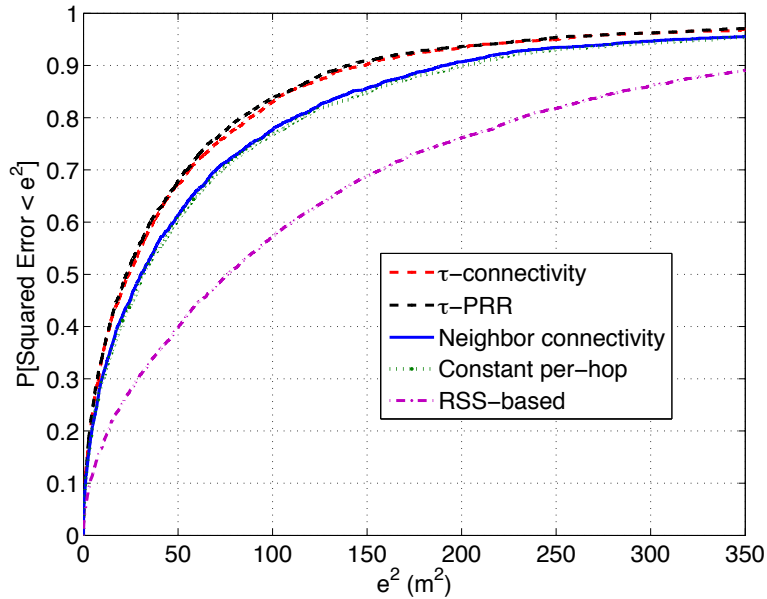


Figure 5.17. CDF plot of the squared errors for network distance estimators (τ -connectivity and τ -PRR) and direct-link measurement estimators (constant per-hop and RSS-based). The error is computed for distance estimation between nodes that are two hops separated.

distance estimator, 90% of the squared error is less than 202.07 m², while for the RSS-based distance estimator, 90% of the squared error is less than 386.98 m². In addition, in the case of NC-based distance estimator, 90% of the squared errors lie below 191 m². Compared to these prior distance estimators, the network distance estimator using τ -connectivity has 90% of the squared errors less than 148.23 m². Similarly, the network distance estimator using τ -PRR has 90% of the squared errors less than 139.33 m².

The average performance in terms of the MSE is shown in Table 5.2. In general, we observe that the network distance estimator reduces the MSE by much as 27% compared to the constant per-hop (CPH) distance estimator, while the decrease in the MSE compared to the neighbor connectivity-based distance estimator is as high as 25%. In addition, the reduction in the MSE compared to the RSS-based distance estimator is as high as 59%.

Table 5.2. Table showing the MSE of the distance estimates between nodes that are two hops separated for different algorithms.

Estimator	MSE (m ²)	% decrease from NC-based	% decrease from CPH	% decrease from RSS-based
τ -connectivity	64.74	23%	25%	58%
τ -PRR	63.15	25%	27%	59%
NC-based	83.70	-	-	-
CPH	86.29	-	-	-
RSS-based	153.75	-	-	-

5.8.4.3 Comparison with Shortest-Path of One-Hop Network Distance

Another way of determining the distance between the nodes that are two hops separated is to use the sum of one-hop network distance along the shortest path between the node pairs. In this subsection, we determine if using the two-hop network distance estimates is better than finding the shortest path from one-hop network distance estimate graph.

In Table 5.3, we tabulate the MSE for both ways of estimating network distance between the nodes that are two hops separated, namely, (a.) two-hop network distance and (b.) shortest-path from one-hop network distance graph. We observe that two-hop network distance performs almost the same as the shortest-path from one-hop network distance graph. In fact, the two-hop network distance is just about 2% better than the shortest-path from one-hop network distance graph.

This is a motivating result and can be desirable in applications like localization

Table 5.3. Table showing the MSE of the distance estimates between nodes that are separated by two hops for two possible network distance estimates.

Network Distance	τ -connectivity	τ -PRR
two-hop	64.74 m ²	63.15 m ²
shortest-path from one-hop graph	66.05 m ²	65.15 m ²

because we need not perform a separate calibration for one-hop and two-hop links. Note that the affine function parameter values for transforming dissimilarity δ to network distance \hat{d} are different for the one-hop links and the two-hop links. One can estimate distance for only one-hop links and use a shortest path algorithm to estimate the distances for two-hop links without a significant affect on the network distance estimator performance.

On the other hand, in applications like mapping of mobile devices where the information that the nodes a and b are one hop away or two hops away is not available, we can still get a reliable network distance estimate by considering the dissimilarity between a and b and as long as there are some common neighbors between a and b . We, however, leave this analysis for future work.

5.8.5 Distance Estimation for Non-Peer-to-Peer Systems

In this subsection, we present an analysis of the performance of the network distance in a system not capable of peer-to-peer communication. Specifically, this subsection is a study of the conditions required on the neighbor ratio $\rho_{a,b}$ for a reliable estimate of network distance.

In order to evaluate the performance of the network distance as a function of $\rho_{a,b}$, we divide the range of $\rho_{a,b}$ into ten equally spaced bins and for each bin determine the links (a, b) whose $\rho_{a,b}$ lie the bin. In Fig. 5.18 we plot the MSE of the network distance estimates for each bin of $\rho_{a,b}$.

From Fig. 5.18, we observe that as $\rho_{a,b}$ increases, the MSE of the distance estimators decreases. An increase in the value of $\rho_{a,b}$ means that relative to the number of total neighbors, the number of common neighbors between two nodes a and b increases, which in turn means that the node pairs are closer to one another. Consequently, the distance can be better estimated, which explains why the MSE decrease when $\rho_{a,b}$ increases.

In addition, we observe that dramatic improvement in the MSE occurs when $0 < \rho_{a,b} < 0.1$ increases to $0.1 < \rho_{a,b} < 0.2$. Increasing the neighbor ratio beyond $\rho_{a,b} = 0.2$ does not have a dramatic improvement in the network distance estimates. As such, we observe that there is a *knee of the curve* at $\rho_{a,b} = 0.1$. We propose that

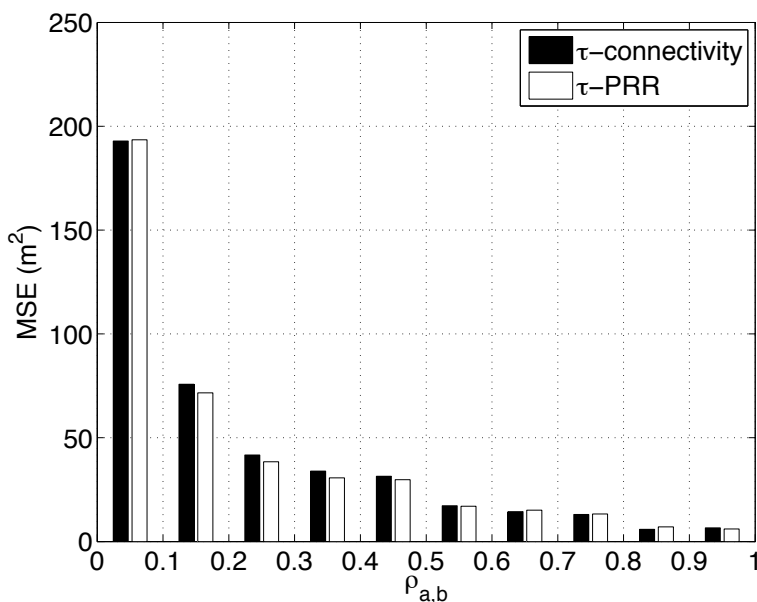


Figure 5.18. MSE of the distance estimators for each ρ bin.

the threshold value ρ required for a reliable network distance estimate is $\rho = 0.1$. In other words, the number of common neighbors that are required for reliable network distance estimates should be at least 0.1 times the number of total neighbors of the two nodes.

Finally, we compare the performance of the network distance estimator with other distance estimators outlined in Section 5.6. In Table 5.4 we tabulate the MSE of the distance estimates for the links that have $\rho_{a,b} > \rho = 0.1$. We see that for links (a, b) with $\rho_{a,b} > 0.1$, the network distance estimators, which have no knowledge about the direct link measurements between a and b , perform better than the estimators which have the direct link measurements between the nodes a and b . Specifically, compared to CPH distance estimator, the network distance estimators reduce the MSE by as much as 34%, while compared to RSS-based distance estimator, the reduction in the MSE is as high as 55%. In addition, even compared to a prior distance estimator that uses the indirect link connectivity measurements between a and b , the network distance estimator reduces the MSE by as much as 25%.

Table 5.4. Table showing the MSE of the different distance estimators for the links that have $\rho_{a,b} > 0.1$.

Estimator	MSE (m ²)	% decrease from NC-based	% decrease from CPH	% decrease from RSS-based
τ -connectivity	32.47	19%	29%	52%
τ -PRR	30.12	25%	34%	55%
NC-based	39.94	-	-	-
CPH	45.47	-	-	-
RSS-based	67.21	-	-	-

5.9 Localization Using Dissimilarities

The results we have presented in the previous section show that the network distance estimate \hat{d} performs better than the existing methods in the literature. Specifically, the proposed network distance estimator performs 27% better than the constant per-hop distance estimator for estimating one-hop distance. Constant per-hop distance estimator is commonly used in connectivity based algorithms, *e.g.*, DV-hop [31]. In addition, the proposed network distance estimator outperforms the RSS-based distance estimation by reducing the MSE by 38% compared to the MSE of the RSS-based estimator.

Once dissimilarity is transformed into network distance, one could use it in different applications, *e.g.*, localization. However, the transformation of dissimilarity δ to network distance estimate \hat{d} requires estimation of the polynomial coefficients, which, if unknown for the environment of deployment, requires a priori environmental knowledge or calibration effort. In this section, we investigate if we can directly use the dissimilarity estimates δ , bypassing the intermediate step of transforming the dissimilarity to network distance estimates.

For our purposes of evaluation, we choose one of the most commonly used localization algorithms in the literature, namely MDS-MAP (*a.k.a* Isomap) [38, 37, 117, 119, 120]. One of the motivating features of using Isomap for our evaluation is that in Isomap, the distance estimates between nodes need to be proportional to geographical distance estimates, but may have an arbitrary unknown proportionality constant. It

produces a relative map but not an absolute map of the nodes. A postprocessing step is usually needed wherein all coordinate estimates are transformed (rotated, scaled and translated) by the transformation that makes the coordinate estimates of the known location nodes best match their *a priori* known coordinates in a least-squares sense. Because of the scaling in this postprocessing step, the distance estimates between nodes need only be proportional to the geographical distance.

5.9.1 Procedure

In Isomap [38], the distances between the non-neighboring nodes are replaced by the distance along the shortest path between the node pair. Isomap does not work well on non-isotropic or nonconvex networks because for these networks the shortest path between all the node pairs will not correlate well with the geographical distance [37]. The purpose of this section is not to propose a new localization algorithm, but to use an existing algorithm to showcase that indirect link measurements can actually be more useful than the direct link measurements.

We divide the deployment area into fourteen small clusters, using a k-means clustering algorithm on the deployment area as shown in Fig. 5.19. The nodes in each cluster in Fig. 5.19 are represented by the same marker shape. In addition, for each cluster, we choose three reference nodes (nodes which have known their location) for the postprocessing step. The reference nodes for each cluster are shown in Fig. 5.19 with a solid *black* line around the marker shape.

5.9.2 Preprocessing for Dissimilarity

Before we can use dissimilarity δ in Isomap, we need to perform a preprocessing step. This is needed because some dissimilarities (especially for smaller geographic distances) are negative, which are not physically meaningful. Consequently a positive constant is added, which is large enough to make all values of δ positive. Specifically, we transform $\delta_{a,b}$ for all links (a,b) to $\hat{\delta}_{a,b}$ as

$$\hat{\delta}_{a,b} = \delta_{a,b} - \min_{(a,b)} \{\delta_{a,b}\}, \quad (5.16)$$

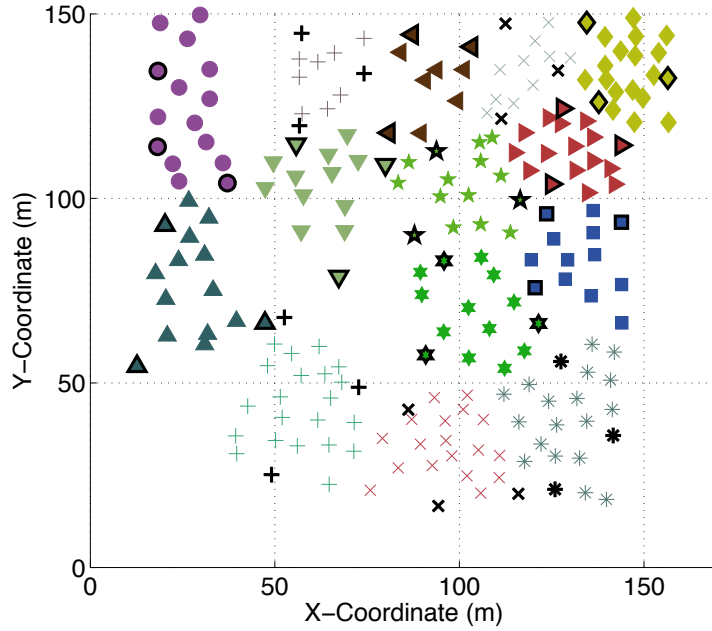


Figure 5.19. Figure showing the nodes in different clusters. Nodes in the same clusters are shown by the same marker type. Also shown are the reference nodes for each clusters, with black solid lines on the boundary of each marker type.

where the minimum is taken over all one-hop and two-hop links. Once transformed, $\hat{\delta}_{a,b}$ can then be used as distance estimates in the Isomap. In this paper, we evaluate two possible ways of using $\hat{\delta}_{a,b}$ as distance estimates, $s_{a,b}$, in the Isomap:

- **Method a:**

$$s_{a,b} = \hat{\delta}_{a,b}, \quad (5.17)$$

for all one-hop and two-hop links (a, b) .

- **Method b:**

$$s_{a,b} = \begin{cases} \hat{\delta}_{a,b}, & \text{if } (a, b) \text{ is one-hop link,} \\ \min_k (\hat{\delta}_{a,k} + \hat{\delta}_{k,b}), & \text{O.W.} \end{cases} \quad (5.18)$$

The main difference between Method a and Method b is that in Method a we use $\hat{\delta}_{a,b}$ as distance estimates for all the one-hop and two-hop nodes. On the other hand, Method b uses $\hat{\delta}_{a,b}$ as distance estimates for only one-hop nodes and uses the shortest-path algorithm on the graph, with $\hat{\delta}_{a,b}$ as the distance between the one-hop

nodes, in order to determine distances between the nodes that are separated by more than one hop.

5.9.3 Results

In this section, we compare localization performance of the two methods described in Section 5.9.2 with the prior distance estimators, which are (a.) Neighbor connectivity-based distance estimator, (b.) Constant per-hop distance estimator, and (c.) RSS-based distance estimator.

We quantify the performance in terms of MSE, defined as

$$MSE = \frac{1}{N} \sum_i \|\mathbf{x}_i - \hat{\mathbf{x}}_i\|^2, \quad (5.19)$$

where \mathbf{x}_i is the actual coordinate of the node i , $\hat{\mathbf{x}}_i$ is the estimated coordinate of the node i and N represents the total number of deployed nodes.

We present the localization performance results under the two settings of determining the links for which we estimate distance using the distance estimator, as described in Sections 5.7 and 5.8. They are,

- Using the PRR on the direct link between the nodes a and b , where we estimate distance only for links whose $PRR > \gamma = 0.1$.
- Using the neighbor ratio, ρ , between a and b , where we estimate distance between the node pairs (a, b) which have $\rho_{a,b} > \rho = 0.1$.

5.9.3.1 Using PRR on Direct Link

In Fig. 5.20 we plot the MSE of the location estimates using the dissimilarities on links with $PRR > 0.1$, as a function of τ . From Fig. 5.20(a) we observe that the MSE when using Method a for distance estimates is lowest when $\tau = 0.2$. Similar results were seen for the distance estimation using network distance, in Fig. 5.10, where the lowest MSE was obtained when $\tau = 0.2$. This would explain why the MSE is lowest for $\tau = 0.2$ when using Method a. In contrast, when using Method b for the distance estimates, the lowest MSE is obtained when $\tau = 0.5$.

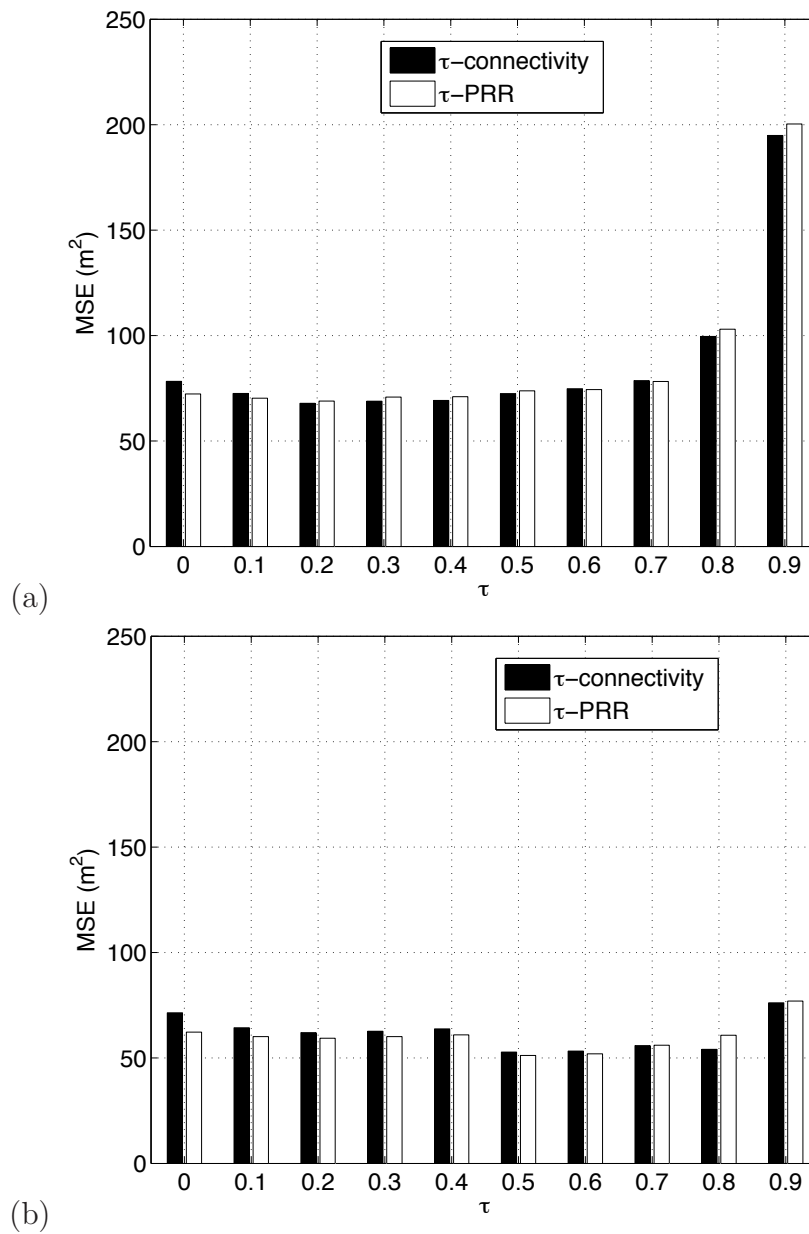


Figure 5.20. MSE of the location estimates using transformed dissimilarity as a function of τ . In (a), method a is used to determine the distance estimates $s_{a,b}$ in Isomap and in (b), method b is used to determine the distance estimates $s_{a,b}$ in Isomap

In Table 5.5, we tabulate the MSE of the dissimilarities along with the MSE using neighbor connectivity (NC)-based distance estimator, constant per-hop distance estimator and RSS-based distance estimator.

In general, from Table 5.5 we observe that localization using dissimilarities have lower MSE compared to the prior distance estimators. We also observe that using Method b for distance estimates in Isomap has better localization performance compared to the Method a. Specifically, using Method b with τ -connectivity, the localization MSE reduces by 27% compared to the CPH distance estimator, while the τ -PRR reduces the MSE by 29% compared to the CPH distance estimator. Compared to the RSS-based distance estimator, the localization MSE decreases by as high as 37%, while the MSE reduces by 14% compared to the NC-based distance estimator. The reason for better performance for method b compared to method a is that the dissimilarity is not linear but affine with respect to geographical distance.

5.9.3.2 Using Neighbor Ratio

In this subsection, we only present results for the transformation by Method b. In Fig. 5.21 we plot the MSE of the location estimates using dissimilarities on the node pairs, which have neighbor ratio $\rho > 0.1$, as a function of τ . We observe that, similar to the PRR case, the minimum MSE is obtained when $\tau = 0.5$.

In Table 5.6, we tabulate the MSE of different estimators. We observe that, overall, the proposed dissimilarities as distance estimates perform better than the prior distance estimators. Specifically, the improvement over NC-based distance

Table 5.5. Table showing the MSE of the location estimates for different distance estimators.

Distance estimator	Method a	Method b
τ -connectivity	67.90 m ²	52.85 m ²
τ -PRR	68.89 m ²	51.27 m ²
NC-based distance	59.60 m ²	59.60 m ²
Const. per-hop distance	71.91 m ²	71.91 m ²
RSS-based distance	80.82 m ²	80.82 m ²

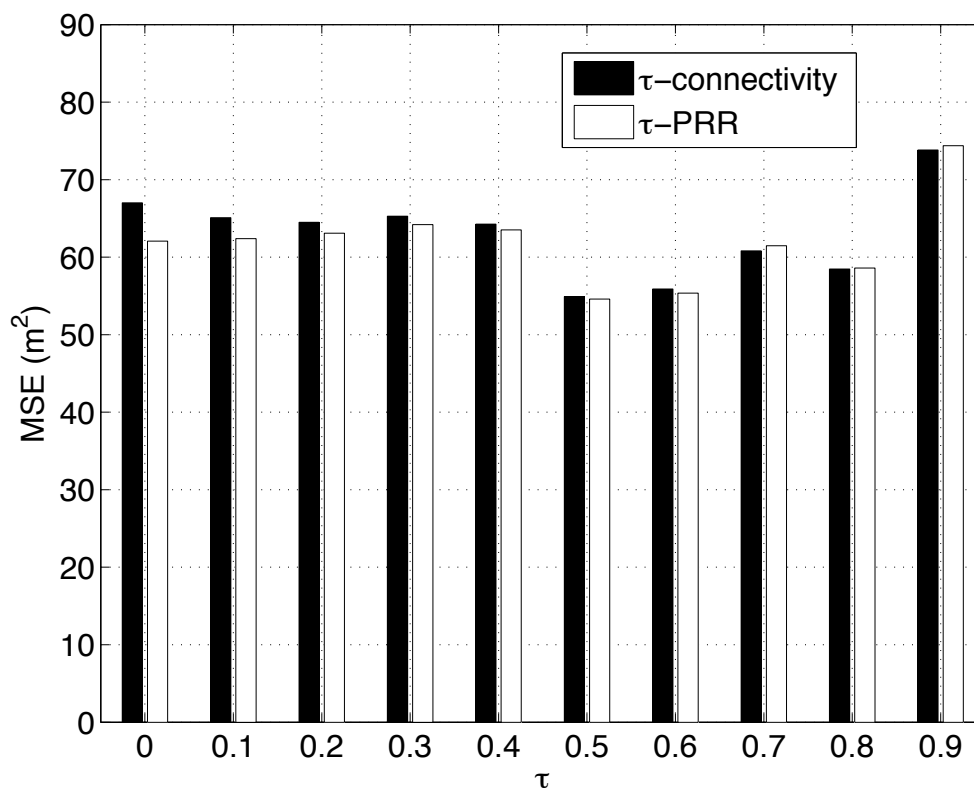


Figure 5.21. MSE of the location estimates using transformed dissimilarity with Method b on node pairs with neighbor ratio $\rho > 0.1$ as a function of τ .

Table 5.6. Table showing the MSE of the location estimates for different distance estimators using neighbor ratio as a parameter to determine the links.

Distance estimator	MSE (m ²)
τ -connectivity	54.90 m ²
τ -PRR	54.46 m ²
NC-based distance	75.16 m ²
Const. per-hop distance	78.50 m ²
RSS-based distance	85.22 m ²

estimator is as high as 28%, while compared to the CPH distance estimator the improvement is 31%. In addition, the improvement over the RSS-based distance estimator is 36%.

5.10 Conclusion

Traditionally, most systems use the direct link measurements for estimating the distance between two nodes a and b . Direct link measurements correspond to the pair-wise measurements made between the nodes a and b . In this paper, we explore the capability to estimate range between the nodes a and b using the indirect link measurements, which are the measurements made by nodes a and b with a node k such that $a \neq k$ and $b \neq k$. We consider range estimation with two modalities of the indirect link measurements, namely binary connectivity and packet reception rate (PRR). We call the proposed estimator the *network distance* estimator.

The study of indirect link measurements for range estimation was motivated by the analyses of correlated shadowing, which indicated that correlations in the indirect measurements can help in reducing the lower bound on localization. In this paper, we propose a framework which quantifies the correlation between the nodes a and b with the connectivity information of a and b with their neighbors, which gives a “dissimilarity” measure between a and b . The dissimilarity does not represent the geographic distance, but gives an estimate of “how far” node b is from node a in a feature space. The network distance estimate is then determined by using a nondecreasing function of the dissimilarity measure.

In this paper we show that for estimating the range between nodes that are one-hop and two-hop separated, the nondecreasing function can be approximated as an affine function. We also show that for the purposes of localization, we can directly use the dissimilarity measure, bypassing the need for estimating the coefficients of the affine function.

Using an extensive measurement campaign in an area of 16,700 square meters, we show that distance estimation using the indirect link measurements alone performs better than distance estimation using the direct link measurements alone. In fact, we find that the proposed estimator, which uses indirect link measurements alone, can improve the range estimation by as much as 38% compared to estimators that use the direct link measurements.

In real world system, we do not intend to ignore the direct link measurements. Instead from this work we intend to emphasize the importance of using indirect link measurements in range estimation. In a real system, when possible, one may combine the direct link and indirect link distance estimates in order to provide a distance estimate better than either alone. However, we leave this estimate fusion for future work.

CHAPTER 6

CONCLUSION

This chapter summarizes key findings before suggesting areas for future work.

6.1 Key Findings

The rising need to locate and track assets necessitates the development of efficient localization algorithms. RSS based localization algorithms are strong candidates because deploying devices that measure RSS is inexpensive. In indoor environment, the RSS measurements are unpredictable because of fading, losses because of walls and obstacles in the path and non-isotropic antenna gain patterns. Efficient modeling and understanding of the statistics of the errors is key in improving any RSS-based localization algorithm. This research aims to provide efficient models for the measured RSS and use the lessons learned from these models to develop and evaluate efficient algorithms that improve localization.

Radio propagation measurement and modeling for a single radio link has been extensively reported in the literature over the past century. Current channel models for multi-hop networks consider shadowing on links to be independent. This is a simplifying assumption because shadowing fading is determined by the environmental obstructions, and geographically proximate links pass through similar obstructions. To this end, there is a need for statistical channel models for multi-hop networks which can model the correlation in shadow fading between proximate links.

The effort to model the shadowing correlation is also motivated by the fact that no existing correlated link shadowing model is valid for arbitrary pairs of links in ad hoc networks. One of the commonly used shadowing models, the Gudmundson model, does not consider link pairs that do not have a common endpoint. An adaptation was proposed by Wang, Tameh and Nix, when both the ends of a link are mobile cannot

be applied directly to ad hoc networks as there would be an ambiguity in which two distances to use in the covariance function. In addition, we prove by counterexample that a naïve application of the Gudmundson model to model joint shadowing losses in a multi-link network does not guarantee a valid covariance matrix.

A new statistical joint path loss model, called NeSh, was presented that relates the shadowing fading on different links in a multi-hop network to the random underlying spatial loss field. We show that the NeSh model agrees with the existing path loss models when considering a single link, and in that essence, NeSh models the second-order statistics of the measured RSS on links. NeSh model was validated using an extensive measurement campaign, involving indoor and outdoor environments and in two different frequency bands, 900 MHz and 2400 MHz. These data sets also demonstrate statistically significant shadowing correlations among particular geometries of link pairs and show that correlated shadowing can be measured in a repeatable experimental setup as well as in natural outdoor environmental sensor network deployments.

A quantitative analysis of effects of the real-world phenomenon of correlated shadowing on link is studied for path connectivity statistics in simple multi-hop networks. The analysis showed the importance of the consideration of shadowing correlation in reliable network design. Using the traditional model the probability of end-to-end path failure is underestimated by a factor of two or more. In addition, when the network is designed for high reliability, the effects of ignoring link shadowing correlations are dramatic.

In a separate study in which this research contributed, it was demonstrated that correlation in link shadowing can actually reduce the lower bound on the localization variance [15]. These results indicate that estimators which consider correlations between link measurements when estimating node's location will aid the effort to achieve the lowest possible variance. Motivated by these results, we study, investigate and experimentally evaluate a class of algorithm called kernel-based localization algorithms.

Kernel-based localization algorithms use *kernel methods*, a class of statistical

learning algorithms, to explicitly learn correlations in RSS measurements using training data and then use these correlations to classify or estimate a node's location. Kernel methods provide a simplified framework for localization without any *a priori* knowledge of the complicated relationship between the measured RSS and position. Instead these relationships are captured by parametrized nonlinear functions. The complexities of the fading environment and the complicated nature of the large-scale real-world deployment require more parameters than are available to a single log-distance path-loss model. In fact, in our experimental campaign, we observe an improvement as high as 55% over the estimator that uses the log-distance path-loss model.

In this research, a general mathematical framework is provided for kernel-based localization algorithms. This enables us to study different kernel-based algorithms in the literature under a unified framework and also facilitates the comparison of different kernel-based localization algorithms. We study four different kernel-based localization algorithms under this framework and compare and contrast their performance using simulations and extensive real-world measurements. The developed framework would also assist future research in the field of kernel-based localization algorithms by providing an understanding of *how* kernel-based algorithms are different from model-based algorithms and *why* kernel-based algorithms perform better.

A simulation example of a simple four AP network is presented to provide better understanding of kernel methods. The results show that the kernel-based algorithms provide better location accuracy compared to the model-based algorithms, in terms of average RMSE. This is because kernel methods provide an adaptive weighting scheme for the APs. Within this weighting scheme, the APs that have significantly different RSS values compared to the tag are weighted less compared to the other APs.

Kernel methods are a strong candidate because the kernel in a kernel-based algorithm provides a spatial similarity measure. Additionally, kernel models are typically linear with respect to the parameters, allowing good analytical properties, yet are nonlinear with respect to the RSS measurements.

Traditionally most range-based localization algorithms use direct link measure-

ment, which is the pairwise measurement between the two nodes, for estimating the distance between the nodes and subsequently their locations. In other words, the range between two nodes a and b is estimated purely based on the measurement made between a and b . In this work, we propose an alternate range estimator for estimating range between the nodes a and b which uses the *indirect link measurements*, that is the measurements made between nodes a and k , for $k \neq b$ and between b and k , for $k \neq a$. We consider range estimation with two modalities of the indirect link measurements, namely binary connectivity and packet reception rate (PRR). We call the proposed estimator as *network distance* estimator.

The study of indirect link measurements for range estimation was motivated by the analyses of correlated shadowing, which indicated that correlations in the indirect measurements can help in reducing the lower bound on localization. In this paper, we propose a framework which quantifies the correlation between the nodes a and b with the connectivity information of a and b with their neighbors, which gives a “dissimilarity” measure between a and b . The dissimilarity does not represent the geographic distance, but gives an estimate of “how far” node b is from node a in a feature space. The network distance estimate is then determined by using a nondecreasing function of the dissimilarity measure.

In this research, we show that for estimating the range between nodes that are one-hop and two-hop separated, the nondecreasing function can be approximated as an affine function. We also show that for the purposes of localization, we can directly use the dissimilarity measure, bypassing the need for estimating the coefficients of the affine function.

Using an extensive measurement campaign in an area of 16,700 square meters, we show that the range estimation using the indirect link measurements alone enables better range estimation than the direct link measurements alone. In fact, we find that the proposed estimator, which uses indirect link measurements alone, can improve the range estimation by as much as 38% compared to estimators that use the direct link measurements.

A considerable part of this research is focused on developing efficient models for a

specific application of RSS-based localization. The developed models, however, find their use in other applications of wireless sensor networks as well. For instance, the NeSh model forms the basis of developing applications like radio tomography imaging, distance estimation using indirect link measurements can be used for the purposes of efficient routing of data packets.

6.2 Future Work

The work of this dissertation has many possible avenues of future research. Some of these avenues are discussed in this section.

In this dissertation, we considered one aspect of improving the channel modeling for multi-hop networks by considering shadowing correlation between links. However, there are some device effects which are not yet modeled. A radio device a that is not in the direct communication range of device b does not mean that the device a does not receive any signal from device b . Rather, it simply means that the signal power from device b was so low that a could not demodulate the signal. We know the RSS measured between a and b is low, but we cannot quantify the value because the RSS value was not measured. This non-measurement of RSS is known as the “censored data” problem in statistics and current channel models do not consider this censoring of measured data. They simply use the measured RSS to model the relationship between RSS and distance. One avenue of future investigation is to model the relationship between RSS and distance using censored regression models. These models add a penalty to links that are supposedly not connected.

So far most RSS-based localization algorithms consider that the gain pattern of the antennas on the sensors are isotropic. In other words, the gain of the antenna is the same at all angles. In large enterprise wide deployment, the sensors are typically attached to walls, close to the power outlets to reduce the cost for replacing batteries and increase their lifetime. The antenna gain of such sensors would not be the same as would be measured in a free space, because of the electromagnetic interaction between the antenna and nearby environment within a few wavelengths of the antenna, *e.g.*, walls. The presence of walls or obstructions in close proximity of the sensors would

have considerable effect on their radiation pattern, which affects the localization accuracy. Future research in the RSS-based localization algorithms should account for this directionality in the antenna gain pattern caused by the environment.

In addition, the gain pattern estimation should be self-calibrating and should have minimum calibration effort. In other words, the models should account for a change in the antenna gain pattern when the environment changes without the need of recalibration. A possible way is to use the measurements made by a sensor with its neighbors. Particularly, efficient modes should be developed which can estimate the antenna gain pattern (and its directionality) of each sensor from the RSS measured by the neighboring sensors.

In this work, we have emphasized the importance of only the spatial correlation between the link pairs for the purposes of localization. A possible extension is to consider the temporal correlations on the link as well. In general, measurements made on a wireless link would exhibit some correlation over time, which would be inversely proportional to the small-scale fading experienced on the link. If the small scale fading is low, then the measurements made on a single link over time would be highly correlated. On the other hand, if the fading is high, then the measurements over time would deviate more from their mean value, thereby decreasing the overall correlation over time. By modeling these spatio-temporal characteristics of the wireless link, one can design better localization algorithms with improved performances.

In general, it has been found in many experimental evaluations that the coordinate estimates vary considerably over time even for a stationary device. Typically, the variance of the coordinate estimates over time is represented by a $1\text{-}\sigma$ covariance ellipse as shown in Chapter 4. The variance of the coordinate estimates over time, especially for a stationary tag, degrades the performances of the localization algorithm and, more generally, degrades the performance of tracking algorithms. A major cause of these variabilities in the coordinate estimates is fading, which causes the RSS measured on a stationary link to vary considerably over time. A possible avenue of future research is to determine what statistics of the measured RSS characterizes the change in the environment, which in turn causes the temporal variations in the

coordinate estimates.

Once the statistic of the measured RSS is determined, we can use it to correct the measured RSS or more generally correct the coordinate estimates. In addition, the determined statistic should be self-configuring and should change with the environment without human intervention. One possible idea is to use the RSS measured between the anchor nodes (or APs) to continuously estimate and track this statistic.

The goal of the localization algorithms considered in this dissertation is that the calibration effort should be minimum and the system should be self-configuring. In particular, we discussed a method in which training is done simultaneously while the system is online, using the pairwise measurements between the anchor nodes (or APs). Specifically, several anchor nodes are deployed at some known locations throughout the deployment area. Each anchor node is a transceiver and can measure the RSS of the packets from other anchor nodes, which constitute the training data for calibration purposes. However, these anchor nodes (or APs) are not deployed densely but are deployed such that maximum spatial coverage is possible with a minimum number of nodes. Because the anchor nodes are placed far apart from one another, there is a “spatial smoothening” by the kernel function which can cause a severe degradation in the system performance. Future research should focus of developing better kernel algorithms, which can overcome the spatial smoothening caused by the kernel functions.

Another possible avenue for future research is to use multiple localization algorithms, with a tunable parameter. The tunable parameter would allow us to change from one localization algorithm to another localization algorithm, or, more generally, use a weighted average of the coordinate estimates from different algorithms.

Future mobile devices will increasingly have multiple wireless technologies. For instance, GPS, bluetooth, 802.11 wireless LAN and near field communication (NFC) are all bundled on a single mobile chip. These different technologies offer multiple sources of location information for a wireless node. A possible avenue for future research is to fuse the measurements from these multiple technologies to infer the location of a wireless node. Efficient data fusion algorithms and techniques should

be developed which can efficiently extract location information from each technology. For instance, location estimates based on 802.15.4 technology can be improved by using the measurements from NFC. An early study of using multiple technologies for localization was done by Pandya *et al.* in [121].

In this research, we have focused on a particular type of RSS-based localization algorithms which uses kernel methods as a tool to learn the correlation in the RSS measurements. However, many model-based algorithms can also be readily adapted to consider link correlations, for example the belief propagation network approaches such as in [122]. A possible direction of future research is to improve the model-based algorithms using methods that consider link correlations. In addition, model-based localization algorithms can be developed that use the spatio-temporal correlations in the RSS measurements.

In many applications, the 2-dimensional (2-d) or 3-dimensional (3-d) coordinate estimate of a sensor node may not be of much importance. For instance, in the scenario of asset tracking in hospitals the 2-d coordinate estimate of the asset is not intuitive information about the location of the asset. In fact, if instead of the 2-d coordinate estimate, the room or area of the asset is reported, the location information is more intuitive. One possible way is to translate the 2-d coordinate estimate to room estimate by determining the room in which the 2-d coordinate lies. However, this may not always give the best performance. Most localization algorithms are designed to reduce the RMSE of the 2-d coordinate estimates. Consider a scenario where a user wants to search for an asset, and the localization algorithm shows that the object is in a room A. In reality, the asset is in the room close to a wall of the room A, but on the wrong side of the room. In this scenario, even though the RMSE of the estimate is low, the room indicated is incorrect. Future research, in these applications, should focus on developing room-based localization algorithms. For instance, kernel-based localization algorithms could be extended into kernel-based classification algorithms, which uses a linear model for classification (instead of regression) [107]. Another extension is to use support vector machines (SVM) to determine a hyperplane that separates the measured RSS into multiple classes.

Location estimates can be used as a foundation in enabling efficient workflow for many applications. For example, in food processing chain automatic location estimates can determine if a particular food product has passed through prescribed steps before it can be launched into the market. For instance, one can determine if all the processing steps are followed by observing the series of location estimates. If the location corresponding to a particular processing step is missing, then one can determine which step has been missed and the processing can repeat from that step onwards. Future research in this direction, algorithms should be developed that filters out spurious location information over time and also apply approaches of “data mining” to extract relevant information from the series of location estimates.

In many applications, tracking and localization go hand in hand. It is possible that tracking of mobile sensors could be done simply by reinitializing the measurement and location process. However, this would not take advantage of mobility to improve localization performance or to reduce bandwidth over time. There have been many tracking algorithms used in the literature, *e.g.*, Kalman filtering, extended Kalman filtering, and more generally particle filtering. In indoor enterprise wide sensor deployment, human motion is constrained by the presence of walls and floors. Accuracy of the tracking algorithms can be improved by using various constraints imposed by the internal structure of the building, *e.g.*, walls and path constraints. In addition, most tracking algorithms track the 2-d coordinate estimates of sensors. Little effort has been made to track the room estimates. Algorithms, based on Markov chains, should be developed and investigated that track the room estimates.

We have proposed a distance estimator that estimates distance between two nodes a and b from the indirect link measurements. We have considered two modalities of indirect link measurements, packet reception rate (PRR) and binary connectivity, *i.e.*, whether two nodes are connected or not. Another modality of indirect link measurements that needs to be explored is the RSS measured on the indirect links.

In this work, we have only explored the capability of indirect link measurements alone and have found that indirect link measurements alone enable better distance estimation than the direct link measurements alone. Another possible avenue of future

research could be to determine an estimator of distance that uses both the direct link measurements and the indirect link measurements.

An advantage of network distance estimator is that the nodes a and b do not need to be capable of peer-to-peer communication. Network distance estimators provide an alternate way of estimating the distance by measuring the RF environment at two locations. This is particularly used in applications where one has to determine how far a single node has moved between time t_1 and t_2 - there is no peer-to-peer measurements between the nodes at the two time instances. A possible avenue of future research could be to map the network distance estimates to how far a node has moved. This could help in improving the performance of inertial measurement system (IMS) which are prone to errors and the errors tend to increase with time in an unbounded manner because of the integration.

In this research, we have shown that the network distance estimators do not have the same accuracy for all links. The accuracy depends on the PRR of the links for which we are estimating the distance. Another direction of future research in network distance is to determine a sufficient statistic based on the indirect link information alone. This could enable us to determine a criterion of when to use network distance especially in the system where peer-to-peer communication is not possible. Furthermore, localization algorithms should be developed which can efficiently tap on the performance of the network distance estimator.

As another research direction, network distance can be used in geographic or geological routing. There are often paths in multi-hop networks that consume less power than the shortest straight line path between two nodes, and network distance (specifically dissimilarity) may be a better representation of the network connectivity. In a recent research [123] the authors have proposed a routing scheme which uses a vector of hop-count to a fixed set of anchor nodes (determined for the entire network) as a node's "virtual coordinate." Our approach of determining the dissimilarity, presented in Chapter 5, is similar in the context that we determine dissimilarity, which is a measure of distance in a virtual embedding space. However, a difference between the approaches is that in our approach we do not consider a predetermined

set of anchor nodes for the entire network. Instead, we consider the hop-count information to the nodes that are “local” to the pair of nodes. Using the proposed dissimilarity measure, future research could enable more energy efficient and scalable routing protocols for large sensor networks with less human moderation and efforts.

REFERENCES

- [1] C. Newport, D. Kotz, Y. Yuan, R. Gray, J. Liu, and C. Elliott, “Experimental evaluation of wireless simulation assumptions,” *Simulation*, vol. 83, no. 9, pp. 643–661, 2007.
- [2] M. Perkins, N. Correal, and B. O’Dea, “Emergent wireless sensor network limitations: A plea for advancement in core technologies,” in *Proceedings of IEEE Sensors*, vol. 2, 2002.
- [3] Awarepoint, “<http://www.awarepoint.com/>,” 2010.
- [4] Ekahau, “<http://www.ekahau.com/>,” 2009.
- [5] M. Hazas, J. Scott, and J. Krumm, “Location-aware computing comes of age,” *Computer*, vol. 37, no. 2, pp. 95–97, 2004.
- [6] N. Patwari, J. Ash, S. Kyperountas, A. Hero III, R. Moses, and N. Correal, “Locating the nodes: Cooperative localization in wireless sensor networks,” *IEEE Signal Processing Magazine*, vol. 22, no. 4, pp. 54–69, 2005.
- [7] N. Correal and N. Patwari, “Wireless sensor networks: Challenges and opportunities,” in *MPRG/Virginia Tech Wireless Symposium*, 2001.
- [8] J. Wilson and N. Patwari, “Radio tomographic imaging with wireless networks,” *IEEE Trans. Mobile Computing*, 2009.
- [9] G. Chen and D. Kotz, “A survey of context-aware mobile computing research,” Technical Report TR2000-381, Dept. of Computer Science, Dartmouth College, Tech. Rep., 2000.
- [10] G. Sun, J. Chen, W. Guo, and K. Liu, “Signal processing techniques in network-aided positioning: A survey of state-of-the-art positioning designs,” *IEEE Signal Processing Magazine*, vol. 22, no. 4, pp. 12–23, 2005.
- [11] A. Sayed, A. Tarighat, and N. Khajehnouri, “Network-based wireless location: challenges faced in developing techniques for accurate wireless location information,” *IEEE Signal Processing Magazine*, vol. 22, no. 4, pp. 24–40, 2005.
- [12] G. Mao, B. Fidan, and B. Anderson, “Wireless sensor network localization techniques,” *Computer Networks*, vol. 51, no. 10, pp. 2529–2553, 2007.
- [13] N. Priyantha, A. Chakraborty, and H. Balakrishnan, “The cricket location-support system,” in *Proceedings of the 6th Annual International Conference on Mobile Computing and Networking (MobiCom ’00)*, 2000, pp. 32–43.

- [14] P. Agrawal and N. Patwari, "Correlated link shadow fading in multi-hop wireless networks," *IEEE Transactions on Wireless Communications*, vol. 8, no. 8, pp. 4024–4036, 2009.
- [15] N. Patwari and P. Agrawal, "Effects of correlated shadowing: Connectivity, localization, and RF tomography," in *Proceedings of the 7th International Conference on Information Processing in Sensor Networks (IPSN '08)*, 2008, pp. 82–93.
- [16] P. Agrawal and N. Patwari, "Kernel methods for RSS-based indoor localization," in *Handbook of Position Location: Theory, Practice and Advances*, S. A. R. Zekavat and R. M. Buehrer, Eds. John Wiley & Sons, Inc., 2011, pp. 457–486.
- [17] G. Marconi, "Wireless telegraphy," *Journal of the IEE*, vol. 28, pp. 273–315, 1899.
- [18] H. Hashemi, "The indoor radio propagation channel," *Proceedings of the IEEE*, vol. 81, no. 7, pp. 943–968, July 1993.
- [19] T. Rappaport, *Wireless communication: Principles and Practice*, 2nd ed. Prentice Hall PTR, New Jersey, 1996.
- [20] H. Bertoni, *Radio Propagation for Modern Wireless Systems*. Prentice Hall Professional Technical Reference, 1999.
- [21] C. Bettstetter and C. Hartmann, "Connectivity of wireless multihop networks in a shadow fading environment," *Wireless Networks*, vol. 11, no. 5, pp. 571–579, September 2005.
- [22] R. Hekmat and P. V. Mieghem, "Connectivity in wireless ad-hoc networks with a log-normal radio model," *Mob. Netw. Appl.*, vol. 11, no. 3, pp. 351–360, 2006.
- [23] D. Kotz, C. Newport, and C. Elliott, "The mistaken axioms of wireless-network research," Dept. of Computer Science, Dartmouth College, Tech. Rep. TR2003-467, July 2003. [Online]. Available: <http://www.cs.dartmouth.edu/reports/abstracts/TR2002-467/>
- [24] P. Bahl and V. Padmanabhan, "RADAR: An in-building RF-based user location and tracking system," in *IEEE Proc. INFOCOM '00*, vol. 2, 2000, pp. 775–784.
- [25] M. Brunato and R. Battiti, "Statistical learning theory for location fingerprinting in wireless LANs," *Computer Networks*, vol. 47, no. 6, pp. 825–845, 2005.
- [26] B. Ferris, D. Hähnel, and D. Fox, "Gaussian processes for signal strength-based location estimation," in *Proc. of Robotics Science and Systems*, 2006.
- [27] X. Nguyen, M. Jordan, and B. Sinopoli, "A kernel-based learning approach to ad hoc sensor network localization," *ACM Transactions on Sensor Networks (TOSN)*, vol. 1, no. 1, p. 152, 2005.

- [28] Y. Ko and N. Vaidya, "Location-aided Routing (LAR) in Mobile Ad hoc Networks," *Wireless Networks*, vol. 6, no. 4, p. 321, 2000.
- [29] M. Mauve, A. Widmer, and H. Hartenstein, "A survey on position-based routing in mobile ad hoc networks," *IEEE Network Magazine*, vol. 15, no. 6, pp. 30–39, 2001.
- [30] R. Jain, A. Puri, and R. Sengupta, "Geographical routing using partial information for wireless ad hoc networks," *IEEE Personal Communications*, vol. 8, no. 1, pp. 48–57, 2001.
- [31] D. Niculescu and B. Nath, "Ad hoc positioning system (aps)," in *Global Telecommunications Conference, (GLOBECOM'01)*, vol. 5, 2001, pp. 2926–2931.
- [32] A. Savvides, H. Park, and M. Srivastava, "The bits and flops of the n-hop multilateration primitive for node localization problems," in *Proceedings of the 1st ACM International Workshop on Wireless Sensor Networks and Applications (WSNA '02)*, 2002, pp. 112–121.
- [33] C. Savarese, J. Rabaey, and K. Langendoen, "Robust positioning algorithms for distributed ad-hoc wireless sensor networks," in *USENIX Technical Annual Conference*, vol. 2, 2002.
- [34] J. Letchner, D. Fox, and A. LaMarca, "Large-scale localization from wireless signal strength," in *Proceedings of the National Conference on Artificial Intelligence*, vol. 20, no. 1, 2005, p. 15.
- [35] T. Roos, P. Myllymäki, H. Tirri, P. Misikangas, and J. Sievänen, "A probabilistic approach to WLAN user location estimation," *International Journal of Wireless Information Networks*, vol. 9, no. 3, pp. 155–164, 2002.
- [36] A. Savvides, C. Han, and M. Srivastava, "Dynamic fine-grained localization in ad-hoc networks of sensors," in *Proceedings of the 7th Annual International Conference on Mobile Computing and Networking (MobiCom '01)*, 2001, pp. 166–179.
- [37] Y. Shang and W. Ruml, "Improved mds-based localization," in *IEEE Proc. INFOCOM '04*, vol. 4, 2004, pp. 2640–2651.
- [38] Y. Shang, W. Ruml, Y. Zhang, and M. Fromherz, "Localization from mere connectivity," in *Proceedings of the 4th ACM International Symposium on Mobile Ad Hoc Networking & Computing (MOBIHOC '03)*, 2003, pp. 201–212.
- [39] G. Hjaltason and H. Samet, "Properties of Embedding Methods for Similarity Searching in Metric Spaces," *IEEE Transactions on Pattern Analysis and Machine Intelligence*, pp. 530–549, 2003.

- [40] L. Tang and M. Crovella, "Virtual landmarks for the internet," in *Proceedings of the 3rd ACM Conference on Internet Measurement (IMC '03)*, 2003, pp. 143–152.
- [41] V. Athitsos and S. Sclaroff, "Estimating 3D hand pose from a cluttered image," *Proceedings of IEEE Computer Society Conference on Computer Vision and Pattern Recognition (CVPR '03)*, vol. 2, 2003.
- [42] L. Ni, Y. Liu, Y. Lau, and A. Patil, "LANDMARC: Indoor location sensing using active RFID," *Transaction on Wireless Networks*, vol. 10, no. 6, pp. 701–710, 2004.
- [43] A. Kushki, K. Plataniotis, and A. Venetsanopoulos, "Kernel-based positioning in wireless local area networks," *IEEE Transactions on Mobile Computing*, vol. 6, no. 6, pp. 689–705, 2007.
- [44] J. Krumm and J. C. Platt, "Minimizing calibration effort for an indoor 802.11 device location measurement system," *Technical Report, Microsoft Corporation*, 2003.
- [45] H. Lim, L. Kung, J. Hou, and H. Luo, "Zero-configuration, robust indoor localization: Theory and experimentation," in *Proceedings of IEEE Infocom*, 2006, pp. 123–125.
- [46] G. Malmgren, "On the performance of single frequency networks in correlated shadow fading," *IEEE Trans. Broadcasting*, vol. 43, no. 2, pp. 155–165, June 1997.
- [47] K. S. Butterworth, K. W. Sowerby, and A. G. Williamson, "Base station placement for in-building mobile communication systems to yield high capacity and efficiency," *IEEE Trans. Communications*, vol. 48, no. 4, pp. 658–669, April 2000.
- [48] T. Klingenbrunn and P. Mogensen, "Modelling cross-correlated shadowing in network simulations," in *IEEE VTC 1999*, vol. 3, Sept. 1999, pp. 1407–1411.
- [49] J. Zhang and V. Aalo, "Effect of macrodiversity on average-error probabilities in a Rician fading channel with correlated lognormal shadowing," *IEEE Trans. Communications*, vol. 49, no. 1, pp. 14–18, Jan. 2001.
- [50] A. Safak and R. Prasad, "Effects of correlated shadowing signals on channel reuse in mobile radio systems," *IEEE Trans. Vehicular Technology*, vol. 40, no. 4, pp. 708–713, Nov. 1991.
- [51] D. Shiu, G. Foschini, M. Gans, and J. Kahn, "Fading correlation and its effect on the capacity of multielement antenna systems," *IEEE Transactions on Communications*, vol. 48, no. 3, pp. 502–513, 2000.

- [52] C. Wang, X. Hong, X. Ge, X. Cheng, G. Zhang, and J. Thompson, "Cooperative mimo channel models: A survey," *IEEE Communications Magazine*, vol. 48, no. 2, pp. 80–87, 2010.
- [53] Y. Chen, L. Hu, C. Yuen, Y. Zhang, Z. Zhang, and P. Rapajic, "Intrinsic measure of diversity gains in generalised distributed antenna systems with cooperative users," *IET Communications*, vol. 3, no. 2, pp. 209–222, 2009.
- [54] R. Szewczyk, J. Polastre, A. Mainwaring, and D. Culler, "Lessons from a sensor network expedition," *Wireless Sensor Networks*, pp. 307–322, 2004.
- [55] K. Srinivasan, M. Jain, J. Choi, T. Azim, E. Kim, P. Levis, and B. Krishnamachari, "The κ factor: Inferring protocol performance using inter-link reception correlation," in *Proceedings of the Sixteenth Annual International Conference on Mobile Computing and Networking (MobiCom '10)*, 2010, pp. 317–328.
- [56] F. Digham, M. Alouini, and M. Simon, "On the energy detection of unknown signals over fading channels," in *IEEE International Conference on Communications, (ICC '03)*, vol. 5, 2003, pp. 3575–3579.
- [57] A. Ghasemi and E. Sousa, "Opportunistic spectrum access in fading channels through collaborative sensing," *Journal of Communications*, vol. 2, no. 2, pp. 71–82, 2007.
- [58] S. Kyperountas, N. Correal, Q. Shi, and Z. Ye, "Performance analysis of cooperative spectrum sensing in Suzuki fading channels," in *2nd International Conference on Cognitive Radio Oriented Wireless Networks and Communications (CrownCom '07)*, 2007, pp. 428–432.
- [59] F. Visser, G. Janssen, and P. Pawelczak, "Multinode spectrum sensing based on energy detection for dynamic spectrum access," in *IEEE Vehicular Technology Conference (VTC Spring '08)*, 2008, pp. 1394–1398.
- [60] M. Di Renzo, F. Graziosi, and F. Santucci, "Cooperative spectrum sensing in cognitive radio networks over correlated log-normal shadowing," in *IEEE 69th Vehicular Technology Conference, (VTC Spring '09)*, 2009, pp. 1–5.
- [61] N. Patwari, Y. Wang, and R. O'Dea, "The importance of the multipoint-to-multipoint indoor radio channel in ad hoc networks," in *IEEE Wireless Communications and Networking Conference*, vol. 2, 2002, pp. 608–612.
- [62] M. Gudmundson, "Correlation model for shadow fading in mobile radio systems," *IEEE Electronics Letters*, vol. 27, no. 23, pp. 2145–2146, November 1991.
- [63] Z. Wang, E. K. Tameh, and A. Nix, "Simulating correlated shadowing in mobile multihop relay/ad-hoc networks," IEEE 802.16 Broadband Wireless Access Working Group, Tech. Rep. IEEE C802.16j-06/060, July 2006.

- [64] N. Patwari and P. Agrawal, "Nesh: A joint shadowing model for links in a multi-hop network," in *IEEE International Conference on Acoustics, Speech and Signal Processing (ICASSP '08)*, 2008, pp. 2873–2876.
- [65] W. Qin, M. Rabbat, and B. Yang, "A correlation model for shadow fading in multi-hop wireless networks," in *Proceedings of the 44th Annual Simulation Symposium*. Society for Computer Simulation International, 2011, pp. 100–104.
- [66] E. Dall'Anese, S. Kim, and G. Giannakis, "Channel gain map tracking via distributed kriging," *IEEE Transactions on Vehicular Technology*, vol. 60, no. 3, pp. 1205–1211, 2011.
- [67] S. Kim, E. Dall'Anese, G. Giannakis, and S. Pupolin, "Collaborative channel gain map tracking for cognitive radios," in *2nd International Workshop on Cognitive Information Processing (CIP '10)*, 2010, pp. 338–343.
- [68] S. Kim, E. Dall'Anese, and G. Giannakis, "Spectrum sensing for cognitive radios using kriged Kalman filtering," in *3rd IEEE International Workshop on Computational Advances in Multi-Sensor Adaptive Processing (CAMSAP '09)*, 2009, pp. 392–395.
- [69] E. Dall'Anese, S. Kim, G. Giannakis, and S. Pupolin, "Power allocation for cognitive radio networks under channel uncertainty," in *IEEE International Conference on Communications (ICC '11)*, 2011, pp. 1–6.
- [70] E. Dall'Anese, S. Kim, and G. Giannakis, "Admission and power control for cognitive radio networks by sequential geometric programming," in *17th International Conference on Digital Signal Processing (DSP '11)*, 2011, pp. 1–8.
- [71] R. L. Moses, D. Krishnamurthy, and R. Patterson, "A self-localization method for wireless sensor networks," *EURASIP Journal on Applied Sig. Proc.*, no. 4, pp. 348–358, Mar. 2003.
- [72] A. Catovic and Z. Sahinoglu, "The Cramér-Rao bounds of hybrid TOA/RSS and TDOA/RSS location estimation schemes," *IEEE Communication Letter*, vol. 8, no. 10, pp. 626–628, Oct. 2004.
- [73] N. Patwari, A. Hero, M. Perkins, N. Correal, and R. O'Dea, "Relative location estimation in wireless sensor networks," *IEEE Transactions on Signal Processing*, vol. 51, no. 8, pp. 2137–2148, 2003.
- [74] A. Savvides, W. Garber, S. Adlakha, R. Moses, and M. B. Srivastava, "On the error characteristics of multihop node localization in ad-hoc sensor networks," in *2nd Intl. Workshop on Inform. Proc. in Sensor Networks (IPSN '03)*, April 2003.

- [75] Y. Ji, S. Biaz, S. Pandey, and P. Agrawal, "ARIADNE: A dynamic indoor signal map construction and localization system," in *Proceedings of the 4th International Conference on Mobile Systems, Applications and Services (MobiSys '06)*, 2006, p. 164.
- [76] A. LaMarca, J. Hightower, I. Smith, and S. Consolvo, "Self-mapping in 802.11 location systems," *Lecture Notes in Computer Science*, vol. 3660, p. 87, 2005.
- [77] D. Niculescu and B. Nath, "VOR base stations for indoor 802.11 positioning," in *Proceedings of the 10th Annual International Conference on Mobile Computing and Networking (MOBICOM '04)*, 2004, pp. 58–69.
- [78] K. Langendoen and N. Reijers, "Distributed localization in wireless sensor networks: A quantitative comparison," *Computer Networks*, vol. 43, no. 4, pp. 499–518, 2003.
- [79] J. Hightower, R. Want, and G. Borriello, "Spoton: An indoor 3d location sensing technology based on rf signal strength," *UW CSE 00-02-02, University of Washington, Department of Computer Science and Engineering, Seattle, WA*, pp. 1–6, 2000.
- [80] A. Coulson, A. G. Williamson, and R. G. Vaughan, "A statistical basis for lognormal shadowing effects in multipath fading channels," *IEEE Transaction on Vehicular Technology*, vol. 46, no. 4, pp. 494–502, April 1998.
- [81] J. Lee and R. Buehrer, "Location estimation using differential rss with spatially correlated shadowing," in *IEEE Global Telecommunications Conference, (GLOBECOM '09)*, 2009, pp. 1–6.
- [82] C. Liu, K. Wu, and T. He, "Sensor localization with ring overlapping based on comparison of received signal strength indicator," in *IEEE International Conference on Mobile Ad-hoc and Sensor Systems (MASS '04)*, 2004, pp. 516–518.
- [83] M. Brunato and C. Kalló, "Transparent location fingerprinting for wireless services," in *Proceedings of Med-Hoc-Net*, vol. 2002, 2002.
- [84] M. Youssef and A. Agrawala, "The Horus location determination system," *Wireless Networks*, vol. 14, no. 3, pp. 357–374, 2008.
- [85] T. King, S. Kopf, T. Haenselmann, C. Lubberger, and W. Effelsberg, "COMPASS: A probabilistic indoor positioning system based on 802.11 and digital compasses," in *Proceedings of the 1st International Workshop on Wireless Network Testbeds, Experimental Evaluation & Characterization*, 2006, p. 40.
- [86] K. Chintalapudi, A. Padmanabha Iyer, and V. Padmanabhan, "Indoor localization without the pain," in *Proceedings of the Sixteenth Annual International Conference on Mobile Computing and Networking (MobiCom '10)*, 2010, pp. 173–184.

- [87] A. Howard, S. Siddiqi, and G. S. Sukhatme, “An experimental study of localization using wireless ethernet,” in *Field and Service Robotics*, ser. Springer Tracts in Advanced Robotics, Yuta, Shin-ichi and Asama, Hajima and Prassler, Erwin and Tsubouchi, Takashi and Thrun, Sebastian, Ed. Springer Berlin / Heidelberg, 2006, pp. 145–153.
- [88] Patwari, Neal and Hero, Alfred O. and Costa, Jose A., “Learning sensor location from signal strength and connectivity,” in *Secure Localization and Time Synchronization for Wireless Sensor and Ad Hoc Networks*, ser. Advances in Information Security, Poovendran, Radha and Roy, Sumit and Wang, Cliff, Ed. Springer US, 2007, vol. 30, pp. 57–81.
- [89] Y. Zhao, N. Patwari, P. Agrawal, and M. Rabbat, “Directed by directionality: Benefiting from the gain pattern of active RFID badges,” *Transactions on Mobile Computing*, July 2010.
- [90] R. Nagpal, “Organizing a global coordinate system from local information on an amorphous computer,” *AI Memo No. 1666, MIT A.I. Laboratory*, 1999.
- [91] L. Kleinrock and J. Silvester, “Optimum transmission radii for packet radio networks or why six is a magic number,” in *Proceedings of the IEEE National Telecommunications Conference*, vol. 4, 1978, pp. 1–4.
- [92] H. Lee, A. Cerpa, and P. Levis, “Improving wireless simulation through noise modeling,” in *Information Processing in Sensor Networks (IPSN’07)*, April 2007.
- [93] S. Seidel and T. Rappaport, “Site-specific propagation prediction for wireless in-building personal communication system design,” *IEEE Trans. Vehicular Technology*, vol. 43, no. 4, pp. 879–891, Nov. 1994.
- [94] M. Hassan-Ali and K. Pahlavan, “A new statistical model for site-specific indoor radio propagation prediction based on geometric optics and geometric probability,” *IEEE Transactions on Wireless Communications*, vol. 1, no. 1, pp. 112–124, 2002.
- [95] G. D. Durgin, *Space-Time Wireless Channel*, 1st ed. Prentice Hall Press, Upper Saddle River, NJ, USA, 2002.
- [96] D. Mallants, B. P. Mohanty, A. Vervoort, and J. Feyen, “Spatial analysis of saturated hydraulic conductivity in a soil with micropores,” *Soil Technology*, 1997.
- [97] N. A. Cressie, *Statistics for Spatial Data*. John Wiley & Sons, Inc., New York, 1991.
- [98] K. Worsley, A. Evans, S. Strother, and J. Tyler, “A linear spatial correlation model, with applications to positron emission tomography,” *Journal of the American Statistical Association*, vol. 86, no. 413, pp. 55–67, March 1991.

- [99] B. D. Ripley, *Spatial Statistics*. John Wiley & Sons, Inc., Hoboken, NJ, USA, 2005.
- [100] G. D. Durgin, T. S. Rappaport, and H. Xu, “Measurements and models for radio path loss and penetration loss in and around homes and trees at 5.85 GHz,” *IEEE Trans. Communications*, vol. 46, no. 11, pp. 1484–1496, Nov. 1998.
- [101] J. Robinson, R. Swaminathan, and E. W. Knightly, “Assessment of urban-scale wireless networks with a small number of measurements,” *Proc. 14th ACM Int’l Conf. Mobile Computing and Networking (MobiCom ’08)*, Sept. 2008.
- [102] P. Agrawal and N. Patwari, “Link shadow correlation model calculation code,” matlab code for public download. [Online]. Available: <http://span.ece.utah.edu>
- [103] “MPR-MIB users manual,” Crossbow Technology Inc, June 2006, revision B.
- [104] “TEP 123 : Collection tree protocol,” <http://www.tinyos.net/tinyos-2.x/doc/html/tep123.html>, August 2006.
- [105] W. W. Hines, D. C. Montgomery, D. M. Goldsman, and C. M. Borror, *Probability and Statistics in Engineering*, 4th ed. John Wiley & Sons, Inc., New York, 2003.
- [106] T. Roos, P. Myllymäki, and H. Tirri, “A statistical modeling approach to location estimation,” *IEEE Transactions on Mobile Computing*, pp. 59–69, 2002.
- [107] C. Bishop, *Pattern Recognition and Machine Learning*. Springer, New York, 2006.
- [108] Y. Gwon and R. Jain, “Error characteristics and calibration-free techniques for wireless LAN-based location estimation,” in *Proceedings of the Second International Workshop on Mobility Management & Wireless Access Protocols (MobiWac ’04)*, 2004, pp. 2–9.
- [109] C. Bishop, *Neural Networks for Pattern Recognition*. Oxford Univ. Press, USA, 2005.
- [110] T. Hastie, R. Tibshirani, and J. Friedman, *The Elements of Statistical Learning: Data mining, Inference, and Prediction*. Springer Verlag, New York, 2009.
- [111] S. Kay, *Fundamentals of Statistical Signal Processing: Estimation Theory*. Prentice-Hall Signal Processing Series, Upper Saddle River (New Jersey), 1993.
- [112] G. Strang, *Linear Algebra and its Applications*. Hartcourt Brace Jovanovich College Publishers, Orlando, FL, 1988.
- [113] L. Paradowski, M. Acad, and P. Warsaw, “Uncertainty ellipses and their application to interval estimation of emitter position,” *IEEE Transactions on Aerospace and Electronic Systems*, vol. 33, no. 1, pp. 126–133, 1997.

- [114] B. Krishnamachari, *Networking Wireless Sensors*. Cambridge Univ Press, New York, NY, USA, 2005.
- [115] M. Zuniga and B. Krishnamachari, "Analyzing the transitional region in low power wireless links," in *First Annual IEEE Communications Society Conference on Sensor and Ad Hoc Communications and Networks, (SECON '04)*, 2004, pp. 517–526.
- [116] A. Woo, T. Tong, and D. Culler, "Taming the underlying challenges of reliable multihop routing in sensor networks," in *Proceedings of the 1st International Conference on Embedded Networked Sensor Systems (SenSys '03)*, 2003, pp. 14–27.
- [117] J. Tenenbaum, V. Silva, and J. Langford, "A global geometric framework for nonlinear dimensionality reduction," *Science*, vol. 290, no. 5500, p. 2319, 2000.
- [118] R. Stoleru and J. Stankovic, "Probability grid: A location estimation scheme for wireless sensor networks," in *First Annual IEEE Communications Society Conference on Sensor and Ad Hoc Communications and Networks, (SECON '04)*, 2004, pp. 430–438.
- [119] A. Ahmed, Y. Shang, and H. Shi, "Variants of multidimensional scaling for node localization," in *Proceedings of the 11th International Conference on Parallel and Distributed Systems - Volume 01 (ICPADS '05)*, vol. 1, 2005, pp. 140–146.
- [120] C. Wang, J. Chen, Y. Sun, and X. Shen, "Wireless sensor networks localization with isomap," in *IEEE International Conference on Communications, (ICC '09)*, 2009, pp. 1–5.
- [121] D. Pandya, R. Jain, and E. Lupu, "Indoor location estimation using multiple wireless technologies," in *14th IEEE Proceedings on Personal, Indoor and Mobile Radio Communications, (PIMRC '03)*, vol. 3, 2003, pp. 2208–2212.
- [122] A. Ihler, J. Fisher III, R. Moses, and A. Willsky, "Nonparametric belief propagation for self-localization of sensor networks," *IEEE Journal on Selected Areas in Communications*, vol. 23, no. 4, pp. 809–819, 2005.
- [123] D. Dhanapala and A. Jayasumana, "Geo-logical routing in wireless sensor networks," in *Proc. 8th Annual IEEE Communications Society Conference on Sensor, Mesh and Ad Hoc Communications and Networks (SECON '11)*, 2011.